

# Information-theoretic Classification Accuracy: A Data-driven Criterion to Combining Ambiguous Outcome Labels in Multi-class Classification

Chihao Zhang<sup>1,2</sup>, Yiling Elaine Chen<sup>3</sup>, Shihua Zhang<sup>\*1,2,4,5</sup>, and Jingyi Jessica Li<sup>\*3, 6</sup>

<sup>1</sup>NCMIS, CEMS, RCSDS, Academy of Mathematics and Systems Science, Chinese Academy of Sciences, Beijing 100190, China

<sup>2</sup>School of Mathematical Sciences, University of Chinese Academy of Sciences, Beijing 100049, China.

<sup>3</sup>Department of Statistics, University of California, Los Angeles, CA 90095

<sup>4</sup>Center for Excellence in Animal Evolution and Genetics, Chinese Academy of Sciences, Kunming 650223, China

<sup>5</sup>Key Laboratory of Systems Biology, Hangzhou Institute for Advanced Study, University of Chinese Academy of Sciences, Chinese Academy of Sciences, Hangzhou 310024, China

<sup>6</sup>Interdepartmental Program in Bioinformatics, Department of Computational Medicine and Department of Biostatistics, University of California, Los Angeles, CA 90095

## Abstract

Outcome labeling ambiguity and subjectivity are ubiquitous in real-world datasets. While practitioners commonly combine ambiguous outcome labels in an ad hoc way to improve the accuracy of multi-class classification, there lacks a principled approach to guide label combination by any optimality criterion. To address this problem, we propose the information-theoretic classification accuracy (ITCA), a criterion that balances the trade-off between prediction accuracy (how well do predicted labels agree with actual labels) and prediction resolution (how many labels are predictable), to guide practitioners on how to combine ambiguous outcome labels. To find the optimal label combination indicated by ITCA, we develop two search strategies: greedy search and breadth-first search. Notably, ITCA and the two search strategies are adaptive to all machine-learning classification algorithms. Coupled with a classification algorithm and a search strategy, ITCA has two uses: improving prediction accuracy and identifying ambiguous labels. We first verify that ITCA achieves high accuracy with both search strategies

---

\*To whom correspondence should be addressed. Email: jli@stat.ucla.edu, zsh@amss.ac.cn

in finding the correct label combinations on synthetic and real data. Then we demonstrate the effectiveness of ITCA in diverse applications including medical prognosis, cancer survival prediction, user demographics prediction, and cell type classification. We also provide theoretical insights into ITCA by studying the oracle and the linear discriminant analysis classification algorithms.

*Keywords:* multi-class classification; information theory; noisy labels; supervised learning; class label combination.

## 1. INTRODUCTION

Machine-learning prediction algorithms play an increasingly important role in data-driven and computer-based scientific research and industrial applications, thanks to the rapid advances in data availability, computing power, and algorithm development. Prominent examples include fraud detection based on historical transactions [Brockett et al., 2002], cardiovascular risk prediction [Wilson et al., 1998, Weng et al., 2017], and risk evaluation for multiple diseases using genomics data [Chen et al., 2016]. Accurate algorithm prediction carries great promise because powerful algorithms can extract wisdom from human experts’ numerous decisions made over the years.

However, a bottleneck in the development of reliable algorithms is the availability of high-quality data, especially in medical diagnosis/prognosis and other biomedical applications. For example, medical records are inherently noisy, containing diagnostic/prognostic outcomes that are mislabeled or labeled inconsistently by graders [Krause et al., 2018]. Further, labeling ambiguity is common in ordinal outcomes—whose ordered levels represent degrees of symptom severity or treatment effectiveness—because of graders’ subjectivity in assigning patients to levels.

Ambiguous outcome labels would inevitably deteriorate the prediction accuracy of algorithms. Nevertheless, prediction accuracy may be boosted by combining the outcome labels that are hard to distinguish in training data, at the cost of losing prediction resolution because label combination reduces the number of predictable outcome labels. Hence, how to find a balance between prediction accuracy and resolution is a computational challenge. Although outcome labels are often combined in an ad hoc way to train algorithms in practices [Feldmann and Steudel, 2000, Hemingway et al., 2013], there lacks a principled approach to guide the combination by any optimality criterion.

Besides outcome prediction, another critical application of machine learning is to refine the outcome labels that are predefined by human experts. For example, in medical informatics, an important task is to use treatment outcomes to retrospectively refine diagnosis categories [Lindenauer et al., 2012, Kale and Korenstein, 2018]. This task can be formulated as a multi-class classification problem, where the features are treatment outcomes and the response is a categorical variable indicating diagnosis categories. In this task, if patients in different diagnosis categories exhibit indistinguishable treatment outcomes, these categories should be combined. Such data-driven prediction has been used to update existing grading systems for diagnosis, such as the Gleason score

for prostatic carcinoma [Epstein et al., 2015], the glomerular filtration rate (GFR) grade for chronic kidney disease, and the ACC/AHA classification for high blood pressure [Muntner et al., 2018]. For another example, in single-cell gene expression data analysis, a typical procedure is to cluster cells based on gene expression levels and subsequently annotate the cell clusters using domain knowledge [Butler et al., 2018]. This procedure is inevitably subjective because how to determine the number of clusters remains a challenging question, and some cell clusters may be hardly distinguishable by gene expression levels. Hence, a principled method is called to guide the decision of combining ambiguous labels defined by the human experts.

How to find an “optimal” class combination is not a trivial problem. The reason is that, even if the prediction is completely random, i.e., assigning data points with random labels irrespective of features, prediction accuracy would still be boosted by label combination. In such an extreme case, the increase in prediction accuracy does not outweigh the decrease in prediction resolution. Hence, our rationale is that label combination must be guided by a criterion that reasonably balances prediction accuracy and resolution. Motivated by this rationale, we propose a criterion from an information theory perspective to evaluate prediction accuracy together with prediction resolution. This data-driven criterion, called the *information-theoretic classification accuracy* (ITCA), guides the combination of class labels given a multi-class classification algorithm. ITCA also allows choosing a multi-class classification algorithm among the available algorithms based on their respective optimal label combinations.

There are two lines of research seemingly related to our work. The first line is classification in the presence of labeling noise [Frénay and Verleysen, 2013]. It includes three major approaches for handling labeling noise: (1) using robust losses or ensemble learning [Freund, 2001, Beigman and Klebanov, 2009]; (2) removing data points that are likely mislabeled [Zhang et al., 2006, Thongkam et al., 2008]; (3) modeling labeling noise using data generative models [Swartz et al., 2004, Kim and Ghahramani, 2008]. The second line is conformal prediction [Vovk et al., 2005], whose core idea is to generalize the prediction from a single label to a set of labels [Balasubramanian et al., 2014]. In detail, given a pre-specified confidence level (e.g., 95%), conformal prediction outputs a set of labels for each data point so that the actual label is contained in the set with probability no less than the confidence level. In summary, both lines of research tackle the labeling noise problem at the level

of individual data points; as a result, neither line can suggest how to combine labels at the global level for all data points, e.g., how to combine labels in a diagnosis or prognosis system.

Unlike these two lines of research, our proposed ITCA is a global criterion that measures prediction accuracy in relation to prediction resolution. Given a multi-class prediction algorithm, say random forest, ITCA is defined as a weighted prediction accuracy, in which each data point is weighted by the entropy attributable to its class. As a result, ITCA balances the trade-off between prediction accuracy and resolution, thus offering guidance for finding an “optimal” class label combination. As the first criterion that guides the combination of class labels, ITCA has broad applications, including medical diagnosis and prognosis, cancer survival prediction, user demographics prediction, and cell type classification. We will demonstrate these applications in Section 4.

A prominent advantage of ITCA is that it is adaptive to all classification algorithms, thus allowing practitioners to choose the most suitable classification algorithm for a specific task. As a side note, one may intuitively consider using a clustering algorithm to combine similar classes; for example, one may use the  $K$ -means algorithm or the hierarchical clustering algorithm to cluster the  $K_0$  class centers into  $K < K_0$  clusters, so that the  $K_0$  observed classes are correspondingly combined into  $K$  classes (see Section 3). However, this intuitive approach has a drawback: since a distance metric is required to define the class centers and their distances, a gap exists between the choices of a metric and a classification algorithm. In other words, clustering-guided class combination based on a certain metric (e.g., Euclidean distance) does not guarantee to optimize the classification accuracy of a specific algorithm (e.g., support vector machine with Gaussian kernel). In contrast, ITCA does not have this drawback because it is defined based on the classification accuracy of the algorithm.

The rest of this paper is structured as follows. In Section 2, we first formulate the problem, define ITCA at the sample and population levels, and explain the intuition behind the definitions. Then we introduce two search strategies—greedy search and breadth-first search—to find the optimal class combination guided by ITCA given a classification algorithm. In Section 3, we use extensive simulation studies to verify the effectiveness of ITCA and the two search strategies. In Section 4, we demonstrate the broad applications of ITCA by applying it to multiple real-world datasets, including prognosis data of traumatic brain injury patients, glioblastoma cancer survival data, mobile phone user behavioral data, and single-cell RNA-seq data. In these applications, we also

show the versatility of ITCA in working with various classification algorithms. Section 5 is the conclusion. Some key details are in Appendix: in Section A, we propose five alternative criteria that may also guide class combination and are compared with ITCA; in Section B.1, we conduct theoretical analysis on two classification algorithms—the oracle and the linear discriminant analysis (LDA)—to characterize ITCA and provide insights for its use in practice; in Section B.2, we propose the soft LDA algorithm to improve LDA for class combination by ITCA; in Section C, we propose a pruning procedure to further reduce the search spaces of the two search strategies. Further details are provided in the Supplementary Material.

## 2. METHOD

### 2.1 Problem formulation

Let  $(\mathbf{X}, Y) \sim \mathcal{P}$  be a random pair where  $\mathbf{X} \in \mathcal{X} \subset \mathbb{R}^d$  is a feature vector,  $Y \in [K_0] := \{1, \dots, K_0\}$  is a class label indicating one of  $K_0$  observed classes that are potentially ambiguous, and  $\mathcal{P}$  is the joint distribution of  $(\mathbf{X}, Y)$ . For a fixed positive integer  $K (< K_0)$ , a class combination is represented by an onto mapping:  $\pi_K : [K_0] \rightarrow [K]$ . For example, if  $K_0 = 4$  classes are combined into  $K = 3$  classes by merging the original classes 3 and 4, then  $\pi_3(1) = 1$ ,  $\pi_3(2) = 2$ ,  $\pi_3(3) = 3$ , and  $\pi_3(4) = 3$ . We define  $\pi_K^{-1}$  as follows:  $\pi_K^{-1}(k) := \{k_0 \in [K_0] : \pi_K(k_0) = k\}$ ,  $\forall k \in [K]$ . Then in this example,  $\pi_3^{-1}(1) = \{1\}$ ,  $\pi_3^{-1}(2) = \{2\}$ ,  $\pi_3^{-1}(3) = \{3, 4\}$ . For notation simplicity, we write  $\pi_3$  as  $\{1, 2, (3, 4)\}$ . Given a class combination  $\pi_K$ , a classification algorithm  $\mathcal{C}$ , and a training dataset  $\mathcal{D}_t$ , we denote by  $\phi_{\pi_K}^{\mathcal{C}, \mathcal{D}_t} : \mathcal{X} \rightarrow [K]$  a multi-class classifier trained by  $\mathcal{C}$  on  $\mathcal{D}_t$  to predict  $K$  combined classes. The prediction is accurate if and only if  $\phi_{\pi_K}^{\mathcal{C}, \mathcal{D}_t}(\mathbf{X}) = \pi_K(Y)$ .

Given  $K$ , how to find an “optimal”  $\pi_K$  is a twofold problem. First, we need an optimality criterion of  $\pi_K$  that balances the trade-off between prediction accuracy and resolution. Mathematically, given a dataset  $\mathcal{D} := \{(\mathbf{X}_i, Y_i)\}_{i=1}^n$ , a class combination  $\pi_K$ , and a classification algorithm  $\mathcal{C}$ , we split  $\mathcal{D}$  into training data  $\mathcal{D}_t$  and evaluation data  $\mathcal{D}_e$ , train a classifier  $\phi_{\pi_K}^{\mathcal{C}, \mathcal{D}_t}$  on  $\mathcal{D}_t$ , and evaluate the prediction accuracy of  $\phi_{\pi_K}^{\mathcal{C}, \mathcal{D}_t}$  on  $\mathcal{D}_e$ . Then we define an optimality criterion of  $\pi_K$  given  $\mathcal{D}_t$ ,  $\mathcal{D}_e$ , and  $\mathcal{C}$ , denoted by  $m(\pi_K; \mathcal{D}_t, \mathcal{D}_e, \mathcal{C})$ , based on the prediction accuracy of  $\phi_{\pi_K}^{\mathcal{C}, \mathcal{D}_t}$  and the resolution of  $\pi_K$ ’s  $K$  combined classes. To define the resolution, we adopt the entropy concept in information theory. The entropy of  $\pi_K$ ’s  $K$  combined classes’ empirical distribution in  $\mathcal{D} = \mathcal{D}_t \cup \mathcal{D}_e$  is

$\sum_{k=1}^K \left( - \sum_{k_0 \in \pi_K^{-1}(k)} \hat{p}_{k_0} \right) \log \left( \sum_{k_0 \in \pi_K^{-1}(k)} \hat{p}_{k_0} \right)$ , where  $\hat{p}_{k_0}$  is the proportion of the  $k_0$ -th original class in  $\mathcal{D}$ , and  $\sum_{k_0 \in \pi_K^{-1}(k)} \hat{p}_{k_0}$  is the proportion of  $\pi_K$ 's  $k$ -th combined class in  $\mathcal{D}$ . Note that this entropy measures the uncertainty of  $\pi_K(Y_1), \dots, \pi_K(Y_n)$  and increases as  $K$  increases or as the balance of the  $K$  classes increases (Figure 1). Hence, we find it reasonable to use this entropy to describe the resolution of  $\pi_K$ . In Section 2.2, we will define  $m(\pi_K; \mathcal{D}_t, \mathcal{D}_e, \mathcal{C})$  as ITCA, a criterion that can be interpreted as an entropy-weighted accuracy, to balance the trade-off between prediction accuracy and resolution.

Second, given the criterion  $m(\cdot; \mathcal{D}_t, \mathcal{D}_e, \mathcal{C})$ , we need a search strategy to find the optimal class combination  $\pi_K^*$  that maximizes the criterion:

$$\pi_K^* = \arg \max_{\pi_K \in \mathcal{A}} m(\pi_K; \mathcal{D}_t, \mathcal{D}_e, \mathcal{C}), \quad (1)$$

where  $\mathcal{A}$  is the set of allowed class combinations. For example, if the outcome labels are ordinal,  $\mathcal{A}$  contains all combinations that only combine adjacent class labels. We will address this search problem in Section 2.3.

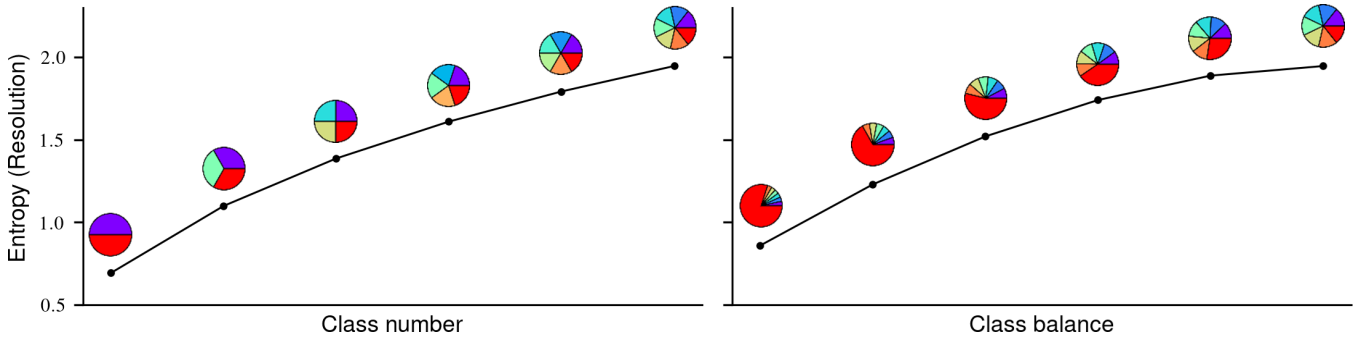


Figure 1: Entropy of the class label distribution reflects the resolution of class labels. Each pie chart indicates a class label distribution. Left: the number of balanced classes increases from left to right. Right: the class distributions are increasingly balanced from left to right. The resolution increases from left to right in both plots, reflected by the entropy increase.

## 2.2 Information-theoretic classification accuracy (ITCA)

Given  $\pi_K$ , a classification algorithm  $\mathcal{C}$ , and a size- $n$  dataset  $\mathcal{D}$  randomly split into training data  $\mathcal{D}_t$  and evaluation data  $\mathcal{D}_e$ , we define the ITCA of  $\pi_K$  at the sample level as

$$\begin{aligned} & \text{ITCA}(\pi_K; \mathcal{D}_t, \mathcal{D}_e, \mathcal{C}) \\ & := \sum_{k=1}^K \left[ - \left( \sum_{k_0 \in \pi_K^{-1}(k)} \hat{p}_{k_0} \right) \log \left( \sum_{k_0 \in \pi_K^{-1}(k)} \hat{p}_{k_0} \right) \right] \cdot \frac{\sum_{(\mathbf{X}_i, Y_i) \in \mathcal{D}_e} \mathbb{I}(\phi_{\pi_K}^{\mathcal{C}, \mathcal{D}_t}(\mathbf{X}_i) = k, \pi_K(Y_i) = k)}{1 \sqrt{\sum_{(\mathbf{X}_i, Y_i) \in \mathcal{D}_e} \mathbb{I}(\pi_K(Y_i) = k)}}, \quad (2) \end{aligned}$$

where  $\mathbb{I}(\cdot)$  is the indicator function,  $\hat{p}_{k_0} := \sum_{i=1}^n \mathbb{I}(Y_i = k_0)/n$  is the proportion of the  $k_0$ -th class in  $\mathcal{D} = \mathcal{D}_t \cup \mathcal{D}_e$ , and  $\phi_{\pi_K}^{\mathcal{C}, \mathcal{D}_t}$  is the classifier trained by the algorithm  $\mathcal{C}$  on  $\mathcal{D}_t$ . In this definition (2), the sum is taken over the  $K$  combined classes defined by  $\pi_K$ ; inside of the sum, for the  $k$ -th combined class, the first term is the contribution of the class to the entropy of  $\pi_K(Y)$ 's empirical distribution in  $\mathcal{D}$ , and the second term is the conditional prediction accuracy of  $\phi_{\pi_K}^{\mathcal{C}, \mathcal{D}_t}$  for the class on the evaluation data  $\mathcal{D}_e$ . In other words, the ITCA of  $\pi_K$  is a weighted out-of-sample prediction accuracy of a classifier trained with  $\pi_K$ 's  $K$  combined classes, whose contributions to the entropy (i.e., resolution) are defined as the weights. Meanwhile, the ITCA of  $\pi_K$  can be regarded as a weighted entropy if we consider the class-conditional prediction accuracies as weights. As a result, ITCA balances the prediction accuracy and resolution.

Note that the ITCA definition in (2), if  $\hat{p}_{k_0}$  is alternatively defined as the proportion of the  $k_0$ -th class in  $\mathcal{D}_e$ , is equivalent to

$$\text{ITCA}^{\text{alt}}(\pi_K; \mathcal{D}_t, \mathcal{D}_e, \mathcal{C}) = \frac{1}{|\mathcal{D}_e|} \sum_{(\mathbf{X}_i, Y_i) \in \mathcal{D}_e} -\log \left( \sum_{k_0 \in \pi_K^{-1}(\pi_K(Y_i))} \hat{p}_{k_0} \right) \cdot \mathbb{I}(\phi_{\pi_K}^{\mathcal{C}, \mathcal{D}_t}(\mathbf{X}_i) = \pi_K(Y_i)), \quad (3)$$

where  $|\mathcal{D}_e|$  is the size of  $\mathcal{D}_e$ . This alternative definition (3) has an intuitive interpretation. Imagine that we represent the  $K_0$  original classes in  $\mathcal{D}_e$  as  $K_0$  non-overlapping intervals in  $[0, 1]$  such that class  $k_0$  is represented by an interval  $I_{k_0}$  of length  $\hat{p}_{k_0}$ ; then  $\cup_{k_0=1}^{K_0} I_{k_0} = [0, 1]$ . With this representation, we can introduce a random variable  $U \sim \text{Uniform}([0, 1])$  such that  $Y = \sum_{k_0=1}^{K_0} k_0 \mathbb{I}(U \in I_{k_0})$ ; that is, the event  $U \in I_{k_0}$  is equivalent to the event  $Y = k_0$ . For a data point  $\mathbf{X}_i \in \mathcal{D}_e$ , when  $\phi_{\pi_K}^{\mathcal{C}, \mathcal{D}_t}$  correctly predicts its combined class label  $\pi_K(Y_i)$ , i.e.,  $\phi_{\pi_K}^{\mathcal{C}, \mathcal{D}_t}(\mathbf{X}_i) = \pi_K(Y_i)$ , we weight this correct prediction in (3) by difficulty, which should be higher if the combined class  $\pi_K(Y_i)$  is

smaller, i.e., the total length of  $\cup_{k_0 \in \pi_K^{-1}(\pi_K(Y_i))} I_{k_0}$  is shorter. Hence, we define the weight as the difference between the entropy of  $\text{Uniform}([0, 1])$  (i.e., the distribution of  $U_i$  without knowledge of  $Y_i$ ) and the entropy of  $\text{Uniform}(\cup_{k_0 \in \pi_K^{-1}(\pi_K(Y_i))} I_{k_0})$  (i.e., the distribution of  $U_i$  conditional on  $\pi_K(Y_i)$ ); this difference is bigger when the total length of  $\cup_{k_0 \in \pi_K^{-1}(\pi_K(Y_i))} I_{k_0}$  is shorter, satisfying our requirement. It can be derived that the entropy of  $\text{Uniform}([0, 1])$  is 0, and the entropy of  $\text{Uniform}(\cup_{k_0 \in \pi_K^{-1}(\pi_K(Y_i))} I_{k_0})$  is  $\log(\sum_{k_0 \in \pi_K^{-1}(\pi_K(Y_i))} \hat{p}_{k_0})$ . Hence, the correct prediction of  $\pi_K(Y_i)$  has the weight  $-\log(\sum_{k_0 \in \pi_K^{-1}(\pi_K(Y_i))} \hat{p}_{k_0})$  as in (3).

To address the issue that ITCA is defined based on one random split on  $\mathcal{D}$  (each data point is used only once for either training or evaluation) in (2), we further define the *R-fold cross-validated (CV) ITCA* as

$$\text{ITCA}^{\text{CV}}(\pi_K; \mathcal{D}, \mathcal{C}) := \frac{1}{R} \sum_{r=1}^R \text{ITCA}(\pi_K; \mathcal{D}_t^r, \mathcal{D}_e^r, \mathcal{C}), \quad (4)$$

where the dataset  $\mathcal{D}$  is randomly split into  $R$  equal-sized folds, with the  $r$ -th fold  $\mathcal{D}_e^r$  serving as the evaluation data and the union of the remaining  $R - 1$  folds  $\mathcal{D}_t^r$  serving as the training data. In the following text, we refer to  $\text{ITCA}^{\text{CV}}$  as the ITCA criterion if without specification.

By definition, ITCA is non-negative and becomes equal to zero when  $K = 1$ , i.e., the degenerate case when all classes are combined as one and classification becomes meaningless. This gives ITCA a nice property: unless all predictions are wrong for all  $K \geq 2$ —an unrealistic scenario, the class combination that maximizes ITCA would not be the degenerate  $\pi_1$ .

To investigate the theoretical properties of ITCA, we define it at the population level as

$$\text{p-ITCA}(\pi_K; \mathcal{D}_t, \mathcal{C}) := \sum_{k=1}^K [-\mathbb{P}(\pi_K(Y) = k) \log \mathbb{P}(\pi_K(Y) = k)] \cdot \mathbb{P}(\phi_{\pi_K}^{\mathcal{C}, \mathcal{D}_t}(\mathbf{X}) = \pi_K(Y) | \pi_K(Y) = k), \quad (5)$$

where  $\phi_{\pi_K}^{\mathcal{C}, \mathcal{D}_t}$  is the classifier trained by the algorithm  $\mathcal{C}$  on a finite training dataset  $\mathcal{D}_t$ . The population is used to evaluate the entropy contributions of  $\pi_K$ 's  $K$  combined classes and the class-conditional prediction accuracies of  $\phi_{\pi_K}^{\mathcal{C}, \mathcal{D}_t}$ . The *population-level ITCA (p-ITCA)* provides the basis of our theoretical analysis in Appendix B.1.

ITCA is aligned with the principle of maximum entropy [Pal et al., 2003], an application of the Occam's razor. For a fixed  $K$ , if the classifier  $\phi_{\pi_K}^{\mathcal{C}, \mathcal{D}_t}$  has the same prediction accuracy for each class, i.e.,  $\mathbb{P}(\phi_{\pi_K}^{\mathcal{C}, \mathcal{D}_t}(\mathbf{X}) = \pi_K(Y) | \pi_K(Y) = k)$  is a constant for all  $k \in [K]$ , then ITCA in (2) is

proportional to the entropy of  $\pi_K(Y)$  and is maximized by the  $\pi_K$  that results in the  $K$  combined classes with the most balanced class probabilities. In the special case where the classifier performs perfect prediction for all  $K$ 's, i.e.,  $\mathbb{P}(\phi_{\pi_K}^{\mathcal{C}, \mathcal{D}_t}(\mathbf{X}) = \pi_K(Y) | \pi_K(Y) = k) = 1$  for all  $k \in [K]$  and all  $K \in [K_0]$ , ITCA becomes monotone increasing in  $K$ , i.e., the higher the class resolution, the larger the entropy.

An advantage of ITCA is that it is adaptive to all machine-learning classification algorithms and its values are comparable for different algorithms. Hence, ITCA allows users to choose the most suitable algorithm for a specific classification task. In a task where prediction accuracy is of primary interest, users may compare algorithms by their optimal ITCA values (whose corresponding class combinations may differ for different algorithms) and choose the algorithm (along with the class combination) that gives the largest optimal ITCA value. Granted, if a classification algorithm has a sufficiently high accuracy for predicting the original  $K_0$  classes, ITCA would not suggest any classes to be combined. Hence, in exploratory data analysis where the goal is to find similar classes, users may use ITCA with a weak classification algorithm (e.g., LDA) so that the class combination found by ITCA can reveal similar classes.

### 2.3 Search strategy

Given the dataset  $\mathcal{D} = \{(\mathbf{X}_i, Y_i)\}_{i=1}^n$ , we aim at finding the optimal class combination that maximizes the ITCA in (4). A naïve strategy is the *exhaustive search*, i.e., computing the ITCA of all allowed class combinations  $\pi_K$ 's for  $2 \leq K \leq K_0$ , whose set is denoted by  $\mathcal{A}$ ; however,  $|\mathcal{A}|$  can be huge even when  $K_0$ , the number of original classes, is moderate (Table 1). Specifically, if the class labels are nominal, the number of allowed combinations,  $|\mathcal{A}|$ , is known as the Bell number [Bell, 1938]. If the class labels are ordinal, only adjacent classes should be combined; then, the number of allowed combinations is  $2^{K_0-1} - 1$  [Feller, 2008]. Since a classification algorithm  $\mathcal{C}$  needs to be trained for every  $\pi_K$  to calculate the ITCA of  $\pi_K$ , a large  $|\mathcal{A}|$  would make the exhaustive search strategy computationally infeasible.

To design an efficient search strategy, we adopt the *greedy search* algorithm. Specifically, we start from  $\pi_{K_0}^* = \pi_{K_0}$ , which does not combine any classes. In the  $k$ -th round ( $1 \leq k \leq K_0 - 2$ ), we find the best combination that maximizes the ITCA among the allowed combinations  $\pi_{K-k}$ 's, which are defined based on the chosen  $\pi_{K-k+1}^*$ . Next, we start from the chosen  $\pi_{K-k}^*$  and repeat this

Label type	$K_0$					
	2	4	6	8	12	16
$ \mathcal{A} $ Nominal	1	14	202	4,139	4,213,596	$\sim 10^{10}$
Ordinal	1	7	31	127	2,047	32,767

Table 1: The number of allowed class combinations given  $K_0$

procedure until the ITCA cannot be improved or  $K_0 - 2$  rounds are finished. This greedy search strategy reduces the search space significantly and is summarized in Algorithm 1. For ordinal class labels, the worst-case complexity of this greedy search strategy is  $\mathcal{O}(K_0^2)$ .

Algorithm 1: Greedy search algorithm

- 
- 1: Input data  $\mathcal{D} = \{(\mathbf{X}_i, Y_i)\}_{i=1}^n$  and a classification algorithm  $\mathcal{C}$ .
  - 2: Set  $K \leftarrow K_0$  and  $\pi_K^* \leftarrow \pi_{K_0}$ .
  - 3: Compute  $\text{ITCA}^{\text{CV}}(\pi_K^*; \mathcal{D}, \mathcal{C})$ .
  - 4: **while**  $K > 2$  **do**
  - 5:     Determine the set of allowed class combinations  $\mathcal{A}_{K-1}$  based on  $\pi_K^*$ .
  - 6:     **for** each allowed class combination  $\pi_{K-1} \in \mathcal{A}_{K-1}$  **do**
  - 7:         Compute  $\text{ITCA}^{\text{CV}}(\pi_{K-1}; \mathcal{D}, \mathcal{C})$ .
  - 8:         **if** there exists no  $\pi_{K-1}$  that achieves  $\text{ITCA}^{\text{CV}}(\pi_{K-1}; \mathcal{D}, \mathcal{C}) > \text{ITCA}^{\text{CV}}(\pi_K^*; \mathcal{D}, \mathcal{C})$  **then**
  - 9:             Break.
  - 10:     **else**
  - 11:          $K \leftarrow K - 1$ ;
  - 12:          $\pi_K^* \leftarrow \arg \max_{\pi_{K-1} \in \mathcal{A}_{K-1}} \text{ITCA}^{\text{CV}}(\pi_{K-1}; \mathcal{D}, \mathcal{C})$ .
  - 13: Return  $\pi_K^*$ .
- 

It is well known that the greedy search strategy may not lead to the globally optimal class combination. Besides the greedy search, another commonly used search strategy is the *breadth-first search (BFS)* summarized in Algorithm 2, which uses a queue to store class combinations that may be further combined. Specifically, given  $\pi_K$  (with  $K \geq 3$ ) removed from the front of queue, we use  $\mathcal{N}(\pi_K)$  to denote the set of allowed combinations  $\pi_{K-1}$ 's that combine any two class defined by  $\pi_K$ . For  $\pi_{K-1} \in \mathcal{N}(\pi_K)$  that has not been visited and improves the ITCA of  $\pi_K$ , the BFS strategy adds  $\pi_{K-1}$  to the end of the queue and considers  $\pi_{K-1}$  as a candidate optimal class combination. The BFS strategy stops when the queue is empty.

The search space of BFS is much larger than that of the greedy search but usually smaller than that of the exhaustive search. For ordinal class labels, BFS may enumerate all allowed class

combinations in the worst case; hence, its worst-case complexity is  $\mathcal{O}(2^{K_0})$ .

Although the greedy search and BFS are heuristic strategies, we will show that they achieve comparable performance to that of the exhaustive search in our experimental results in Section 3.

---

Algorithm 2: Breadth-first search algorithm

---

- 1: Input data  $\mathcal{D} = \{(\mathbf{X}_i, Y_i)\}_{i=1}^n$  and a classification algorithm  $\mathcal{C}$ .
  - 2: Initialize an empty set of combinations  $\mathcal{A}$  and an empty queue  $\mathcal{Q}$ .
  - 3: Compute  $\text{ITCA}^{\text{CV}}(\pi_{K_0}; \mathcal{D}, \mathcal{C})$ .
  - 4:  $\mathcal{A} \leftarrow \mathcal{A} \cup \{\pi_{K_0}\}$ . ▷ Add  $\pi_{K_0}$  to  $\mathcal{A}$ .
  - 5:  $\mathcal{Q}.\text{enqueue}(\pi_{K_0})$ . ▷ Add  $\pi_{K_0}$  to the back of  $\mathcal{Q}$ .
  - 6: **while**  $\mathcal{Q}$  is not empty **do**
  - 7:      $\pi_K \leftarrow \mathcal{Q}.\text{dequeue}()$ . ▷ Remove the front element of  $\mathcal{Q}$  as  $\pi_K$ .
  - 8:     Determine the set of allowed class combinations  $\mathcal{N}(\pi_K)$  based on  $\pi_K$ .
  - 9:     **for** each allowed class combination  $\pi_{K-1} \in \mathcal{N}(\pi_K)$  **do**
  - 10:         **if**  $\pi_{K-1}$  is not visited **then**
  - 11:             Compute  $\text{ITCA}^{\text{CV}}(\pi_{K-1}; \mathcal{D}, \mathcal{C})$ .
  - 12:             **if**  $\text{ITCA}^{\text{CV}}(\pi_{K-1}; \mathcal{D}, \mathcal{C}) > \text{ITCA}^{\text{CV}}(\pi_K; \mathcal{D}, \mathcal{C})$  **then**
  - 13:                  $\mathcal{A} \leftarrow \mathcal{A} \cup \{\pi_{K-1}\}$ . ▷ Add  $\pi_{K-1}$  to  $\mathcal{A}$ .
  - 14:                  $\mathcal{Q}.\text{enqueue}(\pi_{K-1})$ . ▷ Add  $\pi_{K-1}$  to the back of  $\mathcal{Q}$ .
  - 15:             Mark  $\pi_{K-1}$  as visited.
  - 16: Return  $\pi_K^* \leftarrow \arg \max_{\pi \in \mathcal{A}} \text{ITCA}^{\text{CV}}(\pi; \mathcal{D}, \mathcal{C})$ .
- 

## 2.4 Some theoretical remarks

Of note, the ability of ITCA to find the true class combination depends on the classification algorithm. Using the oracle algorithm (see Definition 1 in Appendix B.1) and the LDA algorithm as examples, we analyze the properties of ITCA at a population level. As expected, used with the oracle algorithm, ITCA has a much stronger ability to find the true class combination than used with the LDA algorithm (see Appendix B.1). We also find that, when the LDA is used as a soft classification algorithm, ITCA is more likely to find the true class combination. In a special case where data are drawn from two well-separated Gaussian distributions, we can see that the soft LDA becomes the oracle classification algorithm (see Appendix B.2). Our theoretical analysis also reveals that ITCA is unsuitable for combining observed classes, even if ambiguous, into a large class that dominates in proportion. Moreover, we show that for both greedy search and BFS, the search space of possible class combinations can be further pruned if the classification algorithm satisfies a non-stringent property (see Appendix C). Please refer to Appendix for the detailed results.

### 3. SIMULATION STUDIES

#### 3.1 ITCA outperforms alternative class combination criteria on simulated data

To verify the effectiveness of ITCA, we first compare ITCA with five alternative criteria—*accuracy* (ACC), *mutual information* (MI), *adjusted accuracy* (AAC), *combined Kullback-Leibler divergence* (CKL), and *prediction entropy* (PE)—in simulations. Among the five alternative criteria, ACC is commonly used to evaluate classification algorithms, and MI is often to evaluate clustering algorithms. The rest three alternative criteria, namely AAC, CKL, and PE, are our newly proposed criteria to balance the trade-off between classification accuracy and class resolution from three other perspectives. Please refer to Appendix A and Supplementary Material Section 2.4 for the definitions of the five alternative criteria.

Given the number of observed classes  $K_0$  and the true class combination  $\pi_{K^*}^* : [K_0] \rightarrow [K^*]$ , we first generate  $K^*$  class centers by a random walk in  $\mathbb{R}^d$ . The random walk starts from the center of class 1:  $\boldsymbol{\mu}_1 = \mathbf{0} \in \mathbb{R}^d$ . At time  $k = 2, \dots, K^*$ , the walk chooses a direction at random and takes a step with a fixed length  $l$ ; that is, the center of class  $k$  is  $\boldsymbol{\mu}_k = \boldsymbol{\mu}_{k-1} + l\boldsymbol{v}$ , where  $\boldsymbol{v} \in \mathbb{R}^d$  is a random direction vector with the unit length, i.e.,  $\|\boldsymbol{v}\| = 1$ . To make the true classes distinguishable, we ensure that the minimal pairwise Euclidean distance among  $\boldsymbol{\mu}_1, \dots, \boldsymbol{\mu}_{K^*}$  is greater than  $\sigma$ , i.e., the standard deviation of every feature in each class. Given  $\{\boldsymbol{\mu}_k\}_{k=1}^{K^*}$  and  $\sigma$ , we then define the distribution of  $(\mathbf{X}, Y)$  as follows.

1. The true class  $Y^* \sim \text{discrete uniform}([K^*])$ , i.e.,  $Y^*$  randomly picks a value in  $[K^*]$  with probability  $1/K^*$ .
2. The observed class  $Y \sim \text{discrete uniform}(\pi_{K^*}^{*-1}(Y^*))$ , i.e.,  $Y$  randomly picks a value in  $\pi_{K^*}^{*-1}(Y^*) = \{k_0 \in [K_0] : \pi_{K^*}^*(k_0) = Y^*\} \subset [K_0]$ —the observed classes that belong to the true class  $Y^*$ —with probability  $1/|\pi_{K^*}^{*-1}(Y^*)| = 1/(\sum_{k_0}^{K_0} \mathbb{1}(\pi_{K^*}^*(k_0) = Y^*))$ .
3. The observed feature vector  $\mathbf{X} \sim \mathcal{N}(\boldsymbol{\mu}_{Y^*}, \sigma^2 \mathbf{I}_d)$ , i.e.,  $\mathbf{X}$  follows a  $d$ -dimensional Gaussian distribution with mean  $\boldsymbol{\mu}_{Y^*}$  specified by the true class  $Y^*$ .

Given a dataset  $\{(\mathbf{X}_i, Y_i)\}_{i=1}^n$ , which contains independently and identically distributed (i.i.d.) observations from the above distribution, an ideal criterion of class combination is expected to be maximized at  $\pi_{K^*}^*$ .

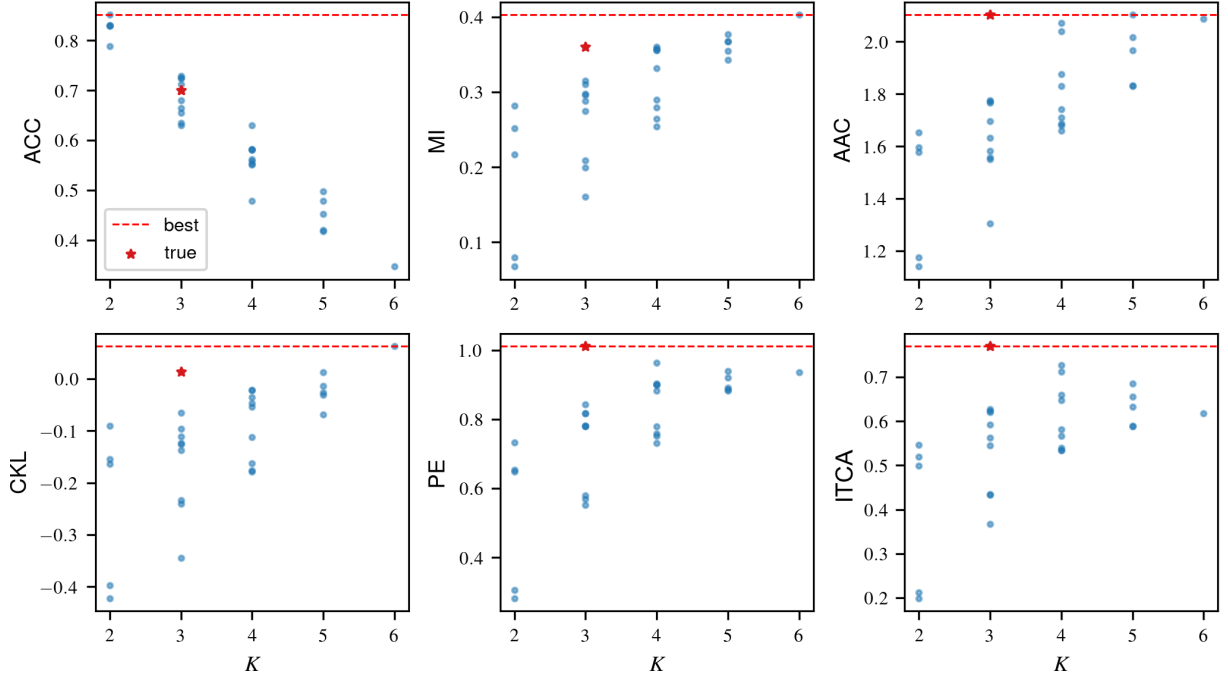


Figure 2: Comparison of ITCA and five alternative criteria using the LDA as the classification algorithm. The dataset is generated with  $K_0 = 6$ ,  $K^* = 3$ ,  $l = 3$ ,  $\sigma = 1.5$ ,  $n = 2000$ , and  $d = 5$ . The true class combination is  $\pi_3^* = \{(1, 2), (3, 4), (5, 6)\}$ . For each criterion (panel), the 31 blue points correspond to the 31 class combinations  $\pi_K$ 's with  $K = 2, \dots, 6$ . The true class combination  $\pi_{K^*}^*$  is marked with the red star, and the best value for each criterion is indicated by a horizontal dashed line. The true class combination is only found by PE and ITCA without close ties.

We generate a simulated dataset with  $K_0 = 6$ ,  $K^* = 3$ ,  $l = 3$ ,  $\sigma = 1.5$ ,  $n = 2000$ , and  $d = 5$ . We assume the true class combination is  $\pi_3^* = \{(1, 2), (3, 4), (5, 6)\}$ , i.e., the 1st and 2nd observed classes belong to one true class, and so do the 3rd and 4th observed classes, as well as the 5th and 6th observed classes. We also assume that the classes are ordinal; that is,  $\mathcal{A}$  contains  $2^5 - 1 = 31$  class combinations (Table 1). Because of the moderate size of  $|\mathcal{A}|$ , we use the exhaustive search to enumerate all allowed class combinations.

Regarding the classification algorithm, we consider the LDA and random forest (RF) [Breiman, 2001]. Figure 2 shows that ITCA using LDA successfully finds the true class combination  $\pi_3^*$ ; that is, when evaluated on the 31  $\pi_K$ 's, ITCA is maximized at  $\pi_3^*$ . As expected, ACC is maximized when the  $K_0 = 6$  observed classes are combined into  $K = 2$  classes; hence, it is not appropriate for guiding class combination. Although better than ACC, MI and two newly proposed criteria

(AAC and CKL) still fail to find  $\pi_3^*$ . Among the alternative criteria, only PE correctly identifies  $\pi_3^*$  because its definition is similar to that of ITCA. The results using RF (Supplementary Material, Figure S1) are consistent with Figure 2.

We design another simulation with  $K^* = 5$  and the true class combination  $\pi_5^* = \{(1, 2), 3, 4, 5, 6\}$ . The results in Figures S2 and S3 (Supplementary Material) show that ITCA outperforms all five alternative criteria, including PE, by finding  $\pi_5^*$  with the largest gap from other class combinations.

To further evaluate the performance of ITCA and the five alternative criteria, we escalate this simulation design by setting  $K_0 = 8$ ; then the number of allowed class combinations is  $2^7 - 1 = 127$  (Table 1). We repeat the simulation for 127 times, each time using one of the 127 allowed class combinations as the true class combination  $\pi_{K^*}^*$ ; the other simulation parameters are kept the same. We use the exhaustive search with LDA or RF to find the best class combination guided by each criterion, denoted by  $\pi_K^m$  for criterion  $m \in \{\text{ITCA, ACC, MI, AAC, CKL, PE}\}$ . To evaluate the performance of criterion  $m$ , we define the distance between  $\pi_K^m$  and  $\pi_{K^*}^*$  as follows. First, we encode each allowed class combination  $\pi_K : [K_0] \rightarrow [K]$  for combining  $K_0$  ordinal classes as a  $(K_0 - 1)$ -dimensional binary vector, as in the “stars and bars” used in combinatorics [Feller, 2008]. For example, the class combination  $\{(1, 2), 3, 4, 5, 6, 7, 8\}$  can be represented by  $12|3|4|5|6|7|8$  and thus encoded as the binary vector  $(0, 1, 1, 1, 1, 1, 1)$ , where the 0 indicates that there is no bar between the original classes 1 and 2, the first 1 indicates that there is a bar between the original classes 2 and 3, etc. Second, we define the distance between  $\pi_K^m$  and  $\pi_{K^*}^*$  as the Hamming distance between their binary encodings; hence, the distance takes an integer value ranging from 0 to  $K_0 - 1$ , with 0 indicating that  $\pi_K^m = \pi_{K^*}^*$ , i.e., the criterion  $m$  finds the true class combination.

We evaluate the performance of each criterion using three criteria: (1) the number of datasets (the larger the better) on which the criterion identifies the true class combination; (2) the average and (3) the maximum Hamming distances (the smaller the better) between the criterion’s best class combination and the true class combination across the 127 datasets. Table 2 shows that, among the six criteria, ITCA has the best performance under all three criteria; PE has the second best performance after ITCA; the other criteria fail to find the true class combination on at least 80% of the datasets. ITCA only misses the true class combination when  $K^* = 2$ , which corresponds to  $\binom{7}{6} = 7$  true class combinations (see Supplementary Material Table S5). This result is confirmed

in a similar analysis with  $K_0 = 6$  (in Supplementary Material Tables S1 and S4), and it can be explained by the theoretic analysis in Appendix B.1, which shows that ITCA would not combine two same-distributed classes when the combined class’ proportion is too large (e.g., larger than 0.5).

Criterion	<u># successes</u>	Average	Max	<u># successes</u>	Average	Max
	# datasets	Hamming	Hamming	# datasets	Hamming	Hamming
	LDA			RF		
ACC	6/127	2.54	6	7/127	2.53	6
MI	7/127	2.51	6	11/127	2.33	6
AAC	15/127	2.02	6	15/127	1.98	6
CKL	3/127	3.68	6	5/127	2.87	5
PE	101/127	0.47	4	94/127	0.46	3
ITCA	<b>120/127</b>	<b>0.12</b>	<b>3</b>	<b>120/127</b>	<b>0.08</b>	<b>2</b>

Table 2: The performance of six criteria on the 127 simulated datasets with  $K_0 = 8$ . The best result in each column is boldfaced.

Strategy	<u># successes</u>	Average	Max	Average # class
	# datasets	Hamming	Hamming	combinations examined
Exhaustive	120/127	0.13	3	127.00
Greedy search	120/127	0.12	3	22.52
BFS	120/127	0.10	2	53.61
Greedy (pruned)	120/127	0.09	2	11.91
BFS (pruned)	120/127	0.09	3	27.20

Table 3: Performance of ITCA using five search strategies and LDA on the 127 simulated datasets with  $K_0 = 8$ .

The above results verify the effectiveness of ITCA in finding the true class combination. In the following, we compare the two proposed search strategies, the greedy search and BFS, with the exhaustive search. Specifically, we use the aforementioned 127 simulated datasets corresponding to  $K_0 = 8$ , and we apply ITCA under the three search strategies, with LDA as the classification algorithm. The top three rows of Table 3 show that the greedy search and BFS are as effective as the exhaustive search in finding the true class combinations. Supplementary Material Table S2 shows similar results for  $K_0 = 6$ . Compared with the exhaustive search, the greedy search and BFS examine fewer class combinations and thus greatly reduce the computational time because each class combination, if examined, needs a separate classifier training.

We note that the search space of the greedy search and BFS can be further pruned if the classification algorithm satisfies a non-stringent property, and we will discuss this pruning procedure in Appendix C. As a preview, the bottom two rows of Table 3 show that pruning reduces the search spaces of the greedy search and BFS while maintaining the performance.

When  $K_0$  is large, it is unrealistic to use the exhaustive search. Here we use  $K_0 = 20$  ordinal classes as an example. Out of the  $2^{19} - 1 \approx 5.24 \times 10^5$  allowed class combinations (Table 1), we randomly select 50 class combinations as the true class combination  $\pi_{K^*}^*$ , whose  $K^*$  ranges from 7 to 16. From each  $\pi_{K^*}^*$ , we generate a dataset with  $n = 10,000$  data points (the other parameters are the same as in the aforementioned simulations). The results show that the greedy search works as well as the BFS (Supplementary Material Table S3): both successfully find the  $\pi_{K^*}^*$  of each dataset. On average, the greedy search only needs to evaluate ITCA on 150.08 class combinations (87.70 combinations with the pruned search space) out of the  $\sim 5.24 \times 10^5$  allowed class combinations. In contrast, the BFS has a much larger search space ( $\sim 10^4$  class combinations). Notably, ITCA has a higher probability of success when  $K^*$  is larger. We discuss this phenomenon in Appendix B.1.

### 3.2 ITCA outperforms alternative class combination criteria on the Iris data

We also compare ITCA with the five alternative class combination criteria on the famous Iris dataset<sup>1</sup>, which contains  $K^* = 3$  classes (corresponding to three types of irises: *setosa*, *versicolor*, and *virginica*) with 50 data points in each class. The *setosa* class is linearly separable from the *versicolor* and *virginica* classes, while *versicolor* and *virginica* are not linearly separable from each other. To prepare the dataset for class combination, we randomly split the *setosa* class into two equal-sized classes, making the number of observed classes  $K_0 = 4$ . Since the four classes are nominal, there are 14 allowed class combinations (Table 1).

For each allowed class combination, we compute the six class combination criteria with LDA as the classification algorithm (Figure 3). Among the six criteria, AAC, CKL, PE, and ITCA successfully find the true class combination  $\pi_{K^*}^*$ . However, only ITCA leads to a clear gap between  $\pi_{K^*}^*$  and the other 13 allowed class combinations. Note that CKL has large error bars because its computation involves the inverses and determinants of sample covariance matrices, whose accurate estimation requires a large sample size. Particularly, ACC has an undesirable result: its maximal

<sup>1</sup><http://archive.ics.uci.edu/ml/datasets/Iris/>

value 1 is obtained at the class combination  $\pi_2$  where the *versicolor* and *virginica* classes are combined. Again, these results confirm the unsuitability of ACC for guiding class combination, and they demonstrate the advantage ITCA has over the five alternative criteria.

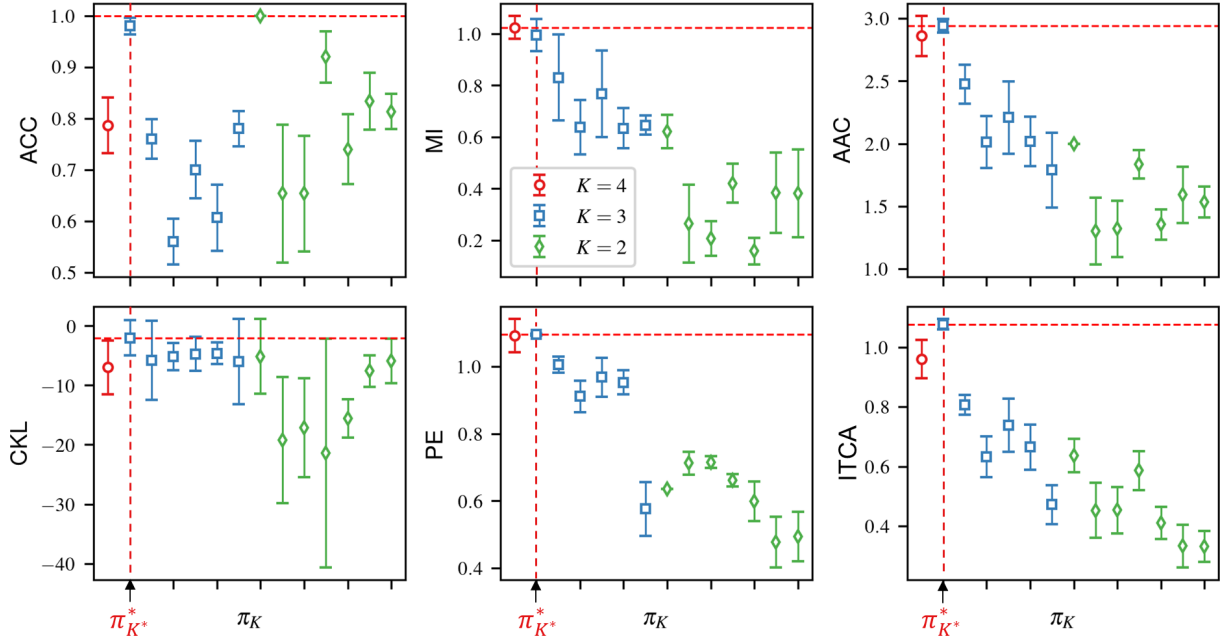


Figure 3: Comparison of ITCA and five alternative criteria using LDA as the classification algorithm on the Iris data.  $K_0 = 4$  and  $K^* = 3$  (with the true class combination  $\pi_{K^*}^*$  marked by the arrow and the red vertical dashed line in every panel). For every allowed class combination  $\pi_K$ , each criterion has its value (calculated by 5-fold CV) marked by a red circle for  $K = 4$ , a blue square for  $K = 3$ , and a green diamond for  $K = 2$ ; each error bar has half its length corresponding to the standard error of the criterion value (i.e., the standard deviation of the 5 criterion values in the 5-fold CV, divided by  $\sqrt{5}$ ). The horizontal line marks each criterion’s best value. Among the six criteria, only AAC, CKL, PE, and ITCA are maximized at  $\pi_{K^*}^*$ , and only ITCA has a clear gap between  $\pi_{K^*}^*$  and all other class combinations.

### 3.3 ITCA outperforms clustering-based class combination

While ITCA provides a powerful data-driven approach for combining ambiguous classes, one may intuitively consider using a clustering algorithm to achieve the same goal. We consider three clustering-based class combination approaches, which are summarized below, and we compare them with ITCA on simulated data under four settings.

**$K$ -means-based class combination.** For the  $k_0$ -th class ( $k_0 = 1, \dots, K_0$ ), we first compute the

$k_0$ -th class center as  $(\sum_{i=1}^n \mathbb{1}(Y_i = k_0)\mathbf{X}_i) / (\sum_{i=1}^n \mathbb{1}(Y_i = k_0))$ . We then use the  $K$ -means clustering to cluster the  $K_0$  class centers into  $K^*$  clusters so that the  $K_0$  observed classes are correspondingly combined into  $K^*$  classes.

**Spectral-clustering-based class combination.** We first compute the  $K^*$ -dimensional spectral embeddings of  $\mathbf{X}_1, \dots, \mathbf{X}_n$  [Ng et al., 2001]. Then we apply the above  $K$ -means-based class combination approach to the  $n$  spectral embeddings to combine the  $K_0$  observed classes into  $K^*$  combined classes.

**Hierarchical-clustering-based class combination.** We first compute the  $K_0$  class centers as in the  $K$ -means-based class combination approach. Then we use the hierarchical clustering with the single, complete, or average linkage to cluster the  $K_0$  class centers into  $K^*$  clusters so that the  $K_0$  observed classes are correspondingly combined into  $K^*$  classes.

Note that all these clustering-based class combination approaches require that  $K^*$  (the true number of classes) is known or estimated by an external approach (e.g., an approach for determining the number of clusters [Tibshirani et al., 2001, Sugar and James, 2003, Pham et al., 2005]), which is by itself a difficult problem in real-world applications. In contrast, ITCA does not require  $K^*$  to be known beforehand; instead, its optimal class combination determines  $K^*$  in a data-driven way.

To benchmark ITCA against the clustering-based class combination approaches, we generate four datasets with two-dimensional features ( $\mathbf{X}_1, \dots, \mathbf{X}_n \in \mathbb{R}^2$ ), which are shown in the four rows of Figure 4. Then we apply the above five clustering-based class combination approaches (three of which are hierarchical clustering with three linkages) and ITCA to the synthetic data; for ITCA, we use the Gaussian kernel support vector machine (SVM) as the classification algorithm.

Figure 4 shows the results of ITCA and the clustering-based class combination approaches with  $K^* = 3$  known: only ITCA successfully finds the true class combination on every dataset. We conclude that ITCA is advantageous over the clustering-based approaches even with a known  $K^*$ . The major reason is that the clustering-based approaches only use the  $K_0$  class centers (whose definition depends on a distance metric) and do not fully use the information in individual data points, which play a central role in the definition of ITCA.

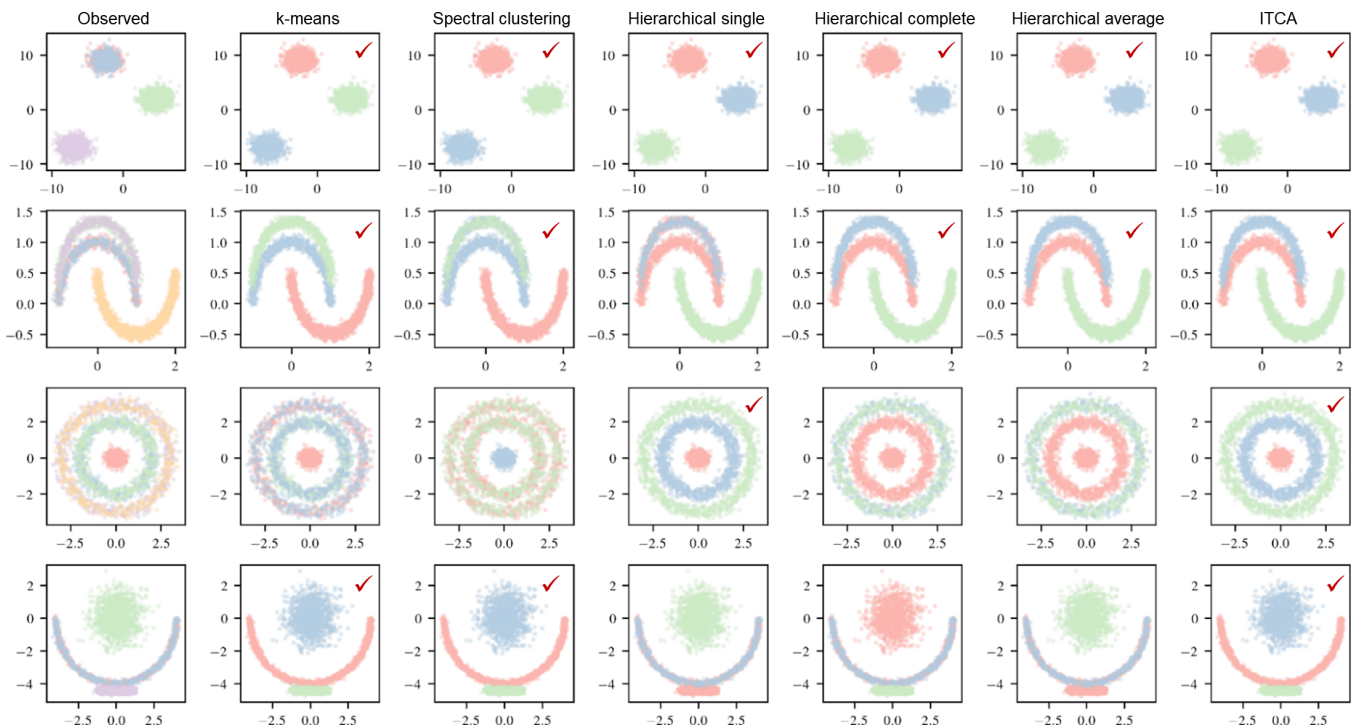


Figure 4: Comparison of clustering-based class combination approaches and ITCA (using Gaussian kernel SVM as the classification algorithm). Each row corresponds to one simulated dataset. From top to bottom, the number of observed classes is  $K_0 = 4, 5, 5,$  and  $4$ , and the number of true classes is  $K^* = 3, 3, 3,$  and  $3$ . In the leftmost column, colors mark the observed classes; in the other columns, the three colors indicate the three combined classes found by each combination approach. Check marks indicate the cases where the true class combinations are found. Only ITCA finds the true class combination on every dataset.

## 4. APPLICATIONS

### 4.1 Prognosis of rehabilitation outcomes of traumatic brain injury patients

According to the Centers for Disease Control and Prevention, traumatic brain injury (TBI) affects an estimated 1.5 million Americans every year<sup>2</sup>. The inpatient TBI rehabilitation care alone costs each patient tens of thousands of dollars per month. However, TBI rehabilitation is proven to be effective for only some but not all patients [Turner-Stokes, 2008]. Therefore, there is a great demand to have an automatic prognosis algorithm that can accurately predict rehabilitation outcomes for individual patients and assist patients' decisions in seeking rehabilitation care. We have access to the

<sup>2</sup>[https://www.cdc.gov/traumaticbraininjury/get\\_the\\_facts.html](https://www.cdc.gov/traumaticbraininjury/get_the_facts.html)

Casa Colina dataset of  $n = 3078$  TBI patients who received inpatient rehabilitation care. Patients’ disability severity was evaluated and recorded by physical therapists in the form of the Functional Independence Measure (FIM) of 17 activities at admission and discharge (Supplementary Material Table S7). The FIM has seven scales ranging from 1 (patient requires total assistance to perform an activity) to 7 (patient can perform the activity with complete independence) [Linacre et al., 1994]. In addition, patients’ characteristics are recorded, including demographics (gender and age) and admission status. This dataset allows the development of an algorithm to predict the efficacy of rehabilitation care for individual patients.

We formulate the task of predicting patients’ rehabilitation outcomes as a multi-class classification problem, where the discharge FIM of each activity is a seven-level ( $K_0 = 7$ ) ordinal outcome and the features are patients’ characteristics and admission FIM. We are motivated to combine outcome levels because the RF algorithm, though being the best-performing algorithm, has low accuracy for predicting the  $K_0$  levels of many activities. Hence, we consult the physical therapists who graded the activities and obtain their suggested combination  $\{1, (2, 3, 4), 5, 6, 7\}$ , which has levels 2–4 combined. However, this expert-suggested class combination is subjective and not activity-specific. Intuitively, we reason that different activities may have different resolutions and thus different outcome level combinations. Hence, we apply ITCA as a data-driven approach to guide the combination of outcome levels for each activity.

Powered with ITCA, we can construct a multilayer prediction framework (Supplementary Material Figure 5), whose  $K_0$  layers (from top to bottom) correspond to the numbers of combined classes  $K = 1, \dots, K_0$ , with the bottommost layer indicating no class combination. There are two ways to construct a framework: greedy-search-based and exhaustive-search-based. In a greedy-search-based framework, layers are constructed by the greedy search (Section 2.3) in a sequential way from bottom up: classes in each layer except the bottommost layer are combined by ITCA from the classes in the layer right below, so the layers would follow a nested structure. In contrast, in an exhaustive-search-based framework, layers are constructed separately from the bottommost layer: each layer has its optimal class combination defined by ITCA and found by the exhaustive search (Section 2.3) given its  $K$ ; thus, there is no nested constraint. Note that  $K_0$  is often not too large in medical diagnosis and prognosis, making the exhaustive search computationally feasible.

Greedy-search-based and exhaustive-search-based frameworks have complementary advantages. On the one hand, the former outputs a data-driven hierarchy of class combinations and is thus more interpretable if the prediction would be conducted for all layers. On the other hand, the latter outputs the optimal class combination for each layer and allows choosing the optimal layer (that maximizes the ITCA); hence, it is more desirable if the prediction would only be conducted for the optimal layer. For example, if healthcare providers would like to predict outcomes at a multilayer resolution, the greedy-search-based framework is more suitable. In contrast, if the priority is to combine outcome levels into the optimal resolution for prediction, the exhaustive-search-based framework would be a better fit.

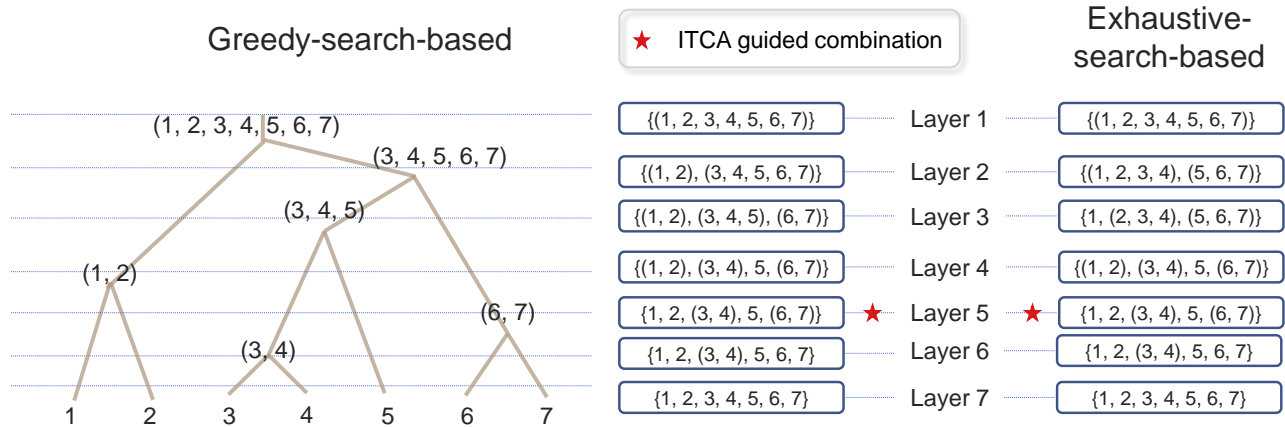


Figure 5: Greedy-search-based and exhaustive-search-based multilayer frameworks for predicting the Toileting activity in the Casa Colina dataset. In either framework, layer  $K$  has a class combination  $\pi_K$  chosen by ITCA. In the greedy-search-based framework, the layers have a tree structure. Layer 5 has the same class combination in both frameworks and is found optimal by ITCA.

We use RF as the classification algorithm for its better accuracy than other popular algorithms’ on the Casa Colina dataset. Leveraging the RF algorithm, we apply the greedy-search-based and exhaustive-search-based multilayer frameworks to predict the rehabilitation outcome of each of the 17 activities. For example, Figure 5 shows the results for predicting the Toileting activity: ITCA indicates the same optimal class combination in both frameworks:  $\{1, 2, (3, 4), 5, (6, 7)\}$  in layer  $K = 5$ , where levels 3 and 4 are combined, and so are levels 6 and 7.

To evaluate the ITCA results for the 17 activities, we calculate the prediction accuracy by RF for our ITCA-guided combinations, the expert-suggested combination, and the hierarchical-clustering-based combinations (defined in Section 3.3; the results are based on the average linkage). Note that the prediction accuracy for different class combinations may differ even if the best guess

algorithm (i.e., the naïve algorithm that assigns data points to the largest class—a baseline control) is used. Hence, for a fair comparison, we evaluate each class combination by the 5-fold CV prediction accuracy improvement of the RF algorithm from the best guess algorithm.

Figure 6 shows the comparison results for eight activities, for which ITCA selects class combinations with  $K$ 's closest to 5 (i.e., the number of combined levels suggested by experts). We find that, compared with the expert-suggested combination and the hierarchical-clustering-based combinations, the ITCA-guided combinations consistently lead to more balanced classes (which are more difficult to predict, as indicated by the lower prediction accuracy of the best guess algorithm) and more significant improvement in prediction accuracy. Figure S5 and Tables S8–S9 (in Supplementary Material) summarize for all 17 activities the ITCA-guided class combinations and their corresponding prediction accuracy (i.e., the ACC criterion defined in Appendix A), as well as the ITCA values.

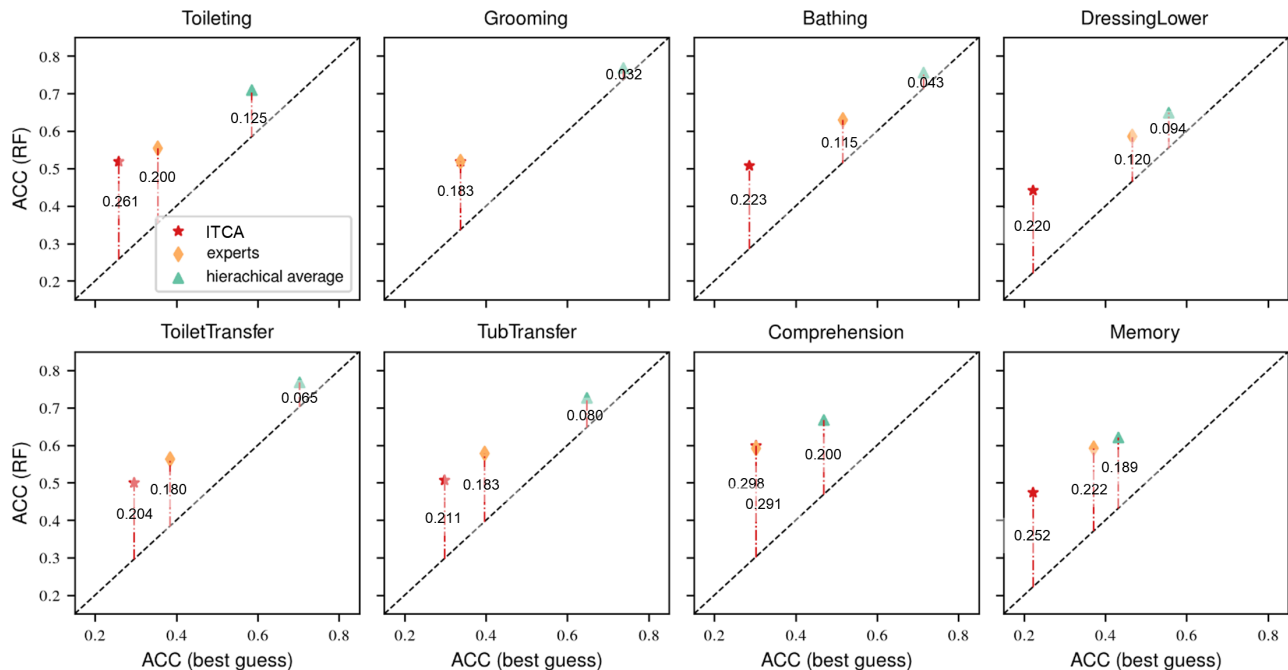


Figure 6: Prediction accuracy for the optimal level combination indicated by ITCA, the expert-suggested combination, and the hierarchical-clustering-based level combinations for the rehabilitation outcomes of eight activities in the Casa Colina dataset. The horizontal axis shows the 5-fold CV prediction accuracy of the best guess algorithm, and the vertical axis shows the accuracy of the RF algorithm. The accuracy improvement of the RF from the best guess is marked on vertical dashed lines. Note that in the “Comprehension” panel, ITCA finds the expert-suggested combination; the two accuracy improvement values (0.298 and 0.291) should be equal in theory, but they are different due to the randomness of data splitting in the 5-fold CV.

As a side note, we argue that it is inappropriate to use the prediction accuracy improvement (from the best guess) as a class combination criterion. The reason is that the prediction accuracy of the best guess, though serving as a baseline accuracy, does not necessarily reflect the class resolution. For example, an outcome encoded as two classes with equal probabilities has a lower resolution than another outcome encoded as three classes with probabilities 0.5, 0.25, and 0.25; however, the best guess algorithm has the same prediction accuracy 0.5 for the two outcomes.

#### 4.2 Prediction of glioblastoma cancer patients’ survival time

Glioblastoma cancer, also known as glioblastoma multiforme (GBM), is the most aggressive type of cancer that begins within the brain. Hence, it is of critical importance to predict GBM patients’ survival time so that appropriate treatments can be provided. In this prediction task, patients’ survival time would be predicted from their clinical measurements.

We download the TCGA GBM dataset from the cBio cancer genomics portal [Cerami et al., 2012]<sup>3</sup>. The dataset contains  $n = 541$  patients’ demographics, gene expression subtypes, therapy, and other clinical information. We remove nine features irrelevant to survival prediction and keep  $d = 36$  features (see Supplementary Material Section 3.2 for the data processing details).

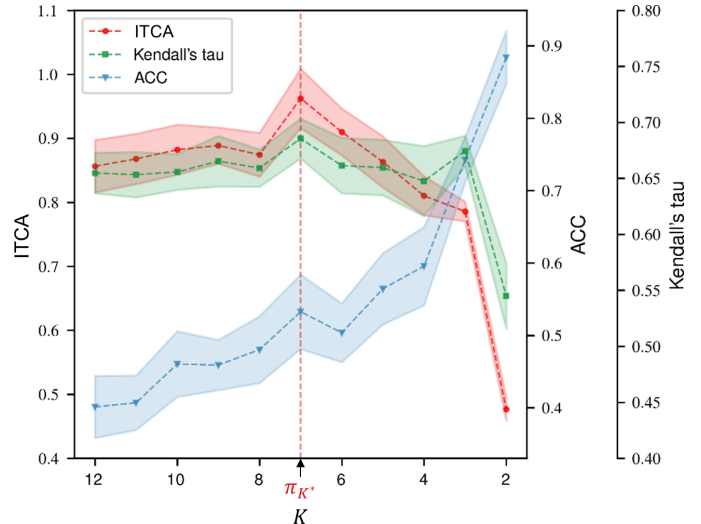
We formulate this survival prediction task as a classification problem instead of a regression problem to demonstrate the use of ITCA, and we compare the performance of the classifier guided by ITCA with that of the Cox regression model. Concretely, we first discretize patients’ survival time into  $K_0 = 12$  intervals:  $[0, 3)$ ,  $[3, 6)$ ,  $[6, 9)$ ,  $[9, 12)$ ,  $[12, 15)$ ,  $[15, 18)$ ,  $[18, 21)$ ,  $[21, 24)$ ,  $[24, 27)$ ,  $[27, 30)$ ,  $[30, 33)$ ,  $[33, +\infty)$ , where  $[0, 3)$  and  $[33, +\infty)$  indicate that the survival time is less than 3 months and at least 33 months, respectively.

We then use ITCA to optimize the survival time intervals for prediction. For the classification algorithm, we use a three-layer neural network (NN) with the ReLU activation function and a modified cross entropy as the loss function for handling censored survival time (see Supplementary Material Section 3.2 and Figure S6). Starting from the observed  $K_0 = 12$  classes, we use ITCA with greedy search to select a class combination for each  $K = 11, \dots, 2$ . For each  $K$  and its selected class combination, we train a NN classifier and show the ITCA and ACC in Figure 7. As expected, as  $K$  decreases, ACC increases, confirming our motivation that ACC cannot be used to guide class

---

<sup>3</sup>The dataset is available at <https://www.cbioportal.org/>

Figure 7: Results of GBM survival prediction. Three criteria, ACC, ITCA and Kendall’s tau coefficient, are shown for  $K$  from  $K_0 = 12$  to 2 (for each  $K$ , a class combination is found by ITCA, and an NN classifier is trained). Each criterion is calculated by the 5-fold CV, and its mean and standard error (i.e., standard deviation of the 5 criterion values in the 5-fold CV, divided by  $\sqrt{5}$ ) are shown. The best class combination  $\pi_K^*$  found by ITCA is indicated by the red vertical dashed line ( $K = 7$ ), where the Kendall’s tau is also maximized.



combination. In contrast, as  $K$  decreases, ITCA first increases until  $K = 7$  and then decreases, confirming that ITCA balances the trade-off between classification accuracy and class resolution.

Following the tradition in survival analysis, we use the Kendall’s tau coefficient (calculated between the predicted outcome and the observed survival time, not the discretized survival time interval, in 5-fold CV) to evaluate the prediction accuracy. Note that the Kendall’s tau is a reasonable accuracy measure for survival prediction because it is an ordinal association measure that allows the predicted outcome to be either discrete (as in our classification formulation) or continuous (as in a regression formulation). Figure 7 shows that the optimal class combination found by ITCA leads to the best Kendall’s tau, verifying that ITCA optimizes the survival time intervals for classifier construction.

We also compare the NN algorithm with two commonly used survival prediction algorithms: the Cox regression [Cox, 1972], a regression algorithm that predicts patients’ risk scores, and the logistic regression (LR), a multi-class classification algorithm that uses the same modified cross entropy loss to predict survival time intervals as the NN algorithm does. We use the Kendall’s tau to evaluate five prediction models: NN and LR classifiers for predicting the original  $K_0$  survival time intervals, NN and LR classifiers for predicting their respective combined intervals guided by ITCA, and a Cox regression model for predicting risk scores (the Kendall’s tau is calculated between negative predicted risk scores and observed survival time). Table 4 shows that the NN classifier trained for ITCA-guided combined intervals has the best prediction accuracy in terms of the Kendall’s tau; moreover, it has the highest ITCA value among the four classifiers. This result again verifies that

ITCA is a meaningful accuracy measure.

Note that the Kendall’s tau is not an appropriate measure to replace ITCA because it requires the response to be a numerical or ordinal variable. Hence, the Kendall’s tau cannot guide the combination of nominal class labels.

Model	ITCA	Kendall’s tau	Average p-value
NN ( $K_0$ survival time intervals)	$0.8565 \pm 0.0410$	$0.6547 \pm 0.0181$	$2.11e-14$
LR ( $K_0$ survival time intervals)	$0.6354 \pm 0.0620$	$0.6024 \pm 0.0244$	$1.64e-11$
NN (ITCA-guided combined intervals)	<b><math>0.9623 \pm 0.0464</math></b>	<b><math>0.6855 \pm 0.0178</math></b>	<b><math>1.27e-15</math></b>
LR (ITCA-guided combined intervals)	$0.8196 \pm 0.0222$	$0.6236 \pm 0.0240$	$5.34e-10$
Cox regression (risk scores)	-	$0.6303 \pm 0.0542$	$2.04e-13$

Each criterion is computed by 5-fold cross validation; its mean and standard error (i.e., standard deviation of the 5 criterion values in the 5-fold CV, divided by  $\sqrt{5}$ ) are listed; the average of the 5 p-values corresponding to the Kendall’s tau coefficients in the 5-fold CV is also listed. The NN algorithm trained with ITCA-guided  $K = 7$  combined intervals achieves the best ITCA value, the best Kendall’s tau, and the most significant average p-value.

Table 4: Performance of survival prediction algorithms on the GBM dataset.

### 4.3 Prediction of user demographics using mobile phone behavioral data

One of the essential tasks in personalized advertising is to predict users’ demographics (gender and age) using behavioral data. A good predictive model is necessary for data-driven marketing decisions. To simplify the prediction of user ages, data scientists often first discretize ages into groups and then construct a multi-class classifier to predict age groups instead of exact ages [Kaggle, 2016]. However, the discretization step is heuristic and unjustified. Here we use ITCA to determine age groups in a principled, data-driven way.

We apply ITCA to the TalkingData mobile user demographics<sup>4</sup>, a public dataset of mobile phone users’ behavioral data in China. Specifically, the dataset contains users’ app usage, mobile device properties, genders, and ages. Our goal is to predict a user’s gender and age from mobile device and app usage.

In detail, we discretize male users’ ages into 17 ordinal groups encoded as M20–, M20–21, . . . , M48–49, and M50+ (where M20–, M20–21, and M50+ indicate male users whose ages are  $< 20$ ,  $\geq 20$  &  $< 21$ , and  $\geq 50$ , respectively). Similarly, we divide female users into 17 ordinal age groups: F20–, F20–21, . . . , F48–49, and F50+. Together, we have  $K_0 = 34$  classes to start with. We

<sup>4</sup>The dataset is available at <https://www.kaggle.com/c/talkingdata-mobile-user-demographics>

use one-hot encoding to convert users’ mobile devices and app usage data into 818 features; after deleting the users with zero values in all features, we retain  $n = 23,556$  users. Then we use XGBoost [Chen and Guestrin, 2016] as the classification algorithm for its successes on similar prediction tasks in Kaggle competitions (see Supplementary Material Section 3.3 for details of data processing and algorithm training procedures).

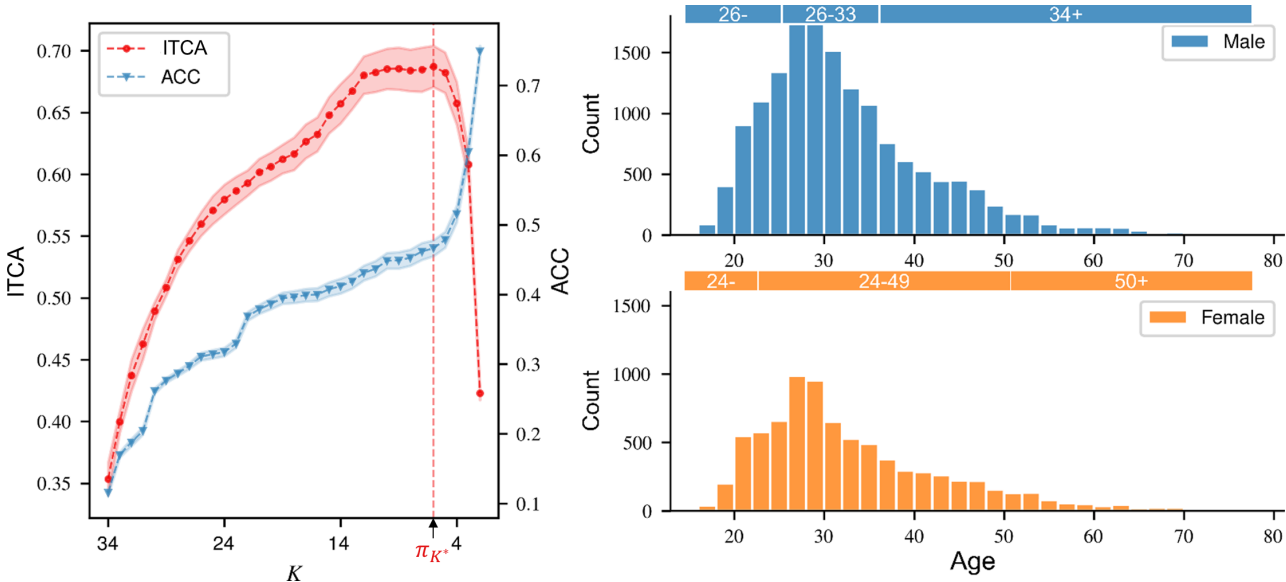


Figure 8: Results on TalkingData mobile user demographics dataset using XGBoost. Left panel: ITCA and ACC versus the number of combined classes  $K$ , which ranges from  $K_0 = 34$  to 2. The criteria are estimated by 5-fold CV, and their standard errors are calculated by the standard deviations in the 5-fold CV divided by  $\sqrt{5}$ . The best class combination  $\pi_K^*$  (with  $K = 6$ ) is indicated by the vertical dashed line. Right upper panel: the histogram of the ages of male users;  $\pi_K^*$  suggests three age groups: M26–, M26–33, and M34+. Right lower panel: the histogram of the ages of female users;  $\pi_K^*$  suggests three age groups: F24–, F24–49, and F50+.

Since 30 out of the 34 classes are exact ages, it is intuitively too challenging to accurately predict the 34 classes simply from users’ phone devices and app usage. This is indeed the case, reflected by the low accuracy ( $< 0.35$ ) of XGBoost (Figure 8). Hence, we use ITCA with the greedy search strategy to combine the 34 ordinal classes into coarser, more meaningful age groups from the prediction perspective. Note that we add the constraint for not combining a male class with a female class .

Interestingly, ITCA suggests three different age groups for the male and female users (male: M26–, M26–33, and M34+; female: F24–, F24–49, and F50+) (Figure 8, right panel). This result reveals a gender difference in the mobile phone behavioral data: female users have a wider middle

age group (24–49 vs. male users’ 26–33). A possible explanation of this gender difference is the well-known gender disparity in career development in China: more males undergo promotion into senior positions in middle 30s compared with females, who tend to slow down career development at young ages for reasons such as marriage and child birth [Wei, 2011]. This explanation is reasonable in that users’ career development and mobile phone use behaviors are likely correlated. Hence, if we interpret the male and female age groups from the perspective of career development, we find a possible explanation of why the age of 34 is a change point for males but not for females, whose middle-to-senior change point is the age of 49, close to the retirement age of most females in China. In summary, ITCA provides a data-driven approach to defining user age groups based on mobile phone behaviors, making it a potentially useful tool for social science research.

#### 4.4 Detection of biologically similar cell types inferred from single-cell RNA-seq data

Recent advances in single-cell sequencing technologies provide unprecedented opportunities for scientists to decipher the mysteries of cell biology [Wang and Navin, 2015, Stuart and Satija, 2019]. An important topic is to discern cell types from single-cell RNA-seq data, which profile transcriptome-wide gene expression levels in individual cells.

Concretely, a single-cell RNA-seq dataset is processed into a data matrix of  $n$  cells and  $d_0$  genes, with the  $(i, j)$ -th entry as the expression level (i.e., log-transformed count of reads or unique molecular identifiers) of the  $j$ -th gene in the  $i$ -th cell. Starting from the matrix, a standard analysis pipeline involves the following steps [Stuart and Satija, 2019]. First, principal component analysis is performed on the data matrix to reduce the column dimension from  $d_0$  to  $d \ll d_0$ , resulting in a principal component matrix of  $n$  cells and  $d$  principal components. Second, a clustering algorithm (e.g., the graph-based Louvain algorithm [Blondel et al., 2008]) is applied to the principal component matrix to cluster the  $n$  cells. Finally, experts use knowledge to manually annotate the cell clusters with cell type labels.

However, the annotated cell types might be ambiguous due to the subjectivity of setting parameter values in the above pipeline (e.g., the number of principal components  $d$  and the clustering algorithm’s parameters) and the uncertainty of the clustering step. As a result, if cells are overclustered, some annotated cell types might be biologically similar.

This problem, the detection of biologically similar cell types, can be formulated as an application

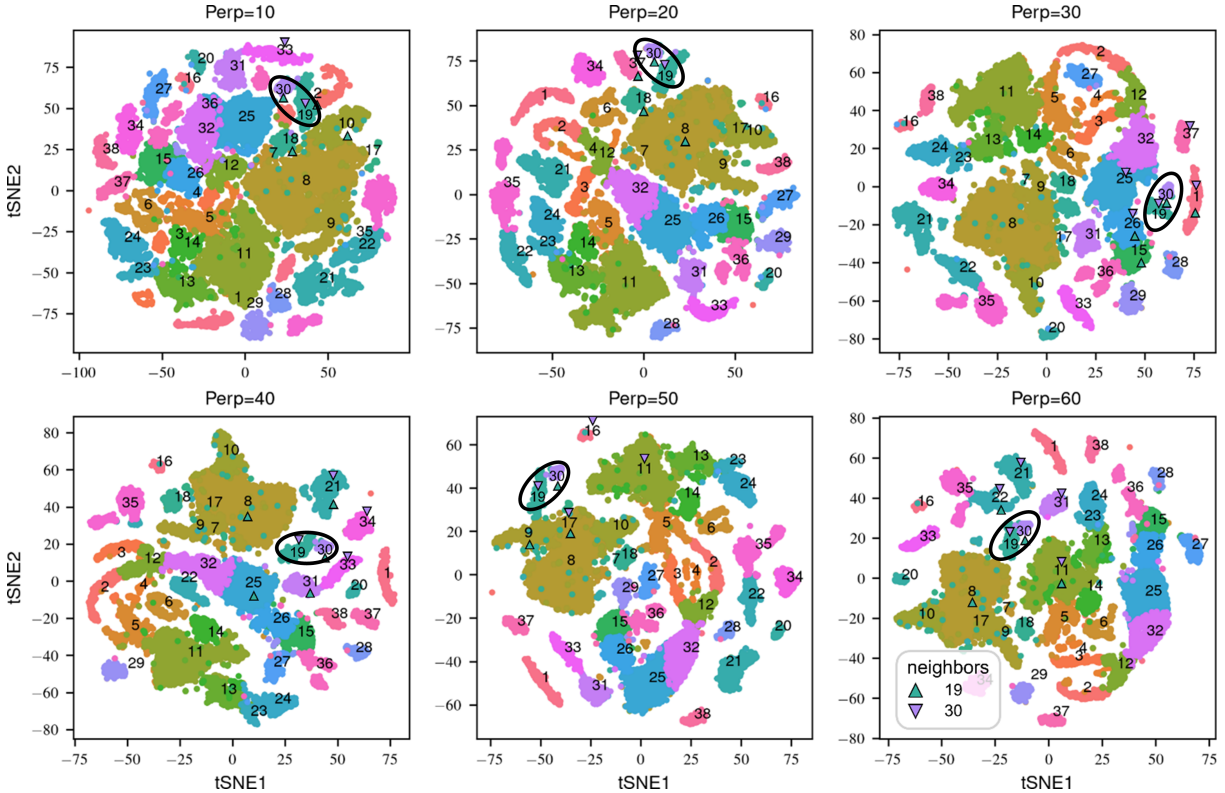


Figure 9: Visualizations of the cells in the hydra single-cell RNA-seq dataset using t-SNE under six perplexity values from 10 to 60. The cell types 19 and 30 are marked by triangles and black circles.

of ITCA. Here, we use a single-cell RNA-seq dataset of hydra [Siebert et al., 2019] as an example<sup>5</sup>. The processed dataset contains  $n = 25,052$  cells annotated into  $K_0 = 38$  cells types (nominal class labels). Following the procedure in [Siebert et al., 2019], we use the first  $d = 40$  principal components as features. We choose the LDA as the classification algorithm for two reasons. First, our goal is to discover ambiguous cell types instead of achieving high prediction accuracy, so it is reasonable to choose a weak classification algorithm. Second, the features are the principal components obtained from the log-transformed counts, and they are found to approximately follow a multivariate Gaussian distribution. Given the large  $K_0$ , we apply ITCA using the greedy search algorithm. The result suggests the combination of cell type 19 (“enEp tentacle”: endodermal epithelial cells in tentacles) and cell type 30 (“enEp tentnem(pd)”: endodermal epithelial cells in tentacle nematocytes—suspected phagocytosis doublets), which indeed have similar cell type labels.

To evaluate this result, we examine cell types 19 and 30 using two-dimensional t-SNE visualization across a wide range of perplexity values (perplexity is the key hyperparameter of t-SNE). The

<sup>5</sup>The dataset is available at Broad Institute’s Single Cell Portal [https://singlecell.broadinstitute.org/single\\_cell/study/SCP260/](https://singlecell.broadinstitute.org/single_cell/study/SCP260/).

t-SNE plots (Figure 9) show that the two cell types are always direct neighbors of each other. We confirm this result by hierarchical clustering: the two cell types share similar gene expression patterns and are barely distinguishable in the first 40 principal components (Figure 10, left panel). As a control, we apply hierarchical clustering to distinguishing cell type 16 (“i\_neuron\_en3”: neuronal cells of the interstitial lineage), whose number of cells is closest to that of cell type 19, from cell type 30. The result shows that, unlike cell types 19 and 30, cell types 16 and 30 are well separated (Figure 10, right panel). Together, these evidence verifies the similarity of cell types 19 and 30, suggesting that ITCA can serve as a useful tool for identifying similar cell types and refining cell type annotations.

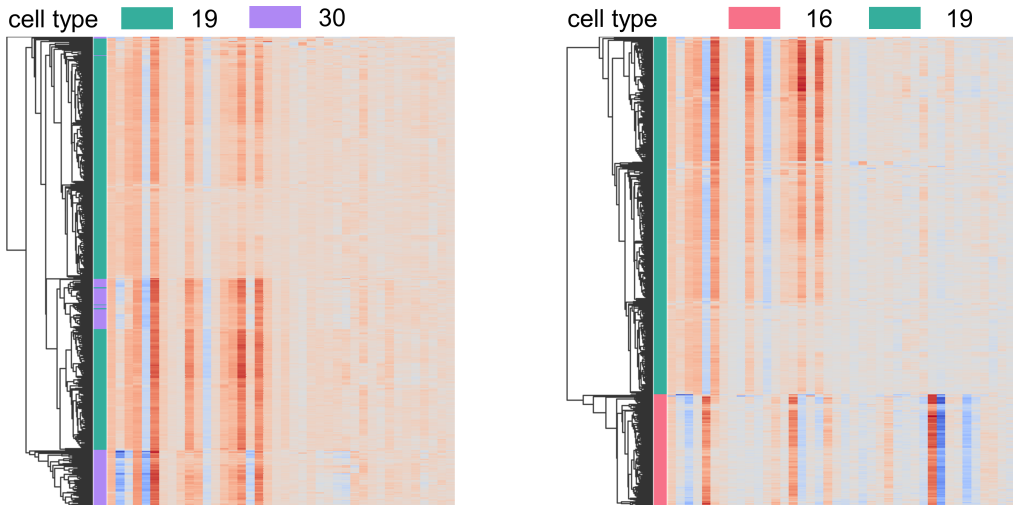


Figure 10: Heatmaps of the first 40 principal components of the hydra single-cell RNA-seq data. Row colors indicate the cell types: green for cell type 19 (458 cells; left and right panels), purple for cell type 30 (134 cells; left panel) and pink for cell type 16 (143 cells; right panel). Hierarchical clustering can hardly distinguish cell types 19 and 30 (left panel) but can well separate cell types 16 and 19 (right panel).

## 5. CONCLUSION

We introduce ITCA, an information-theoretic criterion for combining ambiguous outcome labels in classification tasks; typical examples are in medical and social sciences where class labels are often defined subjectively. ITCA automatically balances the trade-off between the increase in classification accuracy and the loss of class resolution, providing a data-driven criterion to guide class combination. The simulation studies validate the effectiveness of ITCA and the proposed search strategies. The four real-world applications demonstrate the wide application potential. The

theoretical analysis in Appendix B–C characterizes several properties of ITCA and introduces a way to enhance the LDA algorithm for class combination.

One merit of ITCA is its universality: it can be applied with any classification algorithm without modification. While ITCA has an implicit trade-off between classification accuracy and class resolution, it is worth extending ITCA to incorporate user-specified weights for classification accuracy and class resolution. Another open question is how to incorporate users’ predefined classes’ importance to the ITCA definition; that is, users may prefer some important classes to stay as uncombined.

In addition to classification problems, ITCA may potentially serve as a model-free criterion for determining the number of clusters in clustering problems. We will investigate this direction in future work.

## References

- Patrick L Brockett, Richard A Derrig, Linda L Golden, Arnold Levine, and Mark Alpert. Fraud classification using principal component analysis of ridits. *Journal of Risk and Insurance*, 69(3): 341–371, 2002.
- Peter WF Wilson, Ralph B D’Agostino, Daniel Levy, Albert M Belanger, Halit Silbershatz, and William B Kannel. Prediction of coronary heart disease using risk factor categories. *Circulation*, 97(18):1837–1847, 1998.
- Stephen F Weng, Jenna Reys, Joe Kai, Jonathan M Garibaldi, and Nadeem Qureshi. Can machine-learning improve cardiovascular risk prediction using routine clinical data? *Plos One*, 12(4): e0174944, 2017.
- Li Chen, Peng Jin, and Zhaohui S Qin. DIVAN: accurate identification of non-coding disease-specific risk variants using multi-omics profiles. *Genome Biology*, 17(1):252, 2016.
- Jonathan Krause, Varun Gulshan, Ehsan Rahimy, Peter Karth, Kasumi Widner, Greg S Corrado, Lily Peng, and Dale R Webster. Grader variability and the importance of reference standards for evaluating machine learning models for diabetic retinopathy. *Ophthalmology*, 125(8):1264–1272, 2018.
- Uwe Feldmann and Ingo Steudel. Methods of ordinal classification applied to medical scoring systems. *Statistics in Medicine*, 19(4):575–586, 2000.
- Harry Hemingway, Peter Croft, Pablo Perel, Jill A Hayden, Keith Abrams, Adam Timmis, Andrew Briggs, Ruzan Udumyan, Karel GM Moons, Ewout W Steyerberg, et al. Prognosis research strategy (progress) 1: a framework for researching clinical outcomes. *BMJ*, 346, 2013.
- Peter K Lindenauer, Tara Lagu, Meng-Shiou Shieh, Penelope S Pekow, and Michael B Rothberg. Association of diagnostic coding with trends in hospitalizations and mortality of patients with pneumonia, 2003-2009. *JAMA*, 307(13):1405–1413, 2012.
- Minal S Kale and Deborah Korenstein. Overdiagnosis in primary care: framing the problem and finding solutions. *BMJ*, 362:k2820, 2018.

- J. I. Epstein, L. Egevad, M. B. Amin, B. Delahunt, J. R. Srigley, and P. A. Humphrey. Consensus conference on gleason grading of prostatic carcinoma: definition of grading patterns and proposal for a new grading system. *The American Journal of Surgical Pathology*, 40(2):244–252, 2015.
- Paul Muntner, Robert M Carey, Samuel Gidding, Daniel W Jones, Sandra J Taler, Jackson T Wright, and Paul K Whelton. Potential US population impact of the 2017 ACC/AHA high blood pressure guideline. *Journal of the American College of Cardiology*, 71(2):109–118, 2018.
- Andrew Butler, Paul Hoffman, Peter Smibert, Efthymia Papalexi, and Rahul Satija. Integrating single-cell transcriptomic data across different conditions, technologies, and species. *Nature Biotechnology*, 36(5):411–420, 2018.
- Benoît Frénay and Michel Verleysen. Classification in the presence of label noise: a survey. *IEEE Transactions on Neural Networks and Learning Systems*, 25(5):845–869, 2013.
- Yoav Freund. An adaptive version of the boost by majority algorithm. *Machine Learning*, 43(3):293–318, 2001.
- Eyal Beigman and Beata Beigman Klebanov. Learning with annotation noise. In *Proceedings of the Joint Conference of the Annual Meeting of the ACL and the International Joint Conference on Natural Language Processing of the AFNLP*, pages 280–287, 2009.
- Wensheng Zhang, Romdhane Rekaya, and Keith Bertrand. A method for predicting disease subtypes in presence of misclassification among training samples using gene expression: application to human breast cancer. *Bioinformatics*, 22(3):317–325, 2006.
- Jaree Thongkam, Guandong Xu, Yanchun Zhang, and Fuchun Huang. Support vector machine for outlier detection in breast cancer survivability prediction. In *Asia-pacific Web Conference*, pages 99–109. Springer, 2008.
- Tim B Swartz, Yoel Haitovsky, Albert Vexler, and Tae Y Yang. Bayesian identifiability and misclassification in multinomial data. *Canadian Journal of Statistics*, 32(3):285–302, 2004.

- Hyun-Chul Kim and Zoubin Ghahramani. Outlier robust gaussian process classification. In *Joint IAPR International Workshops on Statistical Techniques in Pattern Recognition and Structural and Syntactic Pattern Recognition*, pages 896–905. Springer, 2008.
- Vladimir Vovk, Alex Gammerman, and Glenn Shafer. *Algorithmic learning in a random world*. Springer Science & Business Media, 2005.
- Vineeth Balasubramanian, Shen-Shyang Ho, and Vladimir Vovk. *Conformal prediction for reliable machine learning: theory, adaptations and applications*. Newnes, 2014.
- Nikhil R Pal et al. Uncertainty, entropy and maximum entropy principle—an overview. In *Entropy Measures, Maximum Entropy Principle and Emerging Applications*, pages 1–53. Springer, 2003.
- Eric Temple Bell. The iterated exponential integers. *Annals of Mathematics*, pages 539–557, 1938.
- William Feller. *An introduction to probability theory and its applications, vol 2*. John Wiley & Sons, 2008.
- Leo Breiman. Random forests. *Machine Learning*, 45(1):5–32, 2001.
- Andrew Ng, Michael Jordan, and Yair Weiss. On spectral clustering: Analysis and an algorithm. *Advances in Neural Information Processing Systems*, 14:849–856, 2001.
- Robert Tibshirani, Guenther Walther, and Trevor Hastie. Estimating the number of clusters in a data set via the gap statistic. *Journal of the Royal Statistical Society: Series B (Statistical Methodology)*, 63(2):411–423, 2001.
- Catherine A Sugar and Gareth M James. Finding the number of clusters in a dataset: An information-theoretic approach. *Journal of the American Statistical Association*, 98(463):750–763, 2003.
- Duc Truong Pham, Stefan S Dimov, and Chi D Nguyen. Selection of k in k-means clustering. *Proceedings of the Institution of Mechanical Engineers, Part C: Journal of Mechanical Engineering Science*, 219(1):103–119, 2005.

- Lynne Turner-Stokes. Evidence for the effectiveness of multi-disciplinary rehabilitation following acquired brain injury: a synthesis of two systematic approaches. *Journal of Rehabilitation Medicine*, 40(9):691–701, 2008.
- John Michael Linacre, Allen W Heinemann, Benjamin D Wright, Carl V Granger, and Byron B Hamilton. The structure and stability of the functional independence measure. *Archives of Physical Medicine and Rehabilitation*, 75(2):127–132, 1994.
- Ethan Cerami, Jianjiong Gao, Ugur Dogrusoz, Benjamin E. Gross, Selcuk Onur Sumer, Bülent Arman Aksoy, Anders Jacobsen, Caitlin J. Byrne, Michael L. Heuer, Erik Larsson, Yevgeniy Antipin, Boris Reva, Arthur P. Goldberg, Chris Sander, and Nikolaus Schultz. The cBio cancer genomics portal: An open platform for exploring multidimensional cancer genomics data. *Cancer Discovery*, 2(5):401–404, 2012.
- David R Cox. Regression models and life-tables. *Journal of the Royal Statistical Society: Series B (methodological)*, 34(2):187–202, 1972.
- Kaggle. Talkingdata mobile user demographics, 2016. URL <https://www.kaggle.com/c/talkingdata-mobile-user-demographics>.
- Tianqi Chen and Carlos Guestrin. Xgboost: A scalable tree boosting system. In *Proceedings of the ACM SIGKDD International Conference on Knowledge Discovery and Data Mining*, pages 785–794, 2016.
- Guoying Wei. Gender comparison of employment and career development in China. *Asian Women*, 27(1):95–114, 2011.
- Yong Wang and Nicholas E Navin. Advances and applications of single-cell sequencing technologies. *Molecular Cell*, 58(4):598–609, 2015.
- Tim Stuart and Rahul Satija. Integrative single-cell analysis. *Nature Reviews Genetics*, 20(5):257–272, 2019.

Vincent D Blondel, Jean-Loup Guillaume, Renaud Lambiotte, and Etienne Lefebvre. Fast unfolding of communities in large networks. *Journal of Statistical Mechanics: Theory and Experiment*, 2008 (10):P10008, 2008.

Stefan Siebert, Jeffrey A Farrell, Jack F Cazes, Yashodara Abeykoon, Abby S Primack, Christine E Schnitzler, and Celina E Juliano. Stem cell differentiation trajectories in hydra resolved at single-cell resolution. *Science*, 365(6451):eaav9314, 2019.

Thomas M Cover. *Elements of information theory*. John Wiley & Sons, 1999.

Jean-Louis Durrieu, Jean-Philippe Thiran, and Finnian Kelly. Lower and upper bounds for approximation of the kullback-leibler divergence between gaussian mixture models. *IEEE International Conference on Acoustics, Speech and Signal Processing*, pages 4833–4836, 2012.

Peter Ahrendt. The multivariate gaussian probability distribution. *Technical University of Denmark, Tech. Rep*, 2005.

F. Pedregosa, G. Varoquaux, A. Gramfort, V. Michel, B. Thirion, O. Grisel, M. Blondel, P. Prettenhofer, R. Weiss, V. Dubourg, J. Vanderplas, A. Passos, D. Cournapeau, M. Brucher, M. Perrot, and E. Duchesnay. Scikit-learn: Machine learning in Python. *Journal of Machine Learning Research*, 12:2825–2830, 2011.

Adam Paszke, Sam Gross, Soumith Chintala, Gregory Chanan, Edward Yang, Zachary DeVito, Zeming Lin, Alban Desmaison, Luca Antiga, and Adam Lerer. Automatic differentiation in pytorch. 2017.

## Appendix A ALTERNATIVE CRITERIA THAT MAY GUIDE CLASS COMBINATION

In addition to ITCA, we consider five alternative criteria that may guide class combination. The first two are commonly used criteria: classification accuracy and mutual information. The last three are our newly proposed criteria to balance the trade-off between classification accuracy and class resolution from three other perspectives.

**Accuracy.** It is the most commonly used criterion to evaluate the performance of a classification algorithm. For a class combination  $\pi_K$ , given a classification algorithm  $\mathcal{C}$  and a size- $n$  dataset  $\mathcal{D}$ , the  $R$ -fold CV accuracy (ACC) is

$$\text{ACC}^{\text{CV}}(\pi_K; \mathcal{D}, \mathcal{C}) := \frac{1}{R} \sum_{r=1}^R \frac{1}{|\mathcal{D}_e^r|} \sum_{(\mathbf{X}_i, Y_i) \in \mathcal{D}_e^r} \mathbb{I}(\phi_{\pi_K}^{\mathcal{C}, \mathcal{D}_e^r}(\mathbf{X}_i) = \pi_K(Y_i)), \quad (6)$$

where the dataset  $\mathcal{D}$  is randomly split into  $R$  equal-sized folds, with the  $r$ -th fold  $\mathcal{D}_e^r$  serving as the evaluation data and the union of the remaining  $R - 1$  folds  $\mathcal{D}_t^r$  serving as the training data, and  $\phi_{\pi_K}^{\mathcal{C}, \mathcal{D}_e^r}$  is the classifier trained by the algorithm  $\mathcal{C}$  on  $\mathcal{D}_t^r$ . Typically,  $\text{ACC}^{\text{CV}}$  is used without class combination because it is maximized as 1 when all classes are combined into one. Hence, intuitively, it is not an appropriate criterion for guiding class combination. In the following text, we refer to  $\text{ACC}^{\text{CV}}$  as the ACC criterion.

**Mutual information.** It measures the dependence between two random variables, which, in the context of classification, can be the observed class label and the predicted class label. In this sense, the mutual information can be used as a criterion of classification accuracy. Following the definition of the mutual information of two jointly discrete random variables [Cover, 1999], we define the  $R$ -fold CV mutual information (MI) of  $\pi_K$  given  $\mathcal{C}$  and  $\mathcal{D}$  as

$$\text{MI}^{\text{CV}}(\pi_K; \mathcal{D}, \mathcal{C}) := \frac{1}{R} \sum_{r=1}^R \sum_{k_0=1}^{K_0} \sum_{k=1}^K \left\{ \frac{\sum_{(\mathbf{X}_i, Y_i) \in \mathcal{D}_e^r} \mathbb{I}(Y_i = k_0, \phi_{\pi_K}^{\mathcal{C}, \mathcal{D}_e^r}(\mathbf{X}_i) = k)}{|\mathcal{D}_e^r|} \cdot \log \left( \frac{|\mathcal{D}_e^r| \sum_{(\mathbf{X}_i, Y_i) \in \mathcal{D}_e^r} \mathbb{I}(Y_i = k_0, \phi_{\pi_K}^{\mathcal{C}, \mathcal{D}_e^r}(\mathbf{X}_i) = k)}{\left( \sum_{(\mathbf{X}_i, Y_i) \in \mathcal{D}_e^r} \mathbb{I}(Y_i = k_0) \right) \left( \sum_{(\mathbf{X}_i, Y_i) \in \mathcal{D}_e^r} \mathbb{I}(\phi_{\pi_K}^{\mathcal{C}, \mathcal{D}_e^r}(\mathbf{X}_i) = k) \right)} \right) \right\}, \quad (7)$$

where in the  $r$ -th fold, the mutual information is calculated for  $\left\{ \left( \phi_{\pi_K}^{\mathcal{C}, \mathcal{D}_t^r}(\mathbf{X}_i), Y_i \right) : (\mathbf{X}_i, Y_i) \in \mathcal{D}_e^r \right\}$ , i.e., between the predicted labels after class combination  $\pi_K$  and the original labels. Note that the mutual information does not require  $K_0 = K$  in (7). The reason why we do not use the mutual information of  $\left\{ \left( \phi_{\pi_K}^{\mathcal{C}, \mathcal{D}_t^r}(\mathbf{X}_i), \pi_K(Y_i) \right) : (\mathbf{X}_i, Y_i) \in \mathcal{D}_e^r \right\}$  (i.e., between the predicted labels and observed labels, both after class combination  $\pi_K$ ) is that it increases as more classes are combined—an undesirable phenomenon. In the following text, we refer to  $\text{MI}^{\text{CV}}$  as the MI criterion.

**Adjusted accuracy.** Neither the ACC criterion nor the MI criterion directly uses the class proportions. However, intuitively, it is easier to predict a data point from a larger class. To address this issue, we propose the *R-fold CV adjusted accuracy (AAC)* to weigh each correctly predicted data point by the inverse proportion of the combined class the data point belongs to:

$$\text{AAC}^{\text{CV}}(\pi_K; \mathcal{D}, \mathcal{C}) := \frac{1}{R} \sum_{r=1}^R \frac{1}{|\mathcal{D}_e^r|} \sum_{(\mathbf{X}_i, Y_i) \in \mathcal{D}_e^r} \frac{\mathbb{I} \left( \phi_{\pi_K}^{\mathcal{C}, \mathcal{D}_t^r}(\mathbf{X}_i) = \pi_K(Y_i) \right)}{\sum_{k_0 \in \pi_K^{-1}(\pi_K(Y_i))} \hat{p}_{k_0}}, \quad (8)$$

where  $\hat{p}_{k_0}$  is the proportion of the  $k_0$ -th original class in  $\mathcal{D}$ , same as in main text (2), so the denominator  $\sum_{k_0 \in \pi_K^{-1}(\pi_K(Y_i))} \hat{p}_{k_0}$  is the proportion of  $Y_i$ 's combined class  $\pi_K(Y_i)$  in  $\mathcal{D}$ . The idea is straightforward: assigning smaller weights to the classes that take up larger proportions. In the following text, we refer to  $\text{AAC}^{\text{CV}}$  in (8) as the AAC criterion. An alternative proposal of the adjusted accuracy is to assign smaller weights to the classes that are combined from more original classes; however, this proposal does not work as well as the AAC criterion (see Supplementary Material Section 2.4).

**Combined Kullback–Leibler divergence.** To balance the trade-off between the prediction accuracy and resolution, we also propose a combined Kullback–Leibler (CKL) divergence criterion that adds up (1) the divergence of the joint feature distribution estimated using combined class labels on the evaluation data  $\mathcal{D}_e$  (denoted by  $\hat{F}_{\pi_K, \mathcal{D}_e} : \mathcal{X} \rightarrow [0, 1]$ ) from that estimated using original class labels (denoted by  $\hat{F}_{\pi_{K_0}, \mathcal{D}_e} : \mathcal{X} \rightarrow [0, 1]$ ) and (2) the divergence of the joint feature distribution estimated using predicted combined class labels (denoted by  $\hat{F}_{\phi_{\pi_K}^{\mathcal{C}, \mathcal{D}_t}, \mathcal{D}_e} : \mathcal{X} \rightarrow [0, 1]$ ), where the classifier  $\phi_{\pi_K}^{\mathcal{C}, \mathcal{D}_t}$  is trained on training data  $\mathcal{D}_t$ ) from that estimated using combined class

labels, i.e.,  $\widehat{F}_{\pi_K, \mathcal{D}_e}$ . Accordingly, the  $R$ -fold CV CKL is defined as

$$\text{CKL}^{\text{CV}}(\pi_K; \mathcal{D}, \mathcal{C}) := \frac{1}{R} \sum_{r=1}^R \left[ D_{\text{KL}} \left( \widehat{F}_{\pi_K, \mathcal{D}_e^r} \parallel \widehat{F}_{\pi_{K_0}, \mathcal{D}_e^r} \right) + D_{\text{KL}} \left( \widehat{F}_{\phi_{\pi_K}^{\mathcal{C}, \mathcal{D}_e^r}} \parallel \widehat{F}_{\pi_K, \mathcal{D}_e^r} \right) \right]. \quad (9)$$

In the following text, we refer to  $\text{CKL}^{\text{CV}}$  as the CKL criterion. A challenge in calculating CKL is the estimation of  $d$ -dimensional joint feature distributions. To circumvent this challenge, we only calculate CKL when all class-conditional feature distributions are approximately Gaussian; that is,  $\widehat{F}_{\pi_{K_0}, \mathcal{D}_e}$ ,  $\widehat{F}_{\pi_K, \mathcal{D}_e}$ , and  $\widehat{F}_{\phi_{\pi_K}^{\mathcal{C}, \mathcal{D}_e}}$  can all be approximated by Gaussian mixture models (see Supplementary Material Section 1 for the computational detail of the KL divergence of two Gaussian mixture models). While this is an overly restrictive assumption, we use CKL as an alternative criterion to benchmark ITCA in simulation studies where this assumption holds (main text Section 3.1).

**Prediction entropy.** The p-ITCA definition in the main text (5) does not equate to but reminds us of the entropy of the distribution of  $(\phi_{\pi_K}^{\mathcal{C}, \mathcal{D}_t}(\mathbf{X}), \pi_K(Y))$  conditional on  $\phi_{\pi_K}^{\mathcal{C}, \mathcal{D}_t}(\mathbf{X}) = \pi_K(Y)$ , which we refer to as the *population-level prediction entropy (p-PE)*:

$$\begin{aligned} \text{p-PE}(\pi_K; \mathcal{D}_t, \mathcal{C}) &= \sum_{k=1}^K -\mathbb{P}(\phi_{\pi_K}^{\mathcal{C}, \mathcal{D}_t}(\mathbf{X}) = \pi_K(Y) = k) \cdot \log \mathbb{P}(\phi_{\pi_K}^{\mathcal{C}, \mathcal{D}_t}(\mathbf{X}) = \pi_K(Y) = k) \\ &= \sum_{k=1}^K [-\mathbb{P}(\pi_K(Y) = k) \log \mathbb{P}(\pi_K(Y) = k)] \cdot \mathbb{P}(\phi_{\pi_K}^{\mathcal{C}, \mathcal{D}_t}(\mathbf{X}) = \pi_K(Y) | \pi_K(Y) = k) \\ &\quad + \sum_{k=1}^K [-\mathbb{P}(\pi_K(Y) = k) \log \mathbb{P}(\phi_{\pi_K}^{\mathcal{C}, \mathcal{D}_t}(\mathbf{X}) = \pi_K(Y) | \pi_K(Y) = k)] \cdot \mathbb{P}(\phi_{\pi_K}^{\mathcal{C}, \mathcal{D}_t}(\mathbf{X}) = \pi_K(Y) | \pi_K(Y) = k), \end{aligned} \quad (10)$$

where first term after the last equal sign is the p-ITCA. Accordingly, at the sample level, the  $R$ -fold CV PE is

$$\begin{aligned} \text{PE}^{\text{CV}}(\pi_K; \mathcal{D}, \mathcal{C}) &:= \frac{1}{R} \sum_{r=1}^R \sum_{k=1}^K - \frac{\sum_{(\mathbf{X}_i, Y_i) \in \mathcal{D}_e^r} \mathbb{I}(\phi_{\pi_K}^{\mathcal{C}, \mathcal{D}_e^r}(\mathbf{X}_i) = \pi_K(Y_i) = k)}{|\mathcal{D}_e^r|} \\ &\quad \cdot \log \left( \frac{\sum_{(\mathbf{X}_i, Y_i) \in \mathcal{D}_e^r} \mathbb{I}(\phi_{\pi_K}^{\mathcal{C}, \mathcal{D}_e^r}(\mathbf{X}_i) = \pi_K(Y_i) = k)}{|\mathcal{D}_e^r|} \right). \end{aligned} \quad (11)$$

In the following text, we refer to  $\text{PE}^{\text{CV}}$  as the PE criterion. We argue that the definition of PE is not as intuitive as that of ITCA because PE only considers the data points that have labels correctly

predicted; hence, compared to ITCA, PE does not fully capture the class resolution information. To compute ITCA, ACC, MI, AAC, CKL, and PE, we set the number of folds in CV to  $R = 5$  in all numerical analyses.

## Appendix B SOME THEORETICAL REMARKS

The simulation studies and applications have empirically verified the effectiveness of ITCA and the two search strategies: greedy search and BFS. One crucial question remains: is ITCA maximized at the true class combination when the sample size  $n \rightarrow \infty$ ? To investigate the asymptotic property of ITCA, we define the population-level ITCA (p-ITCA) (5) in the main text. For clarity, in the following text, we refer to the sample-level definition of ITCA in the main text (2) as s-ITCA, and we refer to the  $\text{ITCA}^{\text{CV}}$  in the main text (4) as  $\text{s-ITCA}^{\text{CV}}$ . We can easily see that s-ITCA converges to p-ITCA in probability.

In the first part of this section, we show that p-ITCA does not always suggest to combine the classes that have the same class-conditional feature distribution; the classes we will refer to as “same-distributed classes” in the following. Although this result seems counter-intuitive, it is aligned with the definition of p-ITCA, which not only considers classification accuracy but also class resolution. If the same-distributed classes dominate in class proportions, p-ITCA may prefer to keep them separate to maintain a not-so-degenerate class resolution (a degenerate resolution means that all classes are combined as one). To investigate the class combination properties of p-ITCA, we define and analyze the class-combination curves and regions of the oracle classification algorithm and the LDA algorithm as examples. The results show that the oracle and LDA algorithms have different class-combination curves and regions. They also guide us to enhance the ability of the LDA algorithm for discovering the true class combination as described in the second part of this section. In the third part of this section, we discuss how to prune the search space of possible class combinations when the classification algorithm satisfies certain conditions.

### B.1 Properties of p-ITCA with the oracle and LDA classification algorithms

**Definition 1** (oracle classification algorithm). *Let there be  $K_0$  observed classes. Let  $S \subseteq [K_0]$  be a set of same-distributed classes that share the same class-conditional feature distribution;  $|S| \geq 2$ . Without loss of generality, we assume that all other classes not in  $S$  have distinct class-conditional*

feature distributions. We denote by  $\mathcal{A}$  the set of class combinations that do not combine a class in  $S$  with a class not in  $S$ . Then we define  $\mathcal{C}^*$  as the oracle classification algorithm if its classifier for any class combination  $\pi_K \in \mathcal{A}$ , denoted by  $\phi_{\pi_K}^{\mathcal{C}^*}$ , satisfies the following property. For any data point  $(\mathbf{X}_i, Y_i)$ ,  $\phi_{\pi_K}^{\mathcal{C}^*}$  predicts the label as  $\pi_K(Y_i)$  if  $Y_i \notin S$  or by picking a label in  $\{\pi_K(k_0) : k_0 \in S\}$  (with probability proportional to class  $k_0$ 's proportion) if  $Y_i \in S$ . In other words,  $\phi_{\pi_K}^{\mathcal{C}^*}(\mathbf{X}_i) \sim \pi_K(Y_i)\mathbb{I}(Y_i \notin S) + \text{Multinomial}(n = 1, \text{support} = \{\pi_K(k_0) : k_0 \in S\}, \text{probabilities} = \{\mathbb{P}(Y = k_0) : k_0 \in S\})\mathbb{I}(Y_i \in S)$ .

The oracle classification algorithm  $\mathcal{C}^*$  is only conceptual and does not require training, so its classifier notation  $\phi_{\pi_K}^{\mathcal{C}^*}$  does not involve a training dataset  $\mathcal{D}_t$ . If there exists a combined class  $k \in [K]$  whose class-conditional feature distribution is different from those of all other combined classes, then the prediction accuracy conditional on that class is  $\mathbb{P}(\phi_{\pi_K}^{\mathcal{C}^*}(\mathbf{X}) = \pi_K(Y) | \pi_K(Y) = k) = 1$ . Recall that the definition of p-ITCA in the main text (5) only involves a classifier's class-conditional prediction accuracies and the class proportions. To facilitate our discussion, we denote the proportion of the  $k_0$ -th observed class as  $p_{k_0} = \mathbb{P}(Y = k_0)$ ,  $k_0 \in [K_0]$  in the following.

Below we investigate how the proportions of two same-distributed classes, say  $p_1$  and  $p_2$ , affect the class combination decision of p-ITCA: whether p-ITCA would suggest the two classes to be combined. In the space of  $(p_1, p_2)$ , denoted by

$$\Omega = \{(p_1, p_2) : p_1 > 0, p_2 > 0, p_1 + p_2 < 1\} \subset [0, 1]^2, \quad (12)$$

we define the class-combination curve and region of a general classification algorithm  $\mathcal{C}$ ; the curve and region are regarding whether the two same-distributed classes should be combined.

**Definition 2** (class-combination curve and region). *Among  $K_0 > 2$  observed classes, suppose there are two same-distributed classes  $S = \{1, 2\}$ , and the other classes all have distinct class-conditional feature distributions. Denote by  $\pi_{K_0-1} = \{(1, 2), \dots, K_0\}$  the class combination that only combines the observed classes 1 and 2 into one class. We consider data-generating populations with varying  $(p_1, p_2) \in \Omega$  in (12), and for each population we evaluate the performance of p-ITCA for combining the observed classes 1 and 2. Given a training dataset  $D_t$  (needed for practical algorithms but not*

for the oracle algorithm) and a classification algorithm  $\mathcal{C}$ , we refer to the curve in  $\Omega$

$$\text{CC}(\pi_{K_0-1}||\pi_{K_0}; \mathcal{D}_t, \mathcal{C}) := \{(p_1, p_2) \in \Omega : \text{p-ITCA}(\pi_{K_0}; \mathcal{D}_t, \mathcal{C}, p_1, p_2) = \text{p-ITCA}(\pi_{K_0-1}; \mathcal{D}_t, \mathcal{C}, p_1, p_2)\} \quad (13)$$

as the class-combination curve (CC) of  $\mathcal{C}$ . For notation clarity,  $p_1$  and  $p_2$  are added to  $\text{p-ITCA}(\pi_{K_0}; \mathcal{D}_t, \mathcal{C})$  and  $\text{p-ITCA}(\pi_{K_0-1}; \mathcal{D}_t, \mathcal{C})$  to indicate that p-ITCA also depends on  $p_1$  and  $p_2$ .

Next, we define the class-combination region (CR) of algorithm  $\mathcal{C}$  as

$$\text{CR}(\pi_{K_0-1}||\pi_{K_0}; \mathcal{D}_t, \mathcal{C}) := \{(p_1, p_2) \in \Omega : \text{p-ITCA}(\pi_{K_0-1}; \mathcal{D}_t, \mathcal{C}, p_1, p_2) - \text{p-ITCA}(\pi_{K_0}; \mathcal{D}_t, \mathcal{C}, p_1, p_2) > 0\}, \quad (14)$$

where  $\pi_{K_0-1}$  improves the p-ITCA of  $\pi_{K_0}$  and thus the two same-distributed classes should be combined.

By the above definition, the following proposition holds for the oracle classification algorithm.

**Proposition 1** (class-combination curve and region of the oracle classification algorithm). *The class-combination curve of the oracle classification algorithm  $\mathcal{C}^*$  has the closed form*

$$\text{CC}(\pi_{K_0-1}||\pi_{K_0}; \mathcal{C}^*) = \{(p_1, p_2) \in \Omega : p_1^2 \log p_1 + p_2^2 \log p_2 = (p_1 + p_2)^2 \log(p_1 + p_2)\}, \quad (15)$$

and the class-combination region is

$$\text{CR}(\pi_{K_0-1}||\pi_{K_0}; \mathcal{C}^*) = \{(p_1, p_2) \in \Omega : p_1^2 \log p_1 + p_2^2 \log p_2 - (p_1 + p_2)^2 \log(p_1 + p_2) > 0\}. \quad (16)$$

*Proof.* Consider the p-ITCA before combing the observed classes 1 and 2,

$$\text{p-ITCA}(\pi_{K_0}; \mathcal{C}^*, p_1, p_2) = \sum_{k_0=1}^{K_0} -p_{k_0} \log p_{k_0} \cdot \mathbb{P}(\phi_{\pi_{K_0}}^{\mathcal{C}^*}(\mathbf{X}) = Y | Y = k_0).$$

Since  $\phi_{\pi_{K_0}}^{\mathcal{C}^*}$  is an oracle classifier, we have

$$\begin{aligned}\mathbb{P}(\phi_{\pi_{K_0}}^{\mathcal{C}^*}(\mathbf{X}) = Y | Y = 1) &= \frac{p_1}{p_1 + p_2}, \\ \mathbb{P}(\phi_{\pi_{K_0}}^{\mathcal{C}^*}(\mathbf{X}) = Y | Y = 2) &= \frac{p_2}{p_1 + p_2}, \\ \mathbb{P}(\phi_{\pi_{K_0}}^{\mathcal{C}^*}(\mathbf{X}) = Y | Y = k_0) &= 1, \quad k_0 = 3, \dots, K_0.\end{aligned}$$

Hence,

$$\text{p-ITCA}(\pi_{K_0}; \mathcal{C}^*, p_1, p_2) = -\frac{p_1^2 \log p_1}{p_1 + p_2} - \frac{p_2^2 \log p_2}{p_1 + p_2} - \sum_{k_0=3}^{K_0} p_{k_0} \log p_{k_0}. \quad (17)$$

Denote by  $\pi_{K_0-1}$  the class combination that only combines the observed classes 1 and 2, i.e.,  $\pi_{K_0-1}(1) = \pi_{K_0-1}(2) = 1$ ,  $\pi_{K_0-1}(k_0) = k_0 - 1$ ,  $\forall k \in [K_0] \setminus \{1, 2\}$ . The p-ITCA of  $\pi_{K_0-1}$  is

$$\begin{aligned}\text{p-ITCA}(\pi_{K_0-1}; \mathcal{C}^*, p_1, p_2) &= -\mathbb{P}(\pi_{K_0-1}(Y) = 1) \log \mathbb{P}(\pi_{K_0-1}(Y) = 1) \cdot \mathbb{P}(\phi_{\pi_{K_0-1}}^{\mathcal{C}^*}(\mathbf{X}) = \pi_{K_0-1}(Y) | \pi_{K_0-1}(Y) = 1) \\ &\quad - \sum_{k=2}^{K_0-1} \mathbb{P}(\pi_{K_0-1}(Y) = k) \log \mathbb{P}(\pi_{K_0-1}(Y) = k) \cdot \mathbb{P}(\phi_{\pi_{K_0-1}}^{\mathcal{C}^*}(\mathbf{X}) = \pi_{K_0-1}(Y) | \pi_{K_0-1}(Y) = k).\end{aligned}$$

Since  $\phi_{\pi_{K_0-1}}^{\mathcal{C}^*}$  is an oracle classifier, we have

$$\mathbb{P}(\phi_{\pi_{K_0-1}}^{\mathcal{C}^*}(\mathbf{X}) = \pi_{K_0-1}(Y) | \pi_{K_0-1}(Y) = k) = 1, \quad \forall k \in [K_0 - 1].$$

Hence,

$$\text{p-ITCA}(\pi_{K_0-1}; \mathcal{C}^*, p_1, p_2) = -(p_1 + p_2) \log(p_1 + p_2) - \sum_{k_0=3}^{K_0} p_{k_0} \log p_{k_0}. \quad (18)$$

Substituting (17) and (18) into the definitions of the class-combination curve (13) and class-combination region (14) and simplifying the forms, we obtain the class-combination curve (15) and class-combination region (16) of the oracle classification algorithm. □

Proposition 1 shows that for the oracle classification algorithm, when one of  $p_1$  and  $p_2$  is close to zero and the other is less than  $e^{-1/2} \approx 0.6$ , by (16) p-ITCA would combine the two classes (Supplementary Material Figure S8, left panel shows the function  $f(p) = p^2 \log p$ , which monotone decreases for  $p \in (0, e^{-1/2})$ ). Otherwise, if  $p_1$  and  $p_2$  have a not-too-small minimum and a large max-

imum, p-ITCA would keep the two classes separate to maintain a not-so-degenerate class resolution (Figure 11, left panel). Roughly speaking, unless one of the two classes is extremely small, p-ITCA would not suggest the two classes to be combined if their total proportion  $p_1 + p_2$  dominates. This result suggests that, even under the ideal scenario (i.e., with the oracle algorithm), p-ITCA would not suggest a combination of two non-trivial classes that would result in a dominant class.

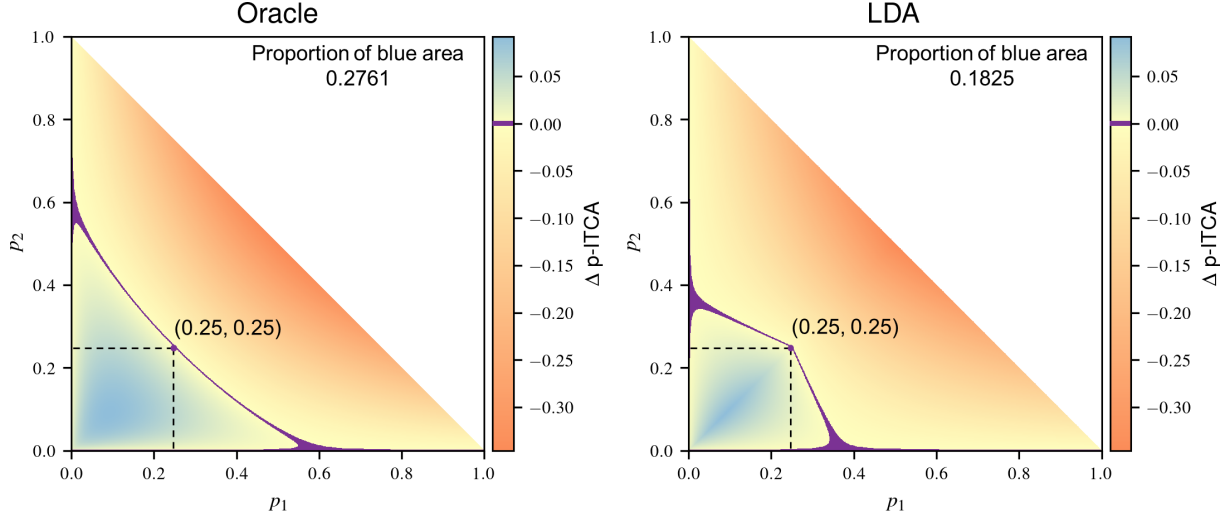


Figure 11: Regarding the combination of two same-distributed classes (with proportions  $p_1$  and  $p_2$ ), the improvement of p-ITCA,  $\Delta p\text{-ITCA}(p_1, p_2; \mathcal{D}_t, \mathcal{C}) := p\text{-ITCA}(\pi_{K_0-1}; \mathcal{D}_t, \mathcal{C}, p_1, p_2) - p\text{-ITCA}(\pi_{K_0}; \mathcal{D}_t, \mathcal{C}, p_1, p_2)$ , of the oracle classification algorithm (left;  $\mathcal{D}_t$  not needed;  $\mathcal{C}^*$ ) and the LDA algorithm (right;  $\mathcal{D}_\infty$ ;  $\mathcal{C}^{\text{LDA}}$ ). The blue areas indicate the class-combination regions of the oracle classification algorithm (16) and the LDA classification algorithm (22) where  $\Delta p\text{-ITCA}(p_1, p_2; \mathcal{D}_t, \mathcal{C}) > 0$  and thus the two classes will be combined. In each panel, the purple boundary ( $|\Delta p\text{-ITCA}| < 10^{-3}$ ) between the blue area and the orange area indicates the class-combination curve of the corresponding algorithm;  $(0.25, 0.25)$  is the point where  $\Delta p\text{-ITCA}(p_1, p_2; \mathcal{D}_t, \mathcal{C}) = 0$  for both classification algorithms; the area of the class-combination region (the proportion of the blue area) is shown in the upper right corner.

Next, we investigate the class-combination curve and region of the LDA algorithm. Different from the oracle classification algorithm, the LDA algorithm has its accuracy depending on the joint distribution of  $(\mathbf{X}, Y)$ , on which we will make some additional assumptions.

**Proposition 2** (class-combination curve and region of LDA). *Suppose there are  $K_0 = 3$  observed classes, which contain two same-distributed classes. Without loss of generality, we assume that*

classes 1 and 2 have the same class-conditional feature distribution  $\mathcal{N}(\mathbf{0}, \sigma^2 \mathbf{I}_d)$ , and that class 3 has the class-conditional feature distribution  $\mathcal{N}(\boldsymbol{\mu}, \sigma^2 \mathbf{I}_d)$  with  $\boldsymbol{\mu} \neq \mathbf{0}$ ; hence,  $\|\boldsymbol{\mu}\|$  is the Euclidean distance between the mean vectors of the two Gaussian distributions. Denote by  $\mathcal{D}_\infty$  the training dataset  $\mathcal{D}_t$  with an infinite sample size, i.e., the LDA model trained on  $\mathcal{D}_\infty$  has parameter estimates as the true parameters. Then, for deciding whether  $\pi_3 = \{1, 2, 3\}$  should be combined as  $\pi_2 = \{(1, 2), 3\}$ , the class-combination curve of the LDA algorithm  $\mathcal{C}^{\text{LDA}}$  has the following form

$$\begin{aligned} & \text{CC}(\pi_2 || \pi_3; \mathcal{D}_\infty, \mathcal{C}^{\text{LDA}}) \\ &= \left\{ (p_1, p_2) \in \Omega : \Phi \left( \frac{\|\boldsymbol{\mu}\|}{2\sigma} + \frac{\sigma}{\|\boldsymbol{\mu}\|} \log \frac{p_{1 \vee 2}}{p_3} \right) p_{1 \vee 2} \log p_{1 \vee 2} + \Phi \left( \frac{\|\boldsymbol{\mu}\|}{2\sigma} - \frac{\sigma}{\|\boldsymbol{\mu}\|} \log \frac{p_{1 \vee 2}}{p_3} \right) p_3 \log p_3 = \right. \\ & \quad \left. \Phi \left( \frac{\|\boldsymbol{\mu}\|}{2\sigma} + \frac{\sigma}{\|\boldsymbol{\mu}\|} \log \frac{p_{1+2}}{p_3} \right) p_{1+2} \log p_{1+2} + \Phi \left( \frac{\|\boldsymbol{\mu}\|}{2\sigma} - \frac{\sigma}{\|\boldsymbol{\mu}\|} \log \frac{p_{1+2}}{p_3} \right) p_3 \log p_3 \right\}, \end{aligned} \quad (19)$$

where  $p_{1 \vee 2} := p_1 \vee p_2 = \max(p_1, p_2)$ ,  $p_{1+2} := p_1 + p_2$ ,  $p_3 = 1 - p_{1+2}$ , and  $\Phi$  is the cumulative distribution function (CDF) of the univariate standard Gaussian distribution. The corresponding class-combination region is

$$\begin{aligned} & \text{CR}(\pi_2 || \pi_3; \mathcal{D}_\infty, \mathcal{C}^{\text{LDA}}) \\ &= \left\{ (p_1, p_2) \in \Omega : \Phi \left( \frac{\|\boldsymbol{\mu}\|}{2\sigma} + \frac{\sigma}{\|\boldsymbol{\mu}\|} \log \frac{p_{1 \vee 2}}{p_3} \right) p_{1 \vee 2} \log p_{1 \vee 2} + \Phi \left( \frac{\|\boldsymbol{\mu}\|}{2\sigma} - \frac{\sigma}{\|\boldsymbol{\mu}\|} \log \frac{p_{1 \vee 2}}{p_3} \right) p_3 \log p_3 \right. \\ & \quad \left. - \Phi \left( \frac{\|\boldsymbol{\mu}\|}{2\sigma} + \frac{\sigma}{\|\boldsymbol{\mu}\|} \log \frac{p_{1+2}}{p_3} \right) p_{1+2} \log p_{1+2} - \Phi \left( \frac{\|\boldsymbol{\mu}\|}{2\sigma} - \frac{\sigma}{\|\boldsymbol{\mu}\|} \log \frac{p_{1+2}}{p_3} \right) p_3 \log p_3 > 0 \right\}. \end{aligned} \quad (20)$$

When  $\|\boldsymbol{\mu}\| \gg \sigma$ , the class-combination curve (19) reduces to

$$\text{CC}(\pi_2 || \pi_3; \mathcal{D}_\infty, \mathcal{C}^{\text{LDA}}) = \{(p_1, p_2) \in \Omega : p_{1 \vee 2} \log p_{1 \vee 2} = p_{1+2} \log p_{1+2}\}. \quad (21)$$

and the class-combination region (20) reduces to

$$\text{CR}(\pi_2 || \pi_3; \mathcal{D}_\infty, \mathcal{C}^{\text{LDA}}) = \{(p_1, p_2) \in \Omega : p_{1 \vee 2} \log p_{1 \vee 2} - p_{1+2} \log p_{1+2} > 0\}. \quad (22)$$

Note that (21) and (22) hold in general for  $K_0 \geq 3$  observed classes regarding whether  $\pi_{K_0}$  should be combined as  $\pi_{K_0-1}$ , which combines classes 1 and 2, when every classes  $k$  with class-conditional feature distribution  $\mathcal{N}(\boldsymbol{\mu}_k, \sigma^2 \mathbf{I}_d)$  satisfies that  $\|\boldsymbol{\mu}_k\| \gg \sigma$ ,  $k = 3, \dots, K_0$ .

*Proof.* Without loss of generality, we assume that  $\boldsymbol{\mu} = (\|\boldsymbol{\mu}\|, 0, \dots, 0)$  because one can always rotate  $\boldsymbol{\mu}$  to obtain  $(\|\boldsymbol{\mu}\|, 0, \dots, 0)$ . With the sample size  $n \rightarrow \infty$ , the parameter estimates of the LDA model converge to the true parameters in probability. In our setting, without class combination (i.e.,  $\pi_3$ ), the LDA algorithm has the following three decision functions for the three observed classes.

$$\begin{aligned}\delta_1^{\pi_3}(\mathbf{X}) &= \log \mathbb{P}(Y = 1 | \mathbf{X}) \text{ up to a constant} = \log p_1, \\ \delta_2^{\pi_3}(\mathbf{X}) &= \log \mathbb{P}(Y = 2 | \mathbf{X}) \text{ up to a constant} = \log p_2, \\ \delta_3^{\pi_3}(\mathbf{X}) &= \log \mathbb{P}(Y = 3 | \mathbf{X}) \text{ up to a constant} = \frac{1}{\sigma^2} \mathbf{X}^T \boldsymbol{\mu} - \frac{\|\boldsymbol{\mu}\|^2}{2\sigma^2} + \log p_3.\end{aligned}$$

Given a new data point  $\mathbf{X}$ , the LDA classifier predicts its label as  $\phi_{\pi_3}^{\mathcal{C}^{\text{LDA}}, \mathcal{D}^\infty}(\mathbf{X}) = \arg \max_{k_0 \in [3]} \delta_{k_0}^{\pi_3}(\mathbf{X})$ .

Consider the p-ITCA definition before combining the observed classes 1 and 2,

$$\text{p-ITCA}(\pi_3; \mathcal{D}_\infty, \mathcal{C}^{\text{LDA}}, p_1, p_2) = \sum_{k_0=1}^3 -p_{k_0} \log p_{k_0} \mathbb{P}(\phi_{\pi_3}^{\mathcal{C}^{\text{LDA}}, \mathcal{D}^\infty}(\mathbf{X}) = Y \mid Y = k_0).$$

Without loss of generality, when  $p_1 > p_2$ , we immediately have  $\delta_1^{\pi_3}(\mathbf{X}) > \delta_2^{\pi_3}(\mathbf{X})$ ,  $\forall \mathbf{X} \in \mathbb{R}^d$ . Hence, we have the following class-conditional prediction accuracies. Conditional on  $Y = 1$ ,

$$\begin{aligned}\mathbb{P}(\phi_{\pi_3}^{\mathcal{C}^{\text{LDA}}, \mathcal{D}^\infty}(\mathbf{X}) = Y \mid Y = 1) &= \mathbb{P}(\delta_3^{\pi_3}(\mathbf{X}) < \delta_1^{\pi_3}(\mathbf{X}) \text{ and } \delta_2^{\pi_3}(\mathbf{X}) < \delta_1^{\pi_3}(\mathbf{X}) \mid Y = 1) \\ &= \mathbb{P}(\delta_3^{\pi_3}(\mathbf{X}) < \delta_1^{\pi_3}(\mathbf{X}) \mid Y = 1) \\ &= \mathbb{P}\left(\frac{1}{\sigma^2} \mathbf{X}^T \boldsymbol{\mu} - \frac{\|\boldsymbol{\mu}\|^2}{2\sigma^2} + \log p_3 < \log p_1 \mid Y = 1\right) \\ &= \mathbb{P}\left(X_1 < \frac{\|\boldsymbol{\mu}\|}{2} + \frac{\sigma^2}{\|\boldsymbol{\mu}\|} \log \frac{p_1}{p_3} \mid Y = 1\right) \\ &= \Phi\left(\frac{\|\boldsymbol{\mu}\|}{2\sigma} + \frac{\sigma}{\|\boldsymbol{\mu}\|} \log \frac{p_1}{p_3}\right),\end{aligned}$$

where  $X_1$  is the first element of  $\mathbf{X}$ , and  $X_1 \mid Y = 1 \sim \mathcal{N}(0, \sigma^2)$ . The fourth equation is based on

$\mathbf{X}^T \boldsymbol{\mu} = \|\boldsymbol{\mu}\|$  because  $\boldsymbol{\mu} = (\|\boldsymbol{\mu}\|, 0, \dots, 0)$ . Conditional on  $Y = 2$ ,

$$\mathbb{P}(\phi_{\pi_3}^{\mathcal{C}^{\text{LDA}}, \mathcal{D}_\infty}(\mathbf{X}) = Y \mid Y = 2) = \mathbb{P}(\delta_3^{\pi_3}(\mathbf{X}) < \delta_2^{\pi_3}(\mathbf{X}) \text{ and } \delta_1^{\pi_3}(\mathbf{X}) < \delta_2^{\pi_3}(\mathbf{X}) \mid Y = 2) = 0.$$

Conditional on  $Y = 3$ ,

$$\begin{aligned} \mathbb{P}(\phi_{\pi_3}^{\mathcal{C}^{\text{LDA}}, \mathcal{D}_\infty}(\mathbf{X}) = Y \mid Y = 3) &= \mathbb{P}(\delta_1^{\pi_3}(\mathbf{X}) < \delta_3^{\pi_3}(\mathbf{X}) \text{ and } \delta_2^{\pi_3}(\mathbf{X}) < \delta_3^{\pi_3}(\mathbf{X}) \mid Y = 3) \\ &= \mathbb{P}(\delta_1^{\pi_3}(\mathbf{X}) < \delta_3^{\pi_3}(\mathbf{X}) \mid Y = 3) \\ &= \mathbb{P}\left(\log p_1 < \frac{1}{\sigma^2} \mathbf{X}^T \boldsymbol{\mu} - \frac{\|\boldsymbol{\mu}\|^2}{2\sigma^2} + \log p_3 \mid Y = 3\right) \\ &= \mathbb{P}\left(X_1 > \frac{\|\boldsymbol{\mu}\|}{2} + \frac{\sigma^2}{\|\boldsymbol{\mu}\|} \log \frac{p_1}{p_3} \mid Y = 3\right) \\ &= \Phi\left(\frac{\|\boldsymbol{\mu}\|}{2\sigma} - \frac{\sigma}{\|\boldsymbol{\mu}\|} \log \frac{p_1}{p_3}\right), \end{aligned}$$

where the last equation holds because  $X_1 \mid Y = 3 \sim \mathcal{N}(\|\boldsymbol{\mu}\|, \sigma^2)$ .

Hence, p-ITCA before combining classes 1 and 2 is

$$\begin{aligned} &\text{p-ITCA}(\pi_3; \mathcal{D}_\infty, \mathcal{C}^{\text{LDA}}, p_1, p_2) \\ &= \begin{cases} -\Phi\left(\frac{\|\boldsymbol{\mu}\|}{2\sigma} + \frac{\sigma}{\|\boldsymbol{\mu}\|} \log \frac{p_1}{p_3}\right) p_1 \log p_1 - \Phi\left(\frac{\|\boldsymbol{\mu}\|}{2\sigma} - \frac{\sigma}{\|\boldsymbol{\mu}\|} \log \frac{p_1}{p_3}\right) p_3 \log p_3 & \text{if } p_1 > p_2 \\ -\Phi\left(\frac{\|\boldsymbol{\mu}\|}{2\sigma} + \frac{\sigma}{\|\boldsymbol{\mu}\|} \log \frac{p_2}{p_3}\right) p_2 \log p_2 - \Phi\left(\frac{\|\boldsymbol{\mu}\|}{2\sigma} - \frac{\sigma}{\|\boldsymbol{\mu}\|} \log \frac{p_2}{p_3}\right) p_3 \log p_3 & \text{otherwise} \end{cases} \\ &= -\Phi\left(\frac{\|\boldsymbol{\mu}\|}{2\sigma} + \frac{\sigma}{\|\boldsymbol{\mu}\|} \log \frac{p_{1 \vee 2}}{p_3}\right) p_{1 \vee 2} \log p_{1 \vee 2} - \Phi\left(\frac{\|\boldsymbol{\mu}\|}{2\sigma} - \frac{\sigma}{\|\boldsymbol{\mu}\|} \log \frac{p_{1 \vee 2}}{p_3}\right) p_3 \log p_3. \end{aligned} \quad (23)$$

After combining classes 1 and 2, the definition of p-ITCA becomes

$$\begin{aligned} \text{p-ITCA}(\pi_2; \mathcal{D}_\infty, \mathcal{C}^{\text{LDA}}, p_1, p_2) &= -p_{1+2} \log p_{1+2} \mathbb{P}(\phi_{\pi_2}^{\mathcal{C}^{\text{LDA}}, \mathcal{D}_\infty}(\mathbf{X}) = \pi_2(Y) \mid \pi_2(Y) = 1) \\ &\quad - p_3 \log p_3 \mathbb{P}(\phi_{\pi_2}^{\mathcal{C}^{\text{LDA}}, \mathcal{D}_\infty}(\mathbf{X}) = \pi_2(Y) \mid \pi_2(Y) = 2). \end{aligned}$$

With  $\pi_2$ , the decision functions of the LDA algorithm becomes

$$\begin{aligned}\delta_1^{\pi_2}(\mathbf{X}) &= \log \mathbb{P}(\pi_2(Y) = 1 | \mathbf{X}) \text{ up to a constant} = \log p_{1+2}, \\ \delta_2^{\pi_2}(\mathbf{X}) &= \log \mathbb{P}(\pi_2(Y) = 2 | \mathbf{X}) \text{ up to a constant} = \frac{1}{\sigma^2} \mathbf{X}^T \boldsymbol{\mu} - \frac{\|\boldsymbol{\mu}\|^2}{2\sigma^2} + \log p_3.\end{aligned}$$

Hence, the LDA classifier  $\phi_{\pi_2}^{\mathcal{C}^{\text{LDA}}, \mathcal{D}_\infty}$  has the following class-conditional prediction accuracies. Conditional on  $\pi_2(Y) = 1$ ,

$$\begin{aligned}\mathbb{P}(\phi_{\pi_2}^{\mathcal{C}^{\text{LDA}}, \mathcal{D}_\infty}(\mathbf{X}) = \pi_2(Y) \mid \pi_2(Y) = 1) &= \mathbb{P}(\delta_2^{\pi_2}(\mathbf{X}) < \delta_1^{\pi_2}(\mathbf{X}) \mid \pi_2(Y) = 1) \\ &= \mathbb{P}\left(\frac{1}{\sigma^2} \mathbf{X}^T \boldsymbol{\mu} - \frac{\|\boldsymbol{\mu}\|^2}{2\sigma^2} + \log p_3 < \log p_{1+2} \mid \pi_2(Y) = 1\right) \\ &= \mathbb{P}\left(X_1 < \frac{\|\boldsymbol{\mu}\|}{2} + \frac{\sigma^2}{\|\boldsymbol{\mu}\|} \log \frac{p_{1+2}}{p_3} \mid \pi_2(Y) = 1\right) \\ &= \Phi\left(\frac{\|\boldsymbol{\mu}\|}{2\sigma} + \frac{\sigma}{\|\boldsymbol{\mu}\|} \log \frac{p_{1+2}}{p_3}\right),\end{aligned}$$

where the last equation holds because  $X_1 \mid \pi_2(Y) = 1 \sim \mathcal{N}(0, \sigma^2)$ .

Conditional on  $\pi_2(Y) = 2$ ,

$$\begin{aligned}\mathbb{P}(\phi_{\pi_2}^{\mathcal{C}^{\text{LDA}}, \mathcal{D}_\infty}(\mathbf{X}) = \pi_2(Y) \mid \pi_2(Y) = 2) &= \mathbb{P}(\delta_2^{\pi_2}(\mathbf{X}) > \delta_1^{\pi_2}(\mathbf{X}) \mid \pi_2(Y) = 2) \\ &= \mathbb{P}\left(\frac{1}{\sigma^2} \mathbf{X}^T \boldsymbol{\mu} - \frac{\|\boldsymbol{\mu}\|^2}{2\sigma^2} + \log p_3 > \log p_{1+2} \mid \pi_2(Y) = 1\right) \\ &= \mathbb{P}\left(X_1 > \frac{\|\boldsymbol{\mu}\|}{2} + \frac{\sigma^2}{\|\boldsymbol{\mu}\|} \log \frac{p_{1+2}}{p_3} \mid \pi_2(Y) = 1\right) \\ &= \Phi\left(\frac{\|\boldsymbol{\mu}\|}{2\sigma} - \frac{\sigma}{\|\boldsymbol{\mu}\|} \log \frac{p_{1+2}}{p_3}\right),\end{aligned}$$

where the last equation holds because  $X_1 \mid \pi_2(Y) = 2 \sim \mathcal{N}(\|\boldsymbol{\mu}\|, \sigma^2)$ .

Hence, p-ITCA after combining classes 1 and 2 becomes

$$\text{p-ITCA}(\pi_2; \mathcal{D}_\infty, \mathcal{C}^{\text{LDA}}, p_1, p_2) = -\Phi\left(\frac{\|\boldsymbol{\mu}\|}{2\sigma} + \frac{\sigma}{\|\boldsymbol{\mu}\|} \log \frac{p_{1+2}}{p_3}\right) p_{1+2} \log p_{1+2} - \Phi\left(\frac{\|\boldsymbol{\mu}\|}{2\sigma} - \frac{\sigma}{\|\boldsymbol{\mu}\|} \log \frac{p_{1+2}}{p_3}\right) p_3 \log p_3 \quad (24)$$

By (23) and (24), we obtain the class-combination curve of LDA in (19) and the class-combination region in (20). When  $\|\boldsymbol{\mu}\| \gg \sigma$ , it is straightforward to see that (19) and (20) reduce to (21) and

(22), respectively.

By similar derivations, we can show that (21) and (22) hold in general for  $K_0 \geq 3$  if the classes 1 and 2 are distinct from the other classes.  $\square$

Similar to Proposition 1, Proposition 2 shows that when one of  $p_1$  and  $p_2$  is close to zero and the other is less than  $e^{-1} \approx 0.37$ , by (22) p-ITCA would combine the two classes (Figure S8, right panel shows the function  $f(p) = p \log p$ , which monotone decreases for  $p \in (0, e^{-1})$ ). If  $p_1$  and  $p_2$  have a not-too-small minimum and a large maximum, p-ITCA would keep the two classes separate to maintain a not-so-degenerate class resolution (Figure 11, right panel). The class-combination curve of LDA is quite different from that of the oracle classification algorithm. Moreover, compared with the oracle classification algorithm, LDA has a smaller chance of discovering the true class combination (shown by the smaller blue area in Figure 11).

## B.2 Improvement of LDA as soft LDA for discovering class combination

Seeing that the LDA algorithm is less powerful than the oracle classification algorithm for discovering the true combination, we consider modifying the LDA algorithm to improve its power. We first review how LDA predicts the class label of a data point  $\mathbf{X}$ . Without loss of generality, we assume that two same-distributed classes  $k_1, k_2 \in [K_0]$  are distinguishable from the remaining  $(K_0 - 2)$  classes. Suppose that classes  $k_1$  and  $k_2$  have a class-conditional feature distribution  $\mathcal{N}(\boldsymbol{\mu}, \sigma^2 \mathbf{I})$ . Note the decision function  $\delta_k^{\pi K_0}(\mathbf{X}) = \frac{1}{\sigma^2} \mathbf{X}^T \boldsymbol{\mu} - \frac{\|\boldsymbol{\mu}\|^2}{2\sigma^2} + \log p_k$  for  $k = k_1$  or  $k_2$ . Hence, if  $p_{k_1} > p_{k_2}$ , then  $\delta_{k_1}^{\pi K_0}(\mathbf{X}) > \delta_{k_2}^{\pi K_0}(\mathbf{X})$  holds for all  $\mathbf{X} \in \mathbb{R}^d$ . Therefore, LDA would never predict that  $Y = k_2$ . In contrast, the oracle classification algorithm acts differently: if a data point  $(\mathbf{X}, Y)$  has  $Y \in \{k_1, k_2\}$ , then the oracle classification algorithm would predict  $Y$  as  $k_1$  or  $k_2$  with probability  $p_1$  or  $p_2$ .

We define soft LDA to mimic the oracle classification algorithm to enhance the ability of LDA for discovering the true class combination. The only difference between soft LDA and LDA is that the soft LDA predicts  $Y$  randomly. Specifically, given a data point  $\mathbf{X}$ , soft LDA computes the decision scores  $\delta_k^{\pi K_0}(\mathbf{X})$  for  $k \in [K_0]$ . Then soft LDA predicts  $Y$  by drawing a sample with size one from a multinomial distribution  $\text{Multinomial}(1, [K_0], \text{softmax}(\boldsymbol{\delta}^{\pi K_0}(\mathbf{X})))$ , where  $\boldsymbol{\delta}^{\pi K_0}(\mathbf{X}) := (\delta_1^{\pi K_0}(\mathbf{X}), \dots, \delta_{K_0}^{\pi K_0}(\mathbf{X}))$  is a  $K_0$ -dimensional vector, and the softmax function normalizes  $\boldsymbol{\delta}^{\pi K_0}(\mathbf{X})$  to a vector of probabilities that sum up to 1.

Interestingly, we show in Proposition 3 that when the data-generating distribution is the LDA model with perfectly separated classes, the soft LDA algorithm trained with an infinite sample size equates the oracle classification algorithm.

**Proposition 3.** *Under the same setting in Proposition 2, when  $\|\boldsymbol{\mu}\|/\sigma \rightarrow \infty$ , the soft LDA classification algorithm is the same as the oracle classification algorithm in Definition 1.*

*Proof.* The decision score of the soft LDA classification algorithm is the same as that of LDA:

$$\boldsymbol{\delta}^{\pi_3}(\mathbf{X}) = (\log p_1, \log p_2, \delta_3^{\pi_3}(\mathbf{X})),$$

where

$$\delta_3^{\pi_3}(\mathbf{X}) = \frac{1}{\sigma^2} \mathbf{X}^T \boldsymbol{\mu} - \frac{\|\boldsymbol{\mu}\|^2}{2\sigma^2} + \log p_3 = \frac{\|\boldsymbol{\mu}\|}{\sigma^2} X_1 - \frac{\|\boldsymbol{\mu}\|^2}{2\sigma^2} + \log p_3,$$

and

$$\text{softmax}(\boldsymbol{\delta}^{\pi_3}(\mathbf{X})) = \left( \frac{p_1}{p_1 + p_2 + \exp(\delta_3^{\pi_3}(\mathbf{X}))}, \frac{p_2}{p_1 + p_2 + \exp(\delta_3^{\pi_3}(\mathbf{X}))}, \frac{\exp(\delta_3^{\pi_3}(\mathbf{X}))}{p_1 + p_2 + \exp(\delta_3^{\pi_3}(\mathbf{X}))} \right).$$

Since

$$X_1 | Y \in \{1, 2\} \sim \mathcal{N}(0, \sigma^2) \quad \text{and} \quad X_1 | Y = 3 \sim \mathcal{N}(\|\boldsymbol{\mu}\|, \sigma^2),$$

we have

$$\delta_3^{\pi_3}(\mathbf{X}) | Y \in \{1, 2\} \sim \mathcal{N}\left(-\frac{\|\boldsymbol{\mu}\|^2}{2\sigma^2} + \log p_3, \frac{\|\boldsymbol{\mu}\|^2}{\sigma^2}\right) \quad \text{and} \quad \delta_3^{\pi_3}(\mathbf{X}) | Y = 3 \sim \mathcal{N}\left(\frac{\|\boldsymbol{\mu}\|^2}{2\sigma^2} + \log p_3, \frac{\|\boldsymbol{\mu}\|^2}{\sigma^2}\right).$$

Hence, when  $\|\boldsymbol{\mu}\|/\sigma^2 \rightarrow \infty$ , we have the following limits in probability.

$$\text{softmax}(\boldsymbol{\delta}^{\pi_3}(\mathbf{X})) | Y \in \{1, 2\} \rightarrow \left( \frac{p_1}{p_1 + p_2}, \frac{p_2}{p_1 + p_2}, 0 \right) \quad \text{and} \quad \text{softmax}(\boldsymbol{\delta}^{\pi_3}(\mathbf{X})) | Y = 3 \rightarrow (0, 0, 1).$$

Recall that soft LDA predicts  $Y$  by drawing a sample with size one from  $(1, [3], \text{softmax}(\boldsymbol{\delta}^{\pi_3}(\mathbf{X})))$ .

Hence, we have

$$\begin{aligned}\mathbb{P}(\phi_{\pi_3}^{\mathcal{C}^{\text{soft LDA}}, \mathcal{D}_\infty}(\mathbf{X}) = 1 \mid Y \in \{1, 2\}) &\rightarrow \frac{p_1}{p_1 + p_2}, \\ \mathbb{P}(\phi_{\pi_3}^{\mathcal{C}^{\text{soft LDA}}, \mathcal{D}_\infty}(\mathbf{X}) = 2 \mid Y \in \{1, 2\}) &\rightarrow \frac{p_2}{p_1 + p_2}, \\ \mathbb{P}(\phi_{\pi_3}^{\mathcal{C}^{\text{soft LDA}}, \mathcal{D}_\infty}(\mathbf{X}) = 3 \mid Y = 3) &\rightarrow 1.\end{aligned}$$

Similarly, we have

$$\begin{aligned}\mathbb{P}(\phi_{\pi_2}^{\mathcal{C}^{\text{soft LDA}}, \mathcal{D}_\infty}(\mathbf{X}) = 1 \mid \pi_2(Y) = 1) &\rightarrow 1, \\ \mathbb{P}(\phi_{\pi_2}^{\mathcal{C}^{\text{soft LDA}}, \mathcal{D}_\infty}(\mathbf{X}) = 2 \mid \pi_2(Y) = 2) &\rightarrow 1.\end{aligned}$$

Hence, the soft LDA algorithm approaches the oracle classification algorithm when  $\|\boldsymbol{\mu}\|/\sigma \rightarrow \infty$ .  $\square$

To numerically verify this result, we generate an array of simulated datasets with  $K_0 = 3$ ,  $K^* = 2$ ,  $l = 5$ ,  $n = 5000$ , and varying  $(p_1, p_2)$ , following the procedure described in Section 3 of the main text. Each dataset, one per  $(p_1, p_2)$  combination, contains 3 classes, with classes 1 and 2 as same-distributed. We set  $0.1 \leq p_1, p_2 \leq 0.7$  and  $p_1 + p_2 \leq 0.8$  for numerical stability. Then we apply LDA and soft LDA to each simulated dataset and compute the improvement of s-ITCA<sup>CV</sup> by combining classes 1 and 2.

Figure 12 shows that the numerical results of s-ITCA<sup>CV</sup> using LDA (lower left panel) match well with the results of p-ITCA using LDA (upper left panel). It is obvious that soft LDA (lower right panel) improves LDA (lower left panel) in terms class combination power (the proportion of blue area). This numerical result is also consistent with the theoretical result in Proposition 3 about the agreement of soft LDA (lower right panel) with oracle (upper right panel).

The improvement of soft LDA over LDA suggests that, for probabilistic classification algorithms, soft prediction of class labels has better power for class combination.

We also used the simulated datasets to numerically approximate the class-combination regions of three commonly used classification algorithms (see Supplementary Material Section 4.2), including random forest (0.2228), gradient boosting trees (0.1961) and neural networks (0.1972); the number

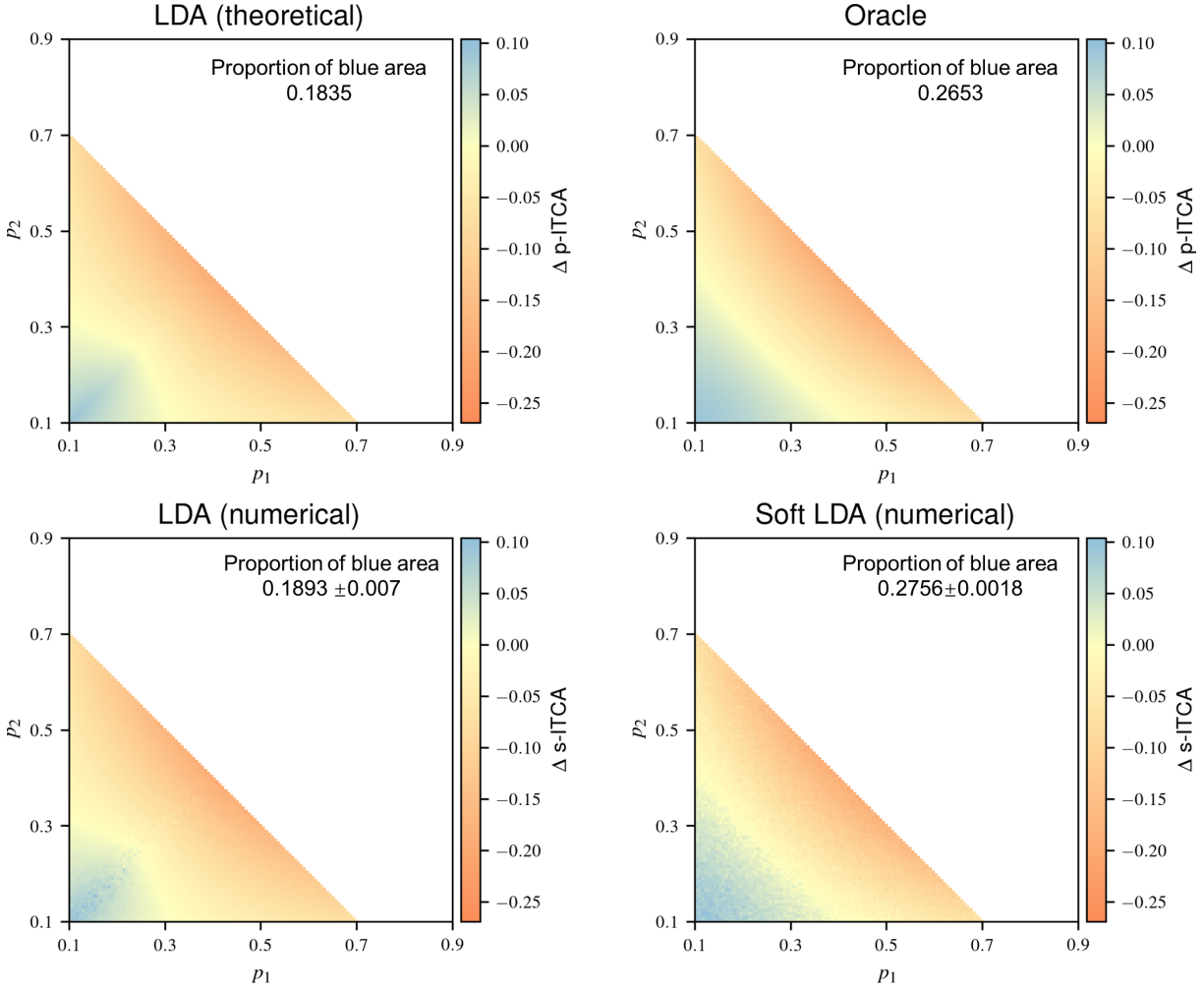


Figure 12: Regarding the combination of two same-distributed classes (with proportions  $p_1$  and  $p_2$ ), the improvement of  $s\text{-ITCA}^{\text{CV}}$  by class combination, i.e.,  $\Delta s\text{-ITCA}^{\text{CV}}(p_1, p_2; \mathcal{D}_t, \mathcal{C}) := s\text{-ITCA}^{\text{CV}}(\pi_{K_0-1}; \mathcal{D}_t, \mathcal{C}, p_1, p_2) - s\text{-ITCA}^{\text{CV}}(\pi_{K_0}; \mathcal{D}_t, \mathcal{C}, p_1, p_2)$  for  $0.1 \leq p_1, p_2 \leq 0.7$  and  $p_1 + p_2 \leq 0.8$ , of the LDA algorithm (bottom left;  $\mathcal{C}^{\text{LDA}}$ ) and the soft LDA algorithm (bottom right;  $\mathcal{C}^{\text{soft LDA}}$ ). The blue areas indicate the class-combination regions where  $\Delta s\text{-ITCA}^{\text{CV}}(p_1, p_2; \mathcal{D}_t, \mathcal{C}) > 0$  and thus the two classes will be combined. For comparison,  $\Delta p\text{-ITCA}$  of the LDA and oracle classification algorithm are shown in the same range of  $(p_1, p_2)$ . In each panel, the yellow boundary between the blue area and the orange area indicates the class-combination curve of the corresponding algorithm; the area of the class-combination region (the proportion of the blue area) is shown in the upper right corner. In the second row, the numerical results are the average of 5-fold CV and the standard deviations of the five folds are shown (divided by  $\sqrt{5}$ ).

in each parenthesis indicates the proportion of blue area. Among the five classification algorithms (LDA, soft LDA, random forest, gradient boosting trees, and neural networks), random forest is second only to soft LDA in terms of finding the true class combination, possibly due to its ensemble nature.

## Appendix C SEARCH SPACE PRUNING

Compared with the exhaustive search, the greedy search and BFS significantly reduce the number of times needed to compute s-ITCA. We note that if the following assumption holds for a classification algorithm, one can further prune the search space of possible class combinations.

**Assumption 1** (classification algorithm property). *Consider a classification algorithm  $\mathcal{C}$ , a training dataset  $\mathcal{D}_t$ . The property states that, for any  $K = 3, \dots, K_0$ , the algorithm  $\mathcal{C}$  satisfies the following inequality for any  $i, j \in [K]$  and the  $\pi_{K-1}^{(i,j)}$  that only combines the (observed or combined) classes  $i$  and  $j$ .*

$$\begin{aligned} & \sum_{k \in [K] \setminus \{i,j\}} \left[ -\mathbb{P} \left( \pi_{K-1}^{(i,j)}(Y) = k \right) \log \mathbb{P} \left( \pi_{K-1}^{(i,j)}(Y) = k \right) \right] \cdot \mathbb{P} \left( \phi_{\pi_{K-1}^{(i,j)}}^{\mathcal{C}, \mathcal{D}_t}(\mathbf{X}) = \pi_{K-1}^{(i,j)}(Y) \mid \pi_{K-1}^{(i,j)}(Y) = k \right) \\ \geq & \sum_{k \in [K] \setminus \{i,j\}} \left[ -\mathbb{P}(\pi_K(Y) = k) \log \mathbb{P}(\pi_K(Y) = k) \right] \cdot \mathbb{P} \left( \phi_{\pi_K}^{\mathcal{C}, \mathcal{D}_t}(\mathbf{X}) = \pi_K(Y) \mid \pi_K(Y) = k \right). \end{aligned} \quad (25)$$

*In other words, the total contribution of other classes (except classes  $i$  and  $j$ ) to p-ITCA does not decrease after classes  $i$  and  $j$  are combined.*

A sufficient condition for Assumption 1 is that a classification algorithm has the same class-conditional prediction accuracies, before and after class combination, for the classes that are not combined. We can easily verify that the oracle, LDA, soft LDA algorithms satisfy this sufficient condition and thus Assumption 1. In addition, Assumption 1 holds for the classification algorithms that use a one-vs-the-rest scheme.

Under Assumption 1, we derive the following condition for class combination by p-ITCA.

**Proposition 4** (class combination condition). *If Assumption 1 holds, classes  $i$  and  $j$  will be com-*

bined by p-ITCA if and only if:

$$\begin{aligned} & \mathbb{P} \left( \phi_{\pi_{K-1}^{(i,j)}}^{\mathcal{C}, \mathcal{D}_t}(\mathbf{X}) = \pi_{K-1}^{(i,j)}(Y) \mid Y \in \{i, j\} \right) \\ & > \frac{p_i \log p_i \mathbb{P}(\phi_{\pi_K}^{\mathcal{C}, \mathcal{D}_t}(\mathbf{X}) = Y \mid Y = i) + p_j \log p_j \mathbb{P}(\phi_{\pi_K}^{\mathcal{C}, \mathcal{D}_t}(\mathbf{X}) = Y \mid Y = j)}{(p_i + p_j) \log(p_i + p_j)}, \quad i, j \in [K]. \end{aligned} \quad (26)$$

*Proof.* The proof is straightforward. Classes  $i$  and  $j$  will be combined if and only if

$$\text{p-ITCA} \left( \pi_{K-1}^{(i,j)}; \mathcal{D}_t, \mathcal{C} \right) > \text{p-ITCA}(\pi_K; \mathcal{D}_t, \mathcal{C}), \quad (27)$$

which is equivalent to

$$\begin{aligned} & \sum_{k' \in [K-1]} \left[ -\mathbb{P} \left( \pi_{K-1}^{(i,j)}(Y) = k' \right) \log \mathbb{P} \left( \pi_{K-1}^{(i,j)}(Y) = k' \right) \right] \cdot \mathbb{P} \left( \phi_{\pi_{K-1}^{(i,j)}}^{\mathcal{C}, \mathcal{D}_t}(\mathbf{X}) = \pi_{K-1}^{(i,j)}(Y) \mid \pi_{K-1}(Y) = k' \right) \\ & > \sum_{k \in [K]} \left[ -\mathbb{P}(\pi_K(Y) = k) \log \mathbb{P}(\pi_K(Y) = k) \right] \cdot \mathbb{P} \left( \phi_{\pi_K}^{\mathcal{C}, \mathcal{D}_t}(\mathbf{X}) = \pi_K(Y) \mid \pi_K(Y) = k \right). \end{aligned} \quad (28)$$

Under Assumption 1, it is straightforward to see that (26) is a sufficient condition for (28), which completes the proof.  $\square$

Proposition 4 provides a rule for pruning the search space. The left-hand side of (26) must be no greater than 1. Hence, if the accuracies  $\mathbb{P}(\phi_{\pi_K}^{\mathcal{C}, \mathcal{D}_t}(\mathbf{X}) = Y \mid Y = i)$  and  $\mathbb{P}(\phi_{\pi_K}^{\mathcal{C}, \mathcal{D}_t}(\mathbf{X}) = Y \mid Y = j)$  are high enough such that the right-hand side is greater than 1, there is no way for (26) to hold, and we can remove  $\pi_{K-1}^{(i,j)}$  from the search space.

Our simulation results show that this pruning strategy is effective and can reduce the number of the s-ITCA evaluations by about half (Tables 3 in the main text and Table S3 in Supplementary Material).

## SUPPLEMENTARY MATERIAL

### 1. APPROXIMATE KL DIVERGENCE BETWEEN TWO GAUSSIAN MIXTURE MODELS

The KL divergence from a Gaussian distribution  $\mathcal{N}(\boldsymbol{\mu}_2, \boldsymbol{\Sigma}_2)$  to another Gaussian distribution  $\mathcal{N}(\boldsymbol{\mu}_1, \boldsymbol{\Sigma}_1)$  has the following closed-form

$$D_{\text{KL}}(\mathcal{N}(\boldsymbol{\mu}_1, \boldsymbol{\Sigma}_1) \parallel \mathcal{N}(\boldsymbol{\mu}_2, \boldsymbol{\Sigma}_2)) = \frac{1}{2} \log \frac{|\boldsymbol{\Sigma}_2|}{|\boldsymbol{\Sigma}_1|} + \frac{1}{2} \text{tr}(\boldsymbol{\Sigma}_2^{-1} \boldsymbol{\Sigma}_1) + \frac{1}{2} (\boldsymbol{\mu}_1 - \boldsymbol{\mu}_2)^T \boldsymbol{\Sigma}_2^{-1} (\boldsymbol{\mu}_1 - \boldsymbol{\mu}_2) - \frac{d}{2}. \quad (29)$$

However, there exists no closed-form KL divergence for Gaussian mixture models (GMMs). Durrieu *et al.* gave the lower and upper bounds for approximating the KL divergence from one GMM to another [Durrieu et al., 2012]. Let  $\mathcal{F} := \sum_{i=1}^K p_i^f \mathcal{N}(\boldsymbol{\mu}_i^f, \boldsymbol{\Sigma}_i^f)$  be a Gaussian mixture model; denote  $\mathcal{F}_i := \mathcal{N}(\boldsymbol{\mu}_i^f, \boldsymbol{\Sigma}_i^f)$  and  $f_i$  as the probability density function (PDF) of  $\mathcal{F}_i$ . Accordingly, denote  $\mathcal{G} := \sum_{j=1}^{K'} p_j^g \mathcal{N}(\boldsymbol{\mu}_j^g, \boldsymbol{\Sigma}_j^g)$ ,  $\mathcal{G}_j := \mathcal{N}(\boldsymbol{\mu}_j^g, \boldsymbol{\Sigma}_j^g)$ , and  $g_j$  as the PDF of  $\mathcal{G}_j$ . The lower bound of the KL divergence from  $\mathcal{G}$  to  $\mathcal{F}$  is

$$D_{\text{KL}}(\mathcal{F} \parallel \mathcal{G}) \geq \underbrace{\sum_{i=1}^K p_i^f \log \frac{\sum_{l=1}^K p_l^f \exp(-D_{\text{KL}}(\mathcal{F}_l \parallel \mathcal{F}_l))}{\sum_{j=1}^{K'} p_j^g t_{ij}}}_{D_{\text{lower}}(\mathcal{F} \parallel \mathcal{G})} - \sum_{i=1}^K p_i^f H(\mathcal{F}_i), \quad (30)$$

where  $t_{ij}$  is the normalization constant:

$$t_{ij} := \int_{\mathcal{X}} f_i(\mathbf{x}) g_j(\mathbf{x}) d\mathbf{x}, \quad (31)$$

which is given by [Ahrendt, 2005]:

$$\log t_{ij} = -\frac{d}{2} \log 2\pi - \frac{1}{2} \log |\boldsymbol{\Sigma}_i^f + \boldsymbol{\Sigma}_j^g| - \frac{1}{2} (\boldsymbol{\mu}_j^g - \boldsymbol{\mu}_i^f)^T (\boldsymbol{\Sigma}_i^f + \boldsymbol{\Sigma}_j^g)^{-1} (\boldsymbol{\mu}_j^g - \boldsymbol{\mu}_i^f), \quad (32)$$

and  $H(\cdot)$  is the entropy of Gaussian distribution:

$$H(\mathcal{F}_i) = \frac{1}{2} \log(2\pi e)^d |\boldsymbol{\Sigma}_i^f| \quad (33)$$

Similarly, the upper bound of the KL divergence from  $\mathcal{G}$  to  $\mathcal{F}$  is:

$$D_{\text{KL}}(f||g) \leq \underbrace{\sum_{i=1}^K p_i^f \log \frac{\sum_{l=1}^K p_l^f t_{il}}{\sum_{j=1}^{K'} p_j^g \exp(-D_{\text{KL}}(\mathcal{F}_i||\mathcal{G}_j))}}_{D_{\text{upper}}(\mathcal{F}||\mathcal{G})}. \quad (34)$$

[Durrieu et al., 2012] proposed using the average of  $D_{\text{upper}}$  and  $D_{\text{lower}}$  to approximate  $D_{\text{KL}}$ :

$$D_{\text{approx}}(\mathcal{F}||\mathcal{G}) := \frac{D_{\text{upper}}(\mathcal{F}||\mathcal{G}) + D_{\text{lower}}(\mathcal{F}||\mathcal{G})}{2}. \quad (35)$$

The experimental results in [Durrieu et al., 2012] show that (35) works well. Hence, we use  $D_{\text{approx}}$  to approximate the two KL divergence functions in the definition of CKL Equation (9) in Appendix.

## 2. MORE SIMULATION DETAILS

### 2.1 The additional results of the performance of six criteria on simulated datasets

Here we present the performance of the six criteria on the simulated data. The datasets are generated by the procedures described in the main text Section 3.1. Table S1 shows the performance of the six criteria where the simulated datasets are generated with  $K_0 = 6$ . The results are consistent with that in the main text Table 2; ITCA outperforms alternative class combination criteria and only failed when  $K^* = 2$ . Table S2 shows the proposed search strategies, namely greedy search and BFS, are almost as effective as the exhaustive search in finding the true class combinations where  $K_0 = 8$ . Table S3 shows that the two search strategies works well even when the number of observed classes  $K_0$  is large.

### 2.2 Additional results where ITCA missed the true class combination

Table S1 and Table 2 in the main text have shown that ITCA is effective for finding the true class combination; ITCA using the LDA classification algorithm missed the true combination on 5 out of 31 datasets when  $K_0 = 6$  and on 7 out of 120 datasets when  $K_0 = 8$ .

Tables S4 and S5 list the 5 and 7 true class combinations missed by ITCA using LDA for  $K_0 = 6$  and 8, respectively. Notably, all these true class combinations belong to  $K^* = 2$ , i.e., the scenario with only two combined classes, where obviously at least one combined class must have a

Criterion	<u># successes</u>	Average	Max	<u># successes</u>	Average	Max
	<u># datasets</u>	Hamming	Hamming	<u># datasets</u>	Hamming	Hamming
	LDA			RF		
ACC	1/31	2.03	4	1/31	2.03	4
MI	8/31	1.42	4	6/31	1.65	4
AAC	9/31	1.03	3	8/31	1.30	3
CKL	7/31	2.42	5	1/31	2.13	4
PE	22/31	0.55	3	22/31	0.42	3
ITCA	<b>26/31</b>	<b>0.23</b>	<b>2</b>	<b>26/31</b>	<b>0.19</b>	<b>2</b>

Table S1: The performance of six criteria on the 31 simulated datasets with  $K_0 = 6$ . The best result in each column is boldfaced.

Strategy	<u># successes</u>	Average	Max	Average # class
	<u># datasets</u>	Hamming	Hamming	combinations examined
Exhaustive	26/31	0.23	2	31.00
Greedy search	26/31	0.23	2	12.13
BFS	26/31	0.19	2	19.19
Greedy (pruned)	26/31	0.19	2	5.71
BFS (pruned)	26/31	0.19	2	8.84

Table S2: Performance of ITCA using five search strategies and LDA on the 31 simulated datasets with  $K_0 = 6$ .

Strategy	<u># successes</u>	Average	Max	Average # class
	<u># datasets</u>	Hamming	Hamming	combinations examined
Greedy	50/50	0.00	0	150.08
BFS	50/50	0.00	0	27226.84
Greedy (pruned)	50/50	0.00	0	87.70
BFS (pruned)	50/50	0.00	0	17155.82

Table S3: Performance of ITCA using five search strategies and LDA on the 50 simulated datasets with  $K_0 = 20$ .

proportion no less than 0.5. Based on our theoretical analysis in Appendix B.1, we know that ITCA would not combine two same-distributed classes when the combined class' proportion is large (see Appendix Figure 11, right panel). Hence, it is expected that ITCA is unlikely to find the true class combination when  $K^* = 2$ . In other words, ITCA is unsuitable for combining observed classes, even if ambiguous, into a large class that dominates in proportion.

On the other hand, ITCA has successfully found the true class combinations when  $K^* \geq 3$  for both  $K_0 = 6$  and 8, demonstrating its effectiveness.

True combination	ITCA-guided combination
$\{(1, 2, 3, 4, 5), 6\}$	$\{1, 2, (3, 4), (5, 6)\}$
$\{(1, 2, 3, 4), (5, 6)\}$	$\{1, 2, (3, 4), (5, 6)\}$
$\{(1, 2, 3), (4, 5, 6)\}$	$\{1, 2, (3, 4), (5, 6)\}$
$\{(1, 2), (3, 4, 5, 6)\}$	$\{1, 2, (3, 4), (5, 6)\}$
$\{1, (2, 3, 4, 5, 6)\}$	$\{1, 2, (3, 4), (5, 6)\}$

Table S4: True class combinations missed by ITCA in Table S1 (simulation study with  $K_0=6$ ).

True combination	ITCA-guided combination
$\{(1, 2, 3, 4, 5, 6, 7), 8\}$	$\{1, 2, 3, 4, (5, 6), (7, 8)\}$
$\{(1, 2, 3, 4, 5, 6), (7, 8)\}$	$\{1, 2, 3, 4, (5, 6), (7, 8)\}$
$\{(1, 2, 3, 4, 5), (6, 7, 8)\}$	$\{1, 2, 3, 4, (5, 6), (7, 8)\}$
$\{(1, 2, 3, 4), (5, 6, 7, 8)\}$	$\{1, 2, 3, 4, (5, 6), (7, 8)\}$
$\{(1, 2, 3), (4, 5, 6, 7, 8)\}$	$\{1, 2, 3, 4, (5, 6), (7, 8)\}$
$\{(1, 2), (3, 4, 5, 6, 7, 8)\}$	$\{1, 2, 3, 4, (5, 6), (7, 8)\}$
$\{1, (2, 3, 4, 5, 6, 7, 8)\}$	$\{1, 2, 3, 4, (5, 6), (7, 8)\}$

Table S5: True class combinations missed by ITCA with LDA in Table 2 (simulation study with  $K_0 = 8$ ).

### 2.3 Comparison of the six criteria

We also evaluate ITCA using random forest (RF) as the classification algorithm. For the true class combination  $\pi_3^* = \{(1, 2), (3, 4), (5, 6)\}$ , the comparison results of ITCA versus the five alternative criteria using RF (Figure S1) are consistent with those using LDA (Figure 2 in the main text).

For another true class combination  $\pi_5^* = \{(1, 2), 3, 4, 5, 6\}$ , the results of the six criteria using LDA are shown in Figure S2. Among the six criteria, only AAC, PE and ITCA find the true class combination. ITCA outperforms the alternative criteria including PE by having the largest gap

between the true class combination and the other class combinations. Specifically, the ITCA value of the true combination is 9% higher than the value of the second-best class combination, while this improvement percentage is only 5.1% for PE. When RF is used as the classification algorithm, the results stay consistent (Figure S3).

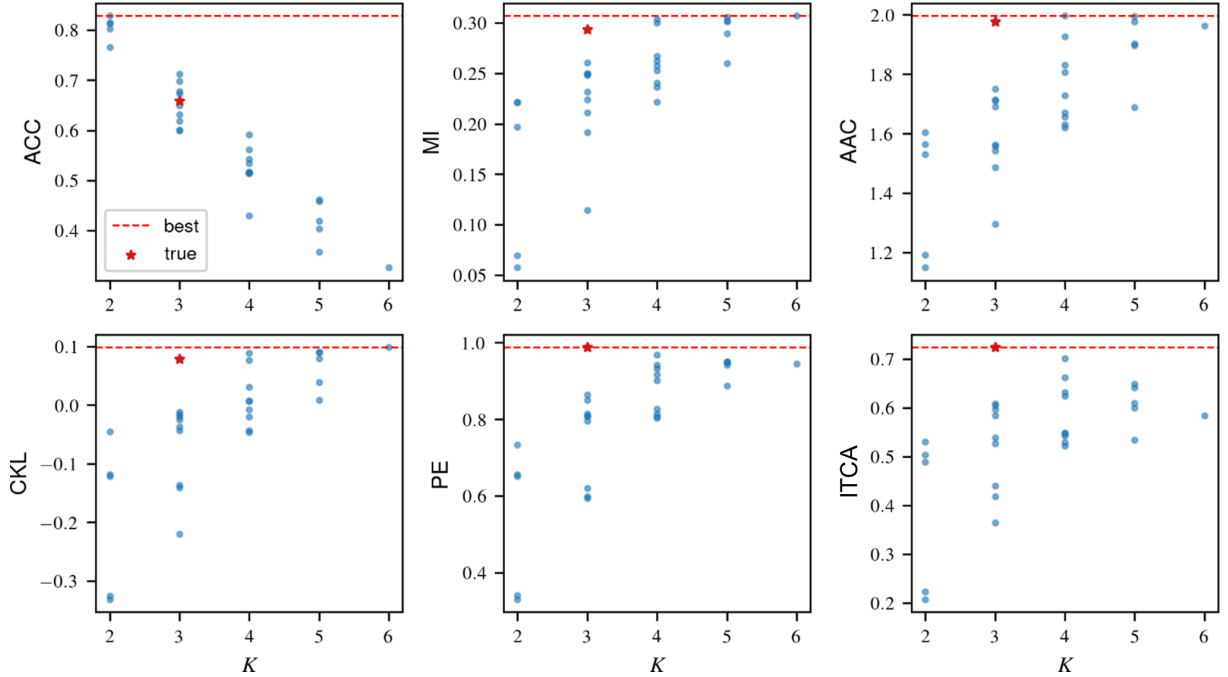


Figure S1: Comparison of ITCA and five other criteria using RF as the classification algorithm. The dataset is generated with  $K_0 = 6$ ,  $K^* = 3$ ,  $l = 3$ ,  $\sigma = 1.5$ ,  $n = 2000$ , and  $d = 5$ . The true class combination is  $\pi_3^* = \{(1, 2), (3, 4), (5, 6)\}$ . For each criterion (panel), the 31 blue points correspond to the 31 class combinations  $\pi_K$ 's with  $K = 2, \dots, 6$ . The true class combination  $\pi_{K^*}^*$  is marked with the red star, and the best value for each criterion is indicated by a horizontal dashed line. The true class combination is only found by PE and ITCA without close ties.

#### 2.4 Alternative definition of the adjusted accuracy (AAC)

In Appendix A, we define the AAC by assigning each (observed or combined) class the weight as the inverse of its class proportion. In other words, smaller classes receive larger weights because they are intuitively more difficult to predict. Here we refer to this definition as ‘‘AAC (proportion)’’ for clarity.

An alternative approach is to weigh each (observed or combined) class by the inverse of the number of observed classes it corresponds to. For example, an observed classes would have a weight of 1, while a class combined from two observed classes would have a weight of  $1/2$ . The intuition is that a class is easier to predict if it is combined from more observed classes. Hence, we refer to

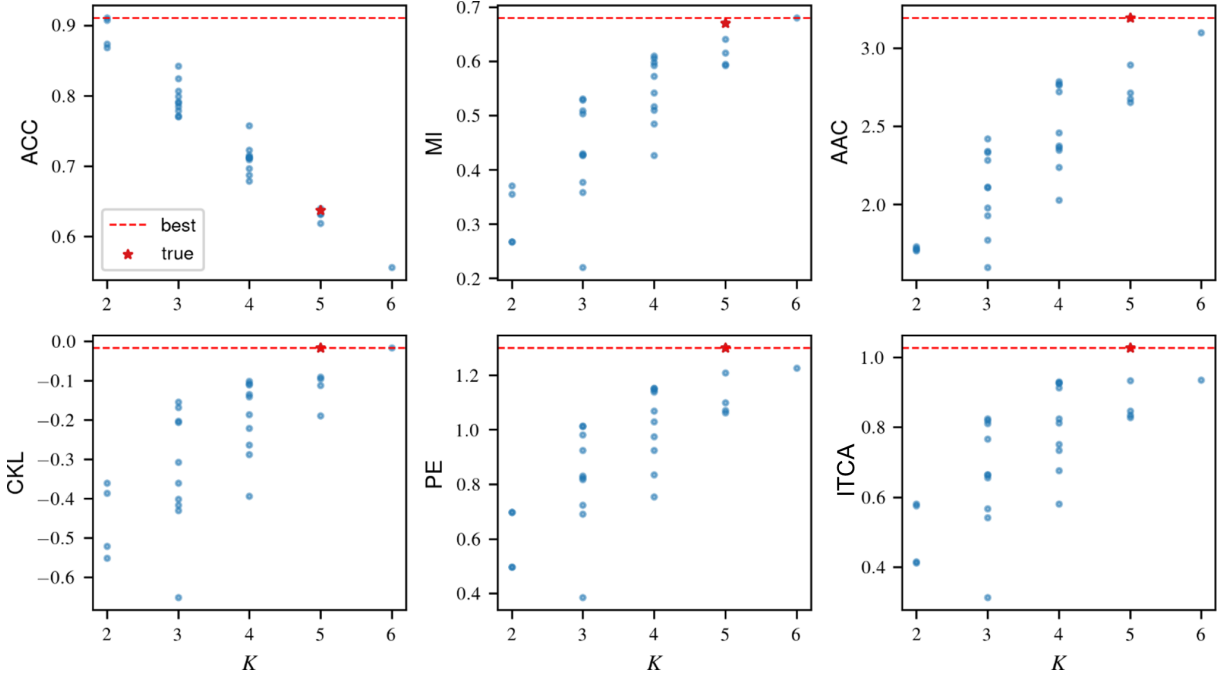


Figure S2: Comparison of ITCA and five other criteria using LDA as the classification algorithm. The dataset is generated with  $K_0 = 6$ ,  $K^* = 5$ ,  $l = 3$ ,  $\sigma = 1.5$ ,  $n = 2000$ , and  $d = 5$ . The true class combination is  $\pi_5^* = \{(1, 2), 3, 4, 5, 6\}$ . For each criterion (panel), the 31 blue points correspond to the 31 class combinations  $\pi_K$ 's with  $K = 2, \dots, 6$ . The true class combination  $\pi_{K^*}$  is marked with the red star, and the best value for each criterion is indicated by a horizontal dashed line. The true class combination is found by AAC, PE and ITCA without close ties.

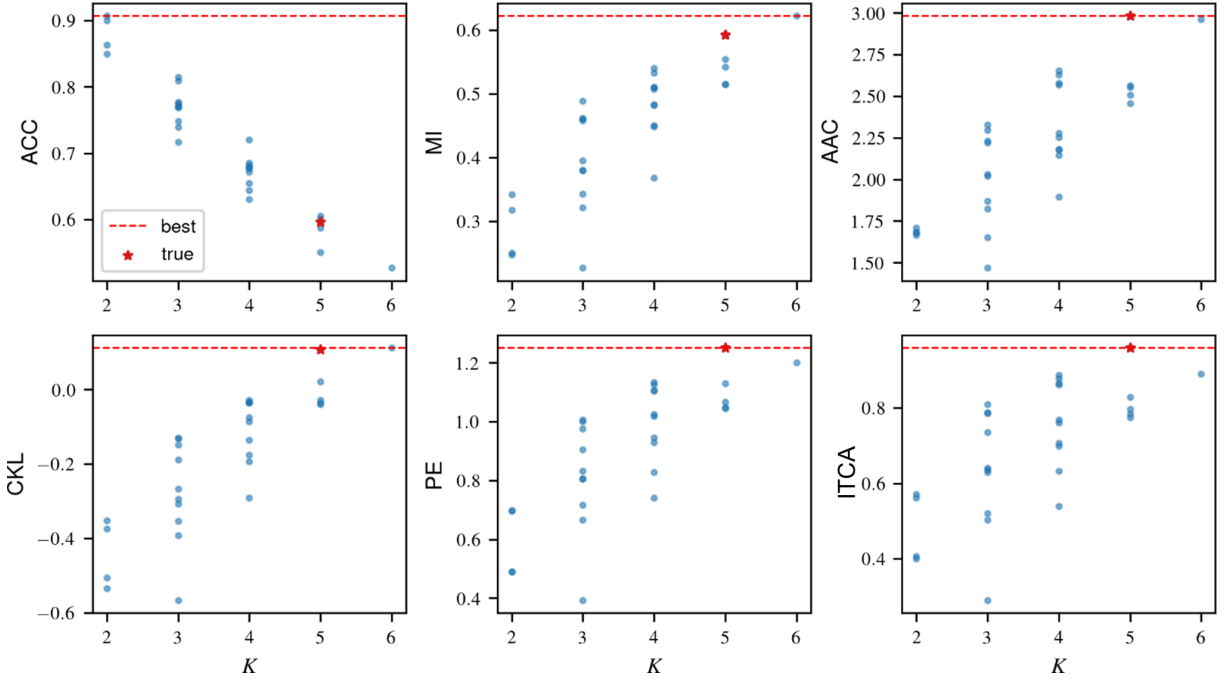


Figure S3: Comparison of ITCA and five other criteria using RF as the classification algorithm. The dataset is generated with  $K_0 = 6$ ,  $K^* = 5$ ,  $l = 3$ ,  $\sigma = 1.5$ ,  $n = 2000$ , and  $d = 5$ . The true class combination is  $\pi_5^* = \{(1, 2), 3, 4, 5, 6\}$ . For each criterion (panel), the 31 blue points correspond to the 31 class combinations  $\pi_K$ 's with  $K = 2, \dots, 6$ . The true class combination  $\pi_{K^*}^*$  is marked with the red star, and the best value for each criterion is indicated by a horizontal dashed line. The true class combination is found by PE and ITCA without close ties.

this alternative definition as “AAC (cardinality)”:

$$\text{AAC (cardinality)}^{\text{CV}}(\pi_K; \mathcal{D}, \mathcal{C}) := \frac{1}{R} \sum_{r=1}^R \frac{1}{|\mathcal{D}_e^r|} \sum_{(\mathbf{X}_i, Y_i) \in \mathcal{D}_e^r} \frac{\mathbb{I}(\phi_{\pi_K}^{\mathcal{C}, \mathcal{D}_e^r}(\mathbf{X}_i) = \pi_K(Y_i))}{|\pi_K^{-1}(\pi_K(Y_i))|}, \quad (36)$$

where the dataset  $\mathcal{D}$  is randomly split into  $R$  equal-sized folds, with the  $r$ -th fold  $\mathcal{D}_e^r$  serving as the evaluation data and the union of the remaining  $R - 1$  folds  $\mathcal{D}_t^r$  serving as the training data,  $\hat{p}_{k_0}$  is the proportion of the  $k_0$ -th original class in  $\mathcal{D}$ , so the denominator  $|\pi_K^{-1}(\pi_K(Y_i))|$  is the number of original classes contained in the combined class  $Y_i$ . In the following text, we refer to  $\text{AAC (cardinality)}^{\text{CV}}$  as the AAC (cardinality) criterion.

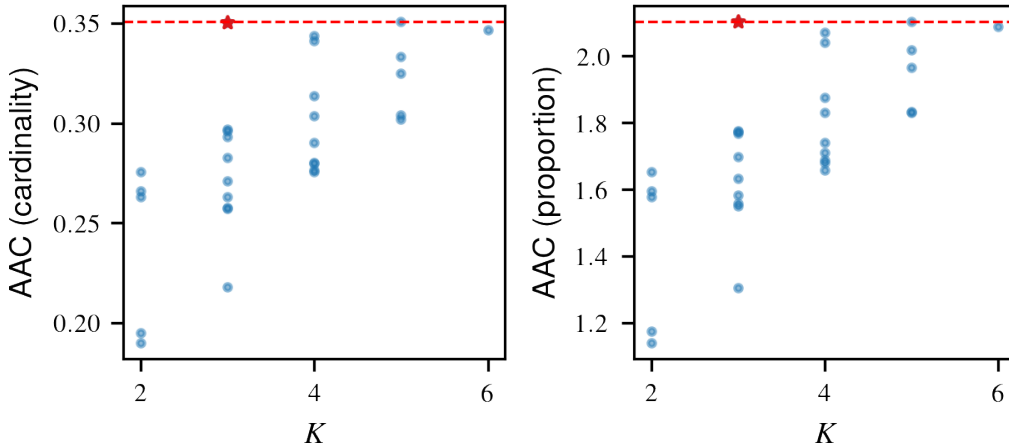


Figure S4: Comparison of AAC (cardinality) and AAC (proportion) using LDA as the classification algorithm. The dataset is generated with  $K_0 = 6$ ,  $K^* = 5$ ,  $l = 3$ ,  $\sigma = 1.5$ ,  $n = 2000$ , and  $d = 5$ . The true class combination is  $\pi_5^* = \{(1, 2), 3, 4, 5, 6\}$ . For each criterion (panel), the 31 blue points correspond to the 31 class combinations  $\pi_K$ 's with  $K = 2, \dots, 6$ . The true class combination  $\pi_{K^*}^*$  is marked with the red star, and the best value for each criterion is indicated by a horizontal dashed line.

Criterion	# successes	Average	Max	# successes	Average	Max
	# datasets	Hamming	Hamming	# datasets	Hamming	Hamming
	$K_0 = 6$			$K_0 = 8$		
AAC (cardinality)	1/31	1.90	3	5/127	2.56	6
AAC (proportion)	9/31	1.03	3	15/127	2.02	6

Table S6: Comparison of two definitions of AAC using LDA on simulated datasets

Figure S4 shows the comparison of AAC (cardinality) and AAC (proportion) for finding  $\pi_5^* = \{(1, 2), 3, 4, 5, 6\}$ . Table S6 lists the overall comparison results of AAC (cardinality) and AAC (proportion).

(proportion) in the simulation studies with  $K_0 = 6$  and 8 (Section 3.1 in the main text). The results show that AAC (proportion) outperforms AAC (cardinality) by finding more true class combinations. Hence, we use AAC (proportion) in the main text.

### 3. MORE APPLICATION DETAILS

#### 3.1 Prognosis of rehabilitation outcomes of traumatic brain injury patients

The Casa Colina dataset includes Functional Independence Measure (FIM) of 17 activities at admission and discharge. For each activity, the discharge FIM is coded as an ordinal outcome with  $K_0 = 7$  levels by physical therapists. Table S7 lists the 17 activities.

Category	Activity
Motor	Eating
	Grooming
	Bathing
	Dressing - upper body
	Dressing - lower body
	Toileting
	Bladder control
	Bower control
	Transfer - bed
	Transfer - toilet
	Transfer - tub
Stairs	
Cognition	Comprehension
	Expression
	Social interaction
	Problem solving
	Memory

Table S7: 17 activities in the Casa Colina dataset

We use RF with 1000 trees as the classification algorithm (with default hyperparameters in the Python `sklearn` package [Pedregosa et al., 2011]), and we compute the ITCA for all allowed class combinations. Since there are seven ordinal outcomes, the number of allowed class combinations is  $2^{7-1} - 1 = 63$ .

Figure S5 shows the ITCA values of all allowed class combinations for each activity. Interestingly, ITCA suggests that most activities should have their outcomes combined into four or five classes, largely consistent with the experts’ suggestion (Table S8). ITCA-guided class combination leads to larger-than-expect increases in the prediction accuracy for many activities, e.g., DressingUpper (Table S9).

Activity	$\pi_K^*$	$K$
Toileting	{1, 2, (3, 4), 5, (6, 7)}	5
Eating	{(1, 2, 3, 4), 5, 6, 7}	4
Grooming	{1, (2, 3, 4), 5, 6, 7}	5
Bathing	{1, (2, 3), 4, 5, (6, 7)}	5
DressingUpper	{(1, 2), (3, 4), 5, (6, 7)}	4
DressingLower	{1, (2, 3), 4, 5, (6, 7)}	5
BladderCtrl	{1, (2, 3, 4), 5, 6, 7}	5
BowelCtrl	{1, 2, (3, 4, 5), 6, 7}	5
BedTransfer	{1, (2, 3), 4, 5, 6, 7}	6
ToiletTransfer	{1, (2, 3), 4, 5, (6, 7)}	5
TubTransfer	{1, (2, 3), 4, 5, (6, 7)}	5
Stairs	{1, (2, 3, 4), (5, 6, 7)}	3
Comprehension	{(1, 2), (3, 4), 5, 6, 7}	5
Expression	{(1, 2, 3), (4, 5), 6, 7}	4
SocialInteraction	{(1, 2, 3), (4, 5), 6, 7}	4
ProblemSolving	{1, (2, 3), 4, 5, 6, 7}	6
Memory	{(1, 2, 3), 4, 5, 6, 7}	5

Table S8: Class combinations suggested by ITCA for the 17 activities.

### 3.2 Prediction of glioblastoma cancer patients’ survival time

**Description of the GBM survival dataset.** The original data consists of 577 patients and 23 features. The dataset contains diagnosis age, gender, gene expression subtypes, therapy and other clinical information.

**Data processing.** We first drop features that are not relevant to the survival prediction, including “Study ID”, “Patient ID”, “Sample ID”, “Cancer Type Detailed”, “Number of Samples Per Patient”, “Oncotree Code”, “Somatic Status”, “Sample Type” and “Cancer Type”. We then impute the missing entries by the feature means and use one-hot coding to represent the categorical features. Since some patients received multiple types of therapies (out of 10 types), we use 10-dimensional binary vectors to indicate patients’ therapy types. After data processing, there are 36 features in

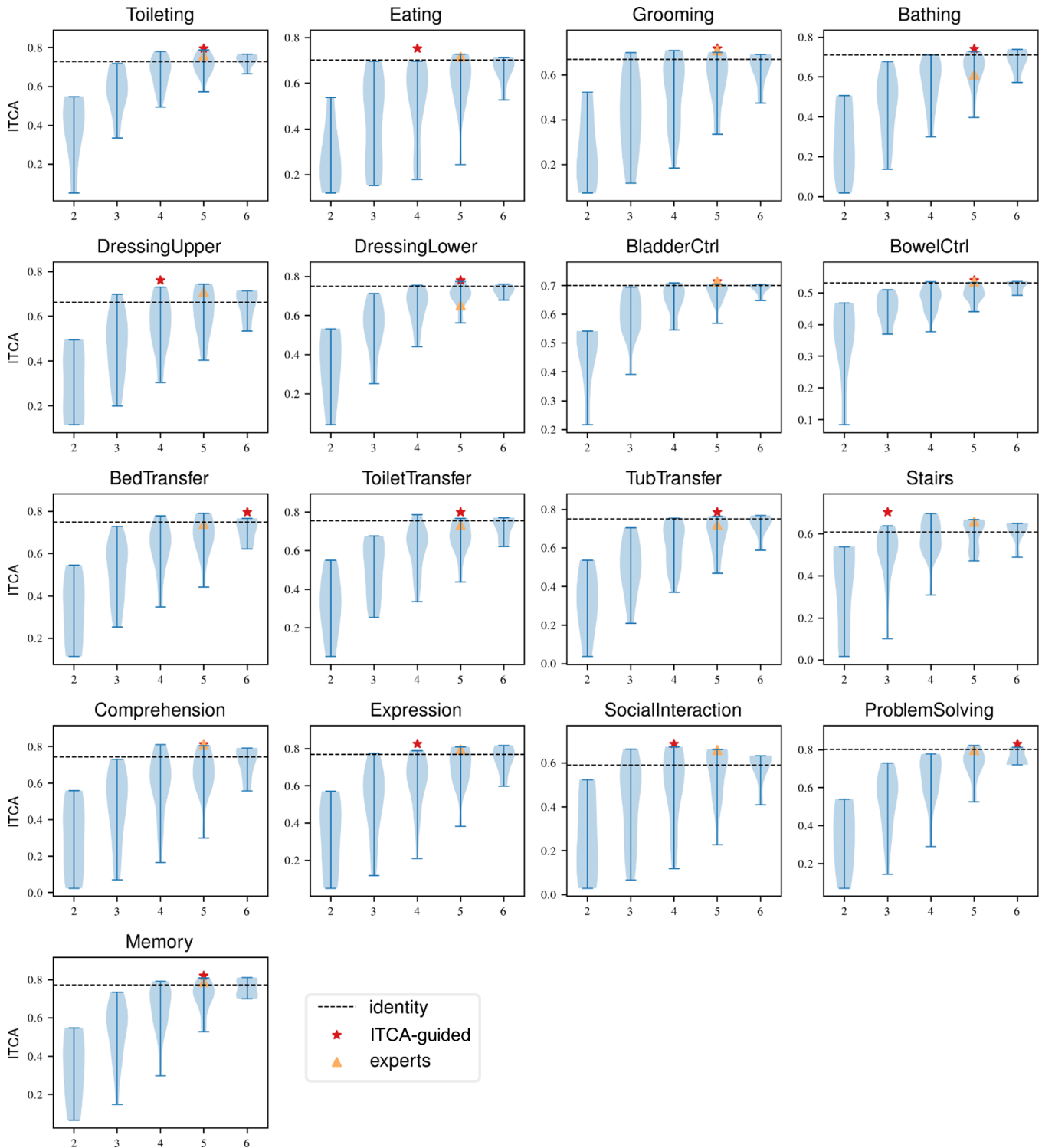


Figure S5: ITCA values of the 63 allowed class combinations for the 17 activities in the Casa Colina dataset. The violin plots show the distribution of ITCA values for each combined class number  $K$ . The dashed horizontal lines indicate the ITCA values of the identity class combination (i.e.,  $\pi_7$  with no classes combined).

Activity	ACC (%)			ITCA (%)			$K$
	Original	Experts	ITCA	Original	Experts	ITCA	
Toileting	44.12(1.26)	55.33(1.13)	52.50(1.05)	72.70(3.29)	75.76(3.16)	79.39(0.87)	5
Eating	57.31(1.36)	57.08(1.18)	61.21(1.24)	70.14(3.94)	71.71(3.20)	75.35(0.54)	4
Grooming	46.36(2.44)	52.44(1.08)	49.94(0.49)	66.91(2.20)	70.97(2.19)	71.73(3.99)	5
Bathing	44.25(1.35)	62.18(1.16)	50.10(1.83)	71.15(1.76)	61.18(2.47)	74.21(2.35)	5
DressingUpper	42.20(1.98)	51.62(1.30)	57.28(1.11)	66.33(3.07)	70.89(1.86)	76.11(3.85)	4
DressingLower	39.76(3.69)	58.45(1.40)	49.74(1.05)	74.88(4.33)	65.23(2.96)	77.93(2.07)	5
BladderCtrl	58.19(0.92)	57.67(2.01)	58.32(2.08)	70.06(3.09)	71.54(2.51)	71.54(2.51)	5
BowelCtrl	65.14(1.43)	65.01(1.90)	64.81(0.79)	53.13(1.28)	53.56(1.27)	53.93(1.96)	5
BedTransfer	42.85(2.21)	55.04(0.95)	46.75(1.46)	74.91(1.30)	74.04(1.54)	79.57(2.86)	6
ToiletTransfer	45.87(1.53)	57.18(2.26)	51.27(0.72)	75.45(1.59)	73.19(2.99)	79.95(3.18)	5
TubTransfer	48.80(0.98)	58.61(1.48)	50.42(1.21)	75.07(2.42)	71.97(2.39)	78.56(2.09)	5
Stairs	52.79(1.26)	59.36(1.47)	65.72(1.02)	60.89(2.39)	65.79(0.87)	70.32(1.36)	3
Comprehension	50.78(1.98)	58.80(1.36)	56.43(2.09)	74.42(1.62)	80.98(3.32)	81.41(2.32)	5
Expression	48.21(1.72)	58.87(1.57)	62.48(1.18)	76.94(2.57)	79.60(2.92)	82.52(2.89)	4
SocialInteraction	51.07(1.07)	56.40(1.80)	60.17(2.35)	59.01(2.81)	65.86(1.30)	68.63(3.93)	4
ProblemSolving	45.03(2.17)	58.84(1.50)	50.03(1.62)	80.13(2.46)	79.98(3.70)	83.03(3.87)	6
Memory	43.34(2.15)	60.04(2.35)	55.33(1.93)	77.23(2.25)	78.83(2.37)	82.02(4.01)	5

Table S9: ACC and ITCA values of the original classes (identical class combination), expert-suggested class combination (the same 5 combined classes for all activities), and ITCA-guided class combinations (listed in Table S8; specific to each activity; the number of combined classes  $K$  in the last column).

total.

**Censored cross entropy loss function.** The neural network is configured to output  $K$  values, and it uses a softmax function to normalize the outputs as  $K$  probabilities that sum to one. The most commonly used loss function for classification is the cross entropy (CE) defined as

$$\text{CE} = - \sum_{i=1}^n \sum_{k=1}^K \mathbb{I}(Y_i = k) \log[\phi_{\pi_K}^{\text{NN}, \mathcal{D}_t}(\mathbf{X}_i)]_k, \quad (37)$$

where  $\{(\mathbf{X}_i, Y_i)\}_{i=1}^n$  is the evaluation dataset,  $\mathcal{D}_t$  is the training dataset,  $[\phi_{\pi_K}^{\text{NN}, \mathcal{D}_t}(\mathbf{X}_i)]_k$  is the  $k$ -th entry of the output vector of the neural network trained for predicting the combined classes indicated by  $\pi_K$ . However, the survival data usually contain many right censored data. The CE loss function is not compatible with such data. To make full use of the censorship information, we introduce the censored cross entropy (CCE):

$$\text{CCE} = - \sum_{i=1}^n \left[ \sum_{k=1}^K O_i I(Y_i = k) \log[\phi_{\pi_K}^{\text{NN}, \mathcal{D}_t}(\mathbf{X}_i)]_k - (1 - O_i) \sum_{k > Y_i} \frac{\hat{p}_k}{1 - \sum_{l \leq Y_i} \hat{p}_l} \log[\phi_{\pi_K}^{\text{NN}, \mathcal{D}_t}(\mathbf{X}_i)]_k \right], \quad (38)$$

where  $O_i$  is binary with  $O_i = 0$  indicating that  $\mathbf{X}_i$  is right censored, and  $\hat{p}_k$  is the proportion of the  $k$ -th (observed or combined) class in  $\mathcal{D}$ . When  $\mathbf{X}_i$  is not censored, its contribution to CCE is the same as to CE; when  $\mathbf{X}_i$  is censored, we compute its contribution to CCE as the cross entropy between the output sub-vector (for the classes later than  $Y_i$ ) and the conditional distribution that the disease occurs later than  $Y_i$ . The empirical results show that the neural network trained with the CCE loss outperforms that with the CE loss (Figure S6).

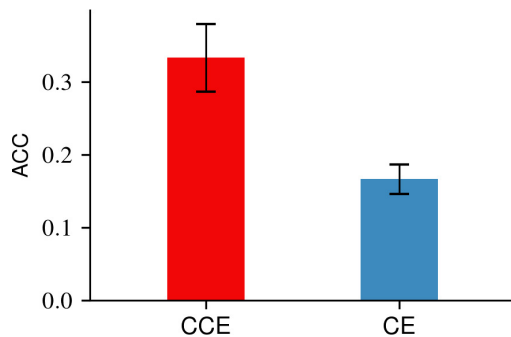


Figure S6: Performance of neural networks trained with the CCE and CE losses. There are  $K = 12$  ordinal classes. The neural networks have three hidden layers with 40 hidden units and the ReLU activation function.

gender_age		
device_id	gender	age
1234	Male	21

app_events			
event_id	app_id	is_installed	is_active
4321	1212	1	1

phone_brand_device_model		
device_id	brand	model
1234	XX	YY

app_labels	
app_id	label_id
1212	game

events		
device_id	event_id	timestamp
1234	4321	2016/1/1-22:00

Figure S7: A view of the TalkingData mobile user demographics dataset. We use five CSV files to construct the features and class labels. Here the five tables are excerpts from the five files and list the relevant fields only.

**Experiment setting.** We implement the neural network with PyTorch [Paszke et al., 2017]. Specifically, we use a three-layered neural network with 40 hidden units each layer. Experimental results show that the ReLU activation outperforms the sigmoid activation function. We use the SGD optimizer with 0.001 learning rate, 0.9 momentum and 0.01 weight decay. Batch size is 64, and we stop the training after 150 epochs.

### 3.3 Prediction of user demographics using mobile phone behavioral data

**Description of the TalkingData mobile user demographics dataset.** This dataset includes several comma separate values (CSV) files as shown in Figure S7. Our training dataset contains 74645 unique device id. The task is to predict a user’s gender and age group (gender\_age table in Figure S7) from his/her phone brand and the applications installed on his/her phone. Readers may refer to the official website<sup>6</sup> for a complete description of the dataset.

**Data processing.** We first construct the device types by concatenating the mobile phone brand and model strings, resulting in around 1600 different types. We denote the device types that appear less than 50 times in the dataset as “others”. There are 440 device types remaining.

We then construct the features of the user behavioral data. Specifically, we use event logs to count which applications are installed on the device. Since there are too many applications, we

<sup>6</sup><https://www.kaggle.com/c/talkingdata-mobile-user-demographics/data>

use the labels of applications instead (app\_label in Figure S7). We also count the users’ earliest, latest, and most used time periods of phone usage every day (24 hours) by the events log. The applications installed are represented by a binary vector, and the device types are encoded with one-hot encoding. We note that the constructed feature vectors are very sparse and there are many users who do not have any activities. We filter out the users whose features vectors have fewer than 5 nonzero values. In summary, there are 23,556 users and 818 features after the data processing.

**Experiment setting.** We use the gradient boost decision tree model (GBT) in XGBoost [Chen et al., 2016] as the classification algorithm. GBT has several critical hyperparameters that may influence the prediction performance, including “subsample” corresponding to the subsample ratio of the training instances, “colsample\_bytree” corresponding to the subsample ratio of columns when constructing each tree, and “gamma” corresponding to the partition on a leaf node. We adopt a greedy strategy to choose the best hyperparameters by the estimated accuracy on the test dataset. Specifically, we first use grid search to find the best value of “subsample” and then fix it to find the best value of “colsample\_bytree”. We fix the three hyperparameters as 0.9, 1.0 and 0, respectively. The learning rate is 0.05 in all experiments.

## 4. MORE THEORETICAL REMARKS

### 4.1 Class-combination regions of the oracle and LDA classification algorithms

Denote  $f_1(p) := p^2 \log p$ . The class-combination region of the oracle classification algorithm can be rewritten as

$$\text{CR}(\pi_{K_0-1} || \pi_{K_0}; \mathcal{C}^*) = \{(p_1, p_2) \in \Omega : f_1(p_1) + f_1(p_2) - f_1(p_{1+2}) > 0\}, \quad (39)$$

where  $\Omega = \{(p_1, p_2) : p_1 > 0, p_2 > 0, p_1 + p_2 < 1\} \subset [0, 1]^2$ , and  $p_{1+2} = p_1 + p_2$ .

Denote  $f_2(p) := p \log p$ . The class-combination region (as  $\|\boldsymbol{\mu}\|/\sigma^2 \rightarrow \infty$ ) of the LDA classification algorithm can be rewritten as

$$\text{CR}(\pi_{K_0-1} || \pi_{K_0}; \mathcal{D}_\infty, \mathcal{C}^{\text{LDA}}) = \{(p_1, p_2) \in \Omega : f_2(p_{1\vee 2}) - f_2(p_{1+2}) > 0\}. \quad (40)$$

where  $p_{1\vee 2} := p_1 \vee p_2$ . Figure S8 shows the plots of  $f_1(p)$ , and  $f_2(p)$  where  $p \in (0, 1]$ .  $f_1(p)$  monotone

decreases for  $p \in (0, e^{-1/2})$  (left panel) and  $f_2(p)$  monotone decreases for  $p \in (0, e^{-1})$  (right panel).

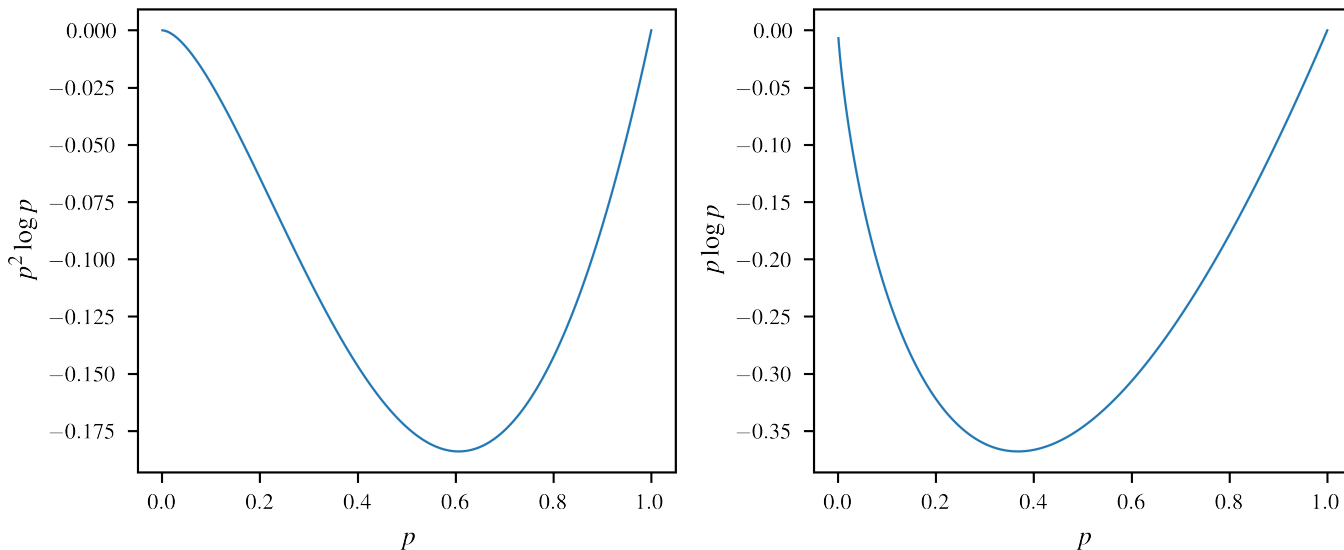


Figure S8: Plots of  $f_1(p) = p^2 \log p$  and  $f_2(p) = p \log p$  where  $p \in (0, 1]$ .

#### 4.2 Class-combination curves and regions of other classification algorithms

We also investigate the class-combination curves of three other commonly used classification algorithms, including random forest (RF), gradient boosting trees (GBT), and neural network (NN). Specifically, we use RF with 50 trees, GBT with 20 trees, and a two-layer NN with 20 hidden units per layer and the ReLU activation function. We use the same procedure to generate the simulated datasets as described in the Figure 12 in the Appendix.

The empirical results of the class-combination regions are shown in Figure S9. We can see that the results of GBT and NN are similar to that of LDA. Compared with GBT and NN, RF is more likely to find the true class combination (the proportion of the blue is the largest). We note that the prediction of RF is based on the majority voting of decision trees. Hence, intuitively, RF has a “soft” nature, putting it in the middle of the oracle classification algorithm and LDA.

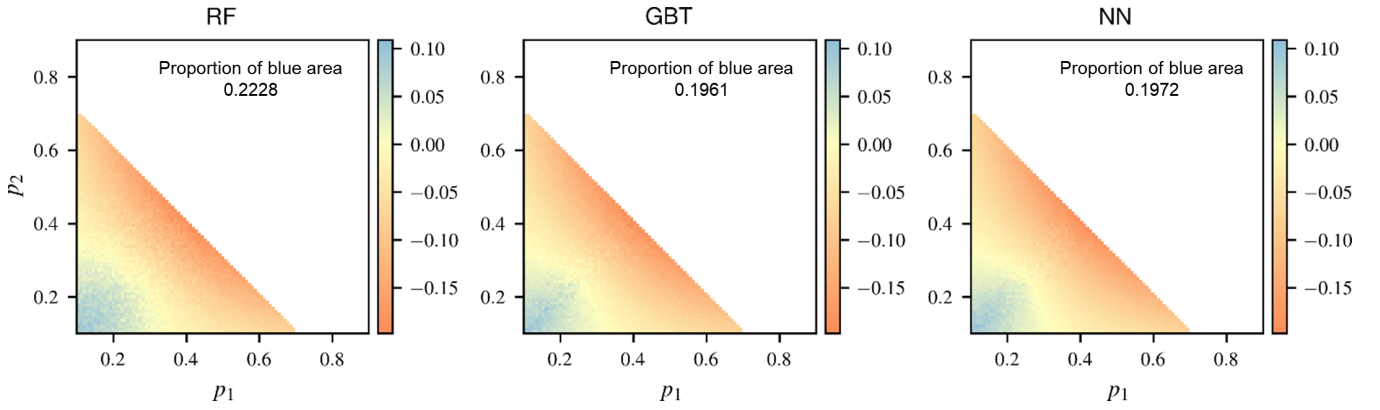


Figure S9: Regarding the combination of two same-distributed classes (with proportions  $p_1$  and  $p_2$ ), the improvement of s-ITCA ,  $\Delta\text{s-ITCA}(p_1, p_2; \mathcal{D}_t, \mathcal{C}) := \text{s-ITCA}(\pi_{K_0-1}; \mathcal{D}_t, \mathcal{C}, p_1, p_2) - \text{s-ITCA}(\pi_{K_0}; \mathcal{D}_t, \mathcal{C}, p_1, p_2)$ , of the RF algorithm (bottom left;  $\mathcal{C}^{\text{RF}}$ ), the GBT algorithm (middle;  $\mathcal{C}^{\text{GBT}}$ ) and the NN algorithm (right;  $\mathcal{C}^{\text{NN}}$ ). The red areas indicate the class-combination regions where  $\Delta\text{s-ITCA}(p_1, p_2; \mathcal{D}_t, \mathcal{C}) > 0$  and thus the two classes will be combined. In each panel, the yellow boundary between the orange area and the blue area is the class-combination curve of the corresponding algorithm. The proportion of the area of the class-combination region (the blue area) is shown in the upper right corner.